

Neuromorphic VLSI Circuits for An Electronic Nose Chip

Thesis by
Kea-Tiong Tang

In Partial Fulfillment of the Requirements
for the Degree of
Doctor of Philosophy

California Institute of Technology
Pasadena, California

2001
(Submitted May 11, 2001)

Acknowledgements

I would like to express my deep gratitude to Professor Rodney M. Goodman for his guidance and interest in this work. Without his numerous encouragements and timely suggestions this work cannot be done. Many helpful and stimulating discussions with Vincent Koosh and Jeff Dickson are also acknowledged. I am also very thankful to my secretary Karin Knott for her always efficient and kindly help.

I would like to gratefully acknowledge my parents Sing-Hua Tang and Sik-Yii Ting, and my wife Monica Li-Chuan Chu. Their forever support and encouragement are the original force to drive me through many obstacles. I would also like to thank the saints from the churches for their unconditional helps and prayers.

If I ever got anything, I would like to give my thanks to my Lord Jesus Christ, for His amazing grace and everlasting supply.

*But by the grace of God I am what I am; and His grace unto me did not turn out in vain.
(1 Corinthians 15:10a)*

Abstract

Human olfaction is still the primary instrument used in many industries to classify the smell or flavor of products. This is a costly process since trained experts are required who can only work for relatively short periods of time. Therefore using machine olfaction to perform the task would be a significant advance. Many researchers have investigated electronic noses, but currently only relatively large "instrument" electronic noses have been built. We have designed an electronic nose on a single silicon chip, including adaption, signal processing, and classification.

The electronic nose chip is composed of four different stages: Sensor stage, Signal Processing stage, Database stage, and Classifier stage.

The sensor stage, as its name suggests, deals with the sensor directly. The sensor we use is a carbon black-organic polymer whose relative resistance change is proportional to the given odor concentration. The function of the sensor stage is to adapt this resistive sensor to a preset baseline value, take the AC signal voltage, then output a current proportional to the signal voltage. So the sensor stage outputs a signal current which contains information about the odor concentration. An adaptive electronics stage, a peak detector, and a transconductance amplifier are designed to complete the sensor stage. Adaptive electronics are implemented to adapt the sensor to be within a proper working range of the circuit while tuning out the environment background. Adaption is done by constructing an adjustable current source. After adaption is done, the bias current value is held, so the sensor voltage at this time contains two different types of information: baseline value and signal value. The peak detector traces the input signal to its maximum value, then holds the value for further signal processing. This is needed because the signal voltage is defined as the difference between the maximum sensor voltage and the baseline sensor voltage. The transconductance amplifier converts voltage to current linearly while functioning as high pass filter. The output current is equal to the difference between the two input voltages multiplied by some gain (called transconductance). The output of the peak detector, the maximum sensor voltage, is used as the noninverting input, while the baseline sensor voltage is used as the inverting input. By the differential input characteristic of the transconductance amplifier, the baseline information is cancelled, and only the signal information remains. Thus, the output current from the transconductance amplifier contains the signal information, i.e., odor concentration.

The signal processing stage performs two important tasks for further signal processing. First, normalization throughout the signal array is realized. Then the Euclidean distance between the signal vector and the data vector is calculated. A normalizer using city-blocks distance is designed and an Euclidean distance calculation circuit is built. A normalization circuit using city-blocks distance is implemented to generate a normalized signal vector. This normalized signal vector is stored in a SRAM through an A/D in the LEARNING State. On the other hand, in the CLASSIFYING state, Euclidean distance between the normalized signal vector and the data vector is calculated. Euclidean distance circuit is implemented to calculate the Euclidean distance between signal vector and data vector. The Euclidean distance is output in the form of a current. This distance measure is utilized for classification.

The database stage stores the signal vector in the data storage device (LEARNING state) or outputs the data vector from the data storage device (CLASSIFYING state). This stage also takes care of the interface between the electronic nose chip and the outside world. A central control unit is designed to generate all the control signals and arrange the time sequence. Eight-bit Static Random-Access Memory (SRAM) is used for data storage. A/D converter is used to convert the signal vector into a digital word. This happens during the LEARNING process. A D/A converter is used to convert the data from SRAM into the data vector. This happens during the CLASSIFYING process. A current copier cell is designed to maintain the value of the data current. Several current copier cells are used to form a data vector. The central control unit is designed to generate all the control signals needed and their time sequence.

The classifier stage receives all the Euclidean distances between signal vector and data vectors, and generates the output corresponding to the shortest Euclidean distance, while inhibiting all the other outputs. The generated output is denoted as the answer to the pattern recognition problem. The current copier cell in the database stage is used to maintain the value of the Euclidean distance current. Several current copier cells are used to generate inputs for the LTA circuit. The Loser-Take-All (LTA) is used for parallel classification. Global inhibition can be done by using an LTA circuit.

Contents

Acknowledgements	iii
Abstract	iv
1 Overview	1
2 Sensor	11
2.1 Introduction	11
2.2 Temporal response	12
2.3 Reproducibility	13
2.4 Linearity	14
2.5 Noise	15
2.6 Sensor array	17
2.7 Percolation theory	19
2.8 Drift	20
3 Chip Floorplan	22
3.1 Introduction	22
3.2 Stages	23
3.2.1 Sensor stage	23
3.2.2 Signal processing stage	23
3.2.3 Database stage	24
3.2.4 Classifier stage	24
3.3 Floorplan	25
4 Sensor Stage	27
4.1 Adaptive electronics	27
4.1.1 Need and advantage	28
4.1.2 Discrete adaptive circuit	28
4.1.3 Digital adaptive circuit	30
4.1.4 First analog adaptive circuit	33
4.1.5 Improved analog adaptive circuit	36
4.1.6 Summary	45

4.2	Peak detector	45
4.2.1	Circuit description	46
4.2.2	Performance and analysis	50
4.3	Transconductance amplifier	52
4.3.1	Circuit description	53
4.3.2	Performance and analysis	55
4.4	Overall performance	58
5	Signal Processing Stage	60
5.1	Signal normalization	61
5.1.1	Need	61
5.1.2	City-blocks distance normalization	64
5.1.3	Translinear principle	65
5.1.4	Circuit description	67
5.1.5	Performance and analysis	69
5.2	Distance measurement	70
5.2.1	Absolute value circuit	71
5.2.2	Euclidean distance circuit	71
5.2.3	Performance and analysis	74
6	Data Storage and Chip Interface	76
6.1	Data storage	76
6.2	Chip interface and control	77
6.2.1	Learning state	78
6.2.2	Classifying state	78
6.2.3	Central control unit	79
6.3	Current copier cell	85
6.3.1	Circuit description	85
6.3.2	Performance and analysis	87
7	Classifier Stage	90
7.1	Serial pattern recognition	90
7.1.1	Description	90
7.1.2	Advantages and disadvantages	92
7.2	Parallel pattern recognition	92
7.2.1	Loser-Take-All circuit	93
7.2.2	Performance	94

7.2.3	Alteration of LTA circuit	95
7.2.4	Drawback and improvement	97
8	Conclusion	101
8.1	Chip performance	102
8.1.1	Power dissipation	102
8.1.2	Longitudinal tests	103
8.1.3	Detection threshold	106
8.1.4	Response to analyte mixtures	108
8.1.5	Temperature dependence	109
8.2	Experimentation methodology	112
8.3	Future works	113
8.3.1	Scalability	113
8.3.2	Full integration	114
	Bibliography	118

List of Figures

2.1	A unique pattern generated from an array of broadly reactive sensors	12
2.2	Temporal resistance response of a typical polymer composite chemiresistor detector .	13
2.3	Resistances of carbon black composites of (a) PEVA and (b) PVP upon 15 repeated exposures to benzene and methanol, respectively	14
2.4	Differential relative resistance increase in a PEO-carbon black composite vs. fraction of analyte vapor pressure exposed to the film	15
2.5	Histograms from a 13-detector array of carbon black-polymer detectors	18
2.6	Relative differential resistance change, $\Delta R/R$, predicted by percolation theory as a function of the relative volume change, $\Delta V/V$, of a carbon black-polymer composite upon swelling	20
3.1	Chip floorplan for electronic nose chip	26
4.1	Sensor stage block diagram	28
4.2	Schematic of the discrete adaptive circuit	29
4.3	Schematic of the digital adaptive circuit	31
4.4	Schematic of the first analog adaptive circuit	34
4.5	Performance of the first analog adaptive circuit	35
4.6	Schematic of the improved analog adaptive circuit	37
4.7	Performance of the linear V/I current source	38
4.8	Output performance of linear V/I current source	42
4.9	Performance of improved analog adaptive circuit	43
4.10	Drift of the sensor voltage	44
4.11	Schematic of the peak detector circuit	46
4.12	Schematic of regenerative latch	48
4.13	Performance of regenerative latch	49
4.14	Performance when maximum voltage is less than 4 V	51
4.15	Performance when maximum voltage is larger than 4 V	52
4.16	Schematic of the transconductance amplifier circuit	54
4.17	Performance of transconductance amplifier	57
4.18	Performance of transconductance amplifier with different bias voltages	58
4.19	Overall performance of the sensor stage	59

5.1	Block diagram of the signal processing stage	61
5.2	Schematic of the city-blocks distance normalization circuit	68
5.3	Performance of city-blocks distance normalization circuit	69
5.4	Schematic of the absolute value circuit	72
5.5	Performance of the absolute value circuit	73
5.6	Schematic of the Euclidean distance circuit	74
5.7	Performance of the Euclidean distance circuit	75
6.1	Block diagram of the database stage	77
6.2	Simplified block diagram of the central control unit	80
6.3	Schematic of the standard current copier circuit	86
6.4	Performance of the current copier	88
7.1	Serial pattern recognition	91
7.2	Parallel pattern recognition	92
7.3	Schematic of the Loser-Take-All circuit	93
7.4	Schematic of the output amplifier	95
7.5	Performance of the LTA circuit (current output)	96
7.6	Performance of the LTA circuit (voltage output)	97
7.7	Performance of the divider circuit	98
7.8	Performance of the WTA circuit	99
7.9	Performance of the alternative LTA circuit	100
8.1	Normalized data patterns	105
8.2	Un-normalized test patterns	107
8.3	Normalized test patterns	108
8.4	3-D plot of the eight different normalized data patterns	109
8.5	3-D plot of the normalized test and data patterns	110
8.6	Maximum relative differential resistance responses of the sensor array when exposed to analyte mixtures	111
8.7	Temperature dependence to three polymer sensors (PEVA,PEO,PV4P)	113
8.8	Circuit diagram for the electronic nose chip	116
8.9	electronic nose chip Layout	117

List of Tables

1.1	Different electronic nose sensor technologies	9
1.2	Available electronic nose instruments	10
2.1	13-element carbon black-organic polymer sensor array	17
4.1	Summary of adaptive circuits	45
6.1	Truth table for RAM Ctrl	82
6.2	State table and function of <i>logic2</i>	83
8.1	Original and normalized data vectors from 10 times exposure to methanol	103
8.2	Average of standard deviation of data vectors stored in the SRAM	104
8.3	Original and normalized test vectors	104
8.4	Euclidean distances	106
8.5	Output currents from the sensor stages in the temperature dependence experiment .	112

Chapter 1 Overview

Olfaction, the sense of smell, is the main sensory system in humans that contributes to the sensation of flavor. Together with other sensations, such as vision and audition, olfaction makes one's life more colorful. Imagine walking in a garden full of beautiful flowers without enjoying their wonderful fragrance, or eating delicious New York steak without smelling it, one can easily conclude that olfaction is so important to our daily life. But it is more than that. There are many applications of olfaction not only for an individual's life but also for the industries. Applications include food product quality control, safety and security, environmental monitoring, indoor air quality, health care, medical diagnosis, pharmaceutical purposes, and military applications. For example, one typical olfaction task is for food manufacturers to test for food freshness, to screen of incoming raw materials, to control food quality, and to monitor for accidental or intentional contamination. Hines at university of Warwick has reported the application for a neural network-based electronic nose to non-destructively determine ripeness of banana and apple[1, 2].

One olfaction task would be involved in safety and security applications. For example, hazardous alarms for toxic and biological agents can be made based on the use of olfaction. Moreover, applications for screening airline passengers and luggage for explosives, and examining vehicles for drugs and contraband at airports, cargo terminals, and border crossings all come to mind. In addition, olfaction is very useful for environmental monitoring. It can be applied to detect pollution and hazardous chemicals that threaten people's life. Odor control is of increasing importance in our lives, such as in automobiles, trains, aircrafts, inside and outside of buildings and factories. Moreover, it can be used to monitor indoor air quality, as well as industrial and agricultural emissions and noxious environmental wastes. Researchers at Warwick university, U.K. have reported an electronic nose system for monitoring the quality of potable water and classifying the strain and growth phase of cyanobacteria in it[3, 4].

Furthermore, odor has been valued by physicians for diagnostic purposes for centuries. Breath, sweat, urine, and stools can be analyzed to provide diagnostic information to medical practitioners. The Chinese have used smell to help diagnose ailments for thousands of years. For example, breath analysis can be used for rapid diagnosis of acute infections, acetone can be detected in the breath of diabetics, and halitosis can be detected for stress or stomach disorders. Gardner has reported the applications of the electronic nose system to predict bacteria type, examine breath, and diagnose

illness[5, 6, 7]. Besides, monitoring of wound infections and body odor in a nursing home would improve the quality of life for the elderly. In addition, olfaction can be applied to screen incoming raw materials, to monitor production processes, and to maintain security in storage and distribution areas in the pharmaceutical industry.

Olfaction can be utilized in the military to find buried landmines. It can also be used for other battlefield applications including biological and chemical agent detection, friend-or-foe identification, monitoring aging warheads and artillery shells, anticipating the creation of explosive environments, and protecting personnel who must handle these dangerous inventory items.

These applications of olfaction raise a demand to find a "nose" that meets the needs. The biological nose is the first thing that comes to mind. In fact, today the human nose is still the primary "instrument" used to assess the smell or flavor of various industrial products. But there are many drawbacks, such as individual variability, fatigue, infections, mental state, subjectivity, exposure to hazardous compounds, etc. Moreover, it is not a good process economically because of the cost to train experts who can only work for relatively short period of time. Thus an alternative "nose" that can imitate the function of the biological nose is needed.

Perhaps the earliest work on odor sensing can be traced back to Moncrieff in 1961[8]. It was actually a mechanical nose. The concepts of early electronic noses were reported by Wilkens and Hatman back in 1964[9], Buck[10] in 1965, and Dravnieks[11] in 1965, but the concept of an electronic nose as an intelligent chemical sensor array system for odor classification was introduced 20 years later by Persaud at Warwick University in UK[12] in 1982 and Ikegami at Hitachi in Japan in 1985 and 1987[13, 14]. The term "electronic nose" appeared around the late 1980s as it was used at a conference in 1987[15]. In 1989, during a session at a NATO Advanced Workshop on Chemosensory Information Processing, artificial olfaction was discussed and the design of an artificial olfactory system was further established[16]. The first conference dedicated to the topic of electronic noses was held in 1990[17].

Since 1990, many researches on a sensor array system for odor classification have been done. Several kinds of electronic nose sensors have been investigated. They fall into five main categories: conductivity sensors, piezoelectric sensors, MOSFETs, optical sensors, and spectrometry-based sensing methods. There are two different types of conductivity sensors: metal oxide[18, 19, 20, 21] and conducting polymer[22, 23, 24, 25]. Both of them exhibit a conductance change when exposed to odors. Metal oxide has been used extensively and available commercially in electronic nose applications. Oxides of tin, zinc, titanium, tungsten, and iridium doped on platinum or palladium are

usually used. Sensor sensitivity ranges from 5 to 500 parts per million. One severe drawback is that its operation temperature is usually very high. On the other hand, conducting polymer sensors usually operate at ambient temperature, so they do not need a special heater. The electronic interface for conducting polymer sensors is very straightforward, making them very suitable for portable instruments. Sensor sensitivity ranges from 0.1 to 100 parts per million. The main drawback of conducting polymer sensors is their high sensitivity to humidity. Thus some ways to tune out the background humidity and sensor drift are necessary.

There are two types of piezoelectric sensors: quartz crystal microbalance (QCM)[26, 27] and surface acoustic-wave (SAW) devices[28, 29]. For the electronic nose applications, they are both configured as mass-change-sensing devices. The QCM device is a resonating polymer-coated disk with metal electrodes on each side connected to a lead wire. In operation, The device resonates at a characteristic frequency when excited with an oscillating signal. When the odor is adsorbed by the polymer, the mass of the device increases, thus the resonance frequency is reduced. The reduction of frequency is inversely proportional to odorant mass adsorbed by the polymer. QCM usually has sensitivity up to 1ng mass change. One of the disadvantage of QCM is when the dimensions are scaled down, the device becomes noisier because of the instabilities due to larger surface-to-volume ratio. Another type of piezoelectric sensor is SAW device. Different from QCM, a Rayleigh wave travels over the surface of the device instead of its volume. SAW sensors operate at much higher frequencies than QCM, hence the frequency change is larger. So the sensitivity of a SAW device can be up to 1pg mass change. Both SAW and QCM devices need more complicated interface electronics.

When the volatile organic compounds come in contact with a catalytic metal, there is a reaction in the metal. By using a MOSFET odor-sensing device this reaction diffuses through its gate and changes the electrical properties of the device[30]. Therefore, the sensitivity and selectivity of the device can be optimized by adjusting the type and thickness of the metal catalyst. Usually several parts per million sensitivity can be achieved. One of the advantages of using a MOSFET odor-sensing device is its excellent compatibility with IC fabrication processes. So the device can be integrated with electronic interface circuits and batch-to-batch variations can be minimized. But remember the catalyzed reaction products have to penetrate the catalytic metal layer for the device to change its electrical properties. Thus the device needs a window to allow reaction products to interact with the gate structures.

Another type of odor-sensing device is optical-fiber sensors[31]. Glass fibers with a thin chemically active material coating on the sides are configured as the sensing devices. The active material contains chemically active fluorescent dyes immobilized in an organic polymer matrix. A light

source at a single frequency is used to interrogate the active material. When an odor is applied to the sensor, a change in color is detected and measured. By forming an array of these optical-fiber devices an electronic nose can be built. Their sensitivity is usually very high, up to low parts per billion. The disadvantages of the device are the complexity of the instrumentation and control system and the limited lifetime due to photobleaching. Dickinson and Kauer at Tufts university have reported convergent, self-encoded bead sensor arrays in the design of an artificial nose[32].

Gas chromatography, mass spectrometry, and light spectrum are the three different types of spectrometry-based sensing methods. The idea is to inject the odor into a spectrometer which generates a spectral response characteristic of the odor, such as separated molecular constituents (gas chromatography), atomic mass profile (mass spectrometry), or transmitted light frequencies (light spectrum). A sensor at the output of the spectrometer detects the characteristic profile. When sampled at various instants, a unique pattern can be obtained as coming from an array of different parallel sensors. The sensitivity is usually parts per billion and good analytical accuracy can be achieved. But this type of odor-sensing devices require complex interface electronics, and they seldom perform in real time in the field.

Table 1.1[33] summaries different technologies for electronic nose sensors, including the principle of operation, their fabrication methods, availability, sensitivity of the sensors, advantages and disadvantages.

Several manufacturers have already commercialized different "electronic noses". They are instruments that are mostly desktop or laptop in size, depending on their features. Since much of the early work of electronic nose technology has been done in Britain, there are many companies such as AromaScan, Bloodhound Sensors, and EEV Chemical Sensor Systems in Britain. There are several other companies in Europe that commercialize electronic nose instruments such as Airsense and Lennartz in German, Alpha M.O.S. in France, and Nordic Sensor Technologies in Sweden. In the United States several companies have joined the electronic nose business, including Cyrano, Electronic Sensor Technologies, Hewlett-Packard, and Sawtek. Table 1.2[33] is a summary of some available electronic nose instruments today in the market, including their sensor type, number of sensors, size of the instrument, and their cost.

Although these "electronic nose" instruments have the ability to mimic the biological nose to some extent so that they can be applied to many industrial uses, they are large in volume with high cost and high operating power. For the applications such as landmine detection in the military use and food freshness examination in the supermarket, it is impractical to bring a desktop or laptop

alongside. Today, electronic nose instruments available in the market are either in size of desktop or laptop, with very few companies researching on palmtop size electronic nose. The purpose of this dissertation is to make a "wearable" electronic nose with the size of, for example, a watch. Therefore, innovative methods have been investigated to build up a low cost, low power, small size, and versatile sensing platform, such as a "electronic nose chip". There have been some efforts designing nose-on-a-chip by several people[30, 34, 35], but a real electronic nose chip has yet been made. So in this dissertation the VLSI circuits needed to build an electronic nose chip are investigated, designed, simulated, and tested.

To design the circuitry needed for the electronic nose chip, the biological nose is studied. The human smell begins with sniffing. When we sniff, air samples that contain molecules of odors move into nostrils, then past curved bony structure called turbinates. The turbinates create a turbulent airflow pattern. Eventually these air molecules would go to the nose's olfactory epithelium coated with thin mucus generated by olfactory mucous membrane. The function of the mucus is to trap the air molecules for further signal processing and maintain the humidity. The olfactory epithelium contains approximately 50 million primary sensory cells. Each of the sensory cells has miniscule filaments that extend from the surface of the epithelium into the watery mucus. Each filament contains a protein which is the molecular receptor that interacts with the incoming odorant molecules. When the air molecule binds to the receptor protein, a cascade of enzymatic reactions is initiated, and odor signals are transmitted from the sensory cells in the epithelium through axons to the brain's olfactory bulb, where it terminates in a cluster of neural networks called glomeruli. These glomeruli neural networks perform recoding, re-mapping, and compression of the sensor signals. Then these signals are sent to olfactory cortex, where classification and recognition really take place.

Learning from the biological nose, this dissertation is devoted to design the circuits needed for building up a novel VLSI-compatible, versatile, low-cost, small volume, electronic nose chip. First, discrete carbon black-organic polymer sensors from Nate Lewis' group at Caltech[25] are chosen to imitate the function of receptor proteins in the biological nose. These polymer sensors exhibit several desired characteristics, such as good sensitivity, linearity, quick response time, and good reproducibility. Moreover, the interface electronics of the polymer sensors can be very simple and compact. Unlike metal oxide sensors, these polymer sensors operate at room temperature. Because of its characteristics, the carbon black-organic polymer is a very suitable candidate for the wearable electronic nose. Maybe one major drawback of the polymer sensor is its strong sensitivity to humidity. So an adaptive circuit which can tune out the environment background needs to be designed.

The sensor signal is read from the output of the adaptive circuit. By forming an array of different polymer sensors a signal vector can be generated. However, this signal vector is still "raw" and needs some further signal processing. First of all, the signal vector needs to be normalized because the odor concentration is usually unknown. This normalized signal vector is either stored in the memory for database storage or compared with existing data vectors. The comparison between the normalized signal vector and existing data vectors are done by performing Euclidean distance calculation. A nearest neighbor classifier is then implemented to imitate the function as glomeruli neural network.

Normalization and Euclidean distance calculation are done by designing circuits that perform these functions. Bipolar transistors are chosen because of the simplicity resulting from their excellent exponential characteristic. Signals are processed in current mode rather than voltage mode because it is much easier to perform addition, subtraction, and many mathematical calculations in current mode. Therefore, a transconductance amplifier is needed to convert the sensor signal into current before normalization.

Integrated sensor has been researched by Jeff Dickson in our group[36, 37]. Therefore, only VLSI circuits needed are investigated in the first generation electronic nose chip. A standard SRAM is chosen as the memory to store the data vectors instead of on-chip memory cells. Since SRAM, A/D, and D/A are all existing parts available in the market today, this dissertation concentrates on the other building blocks of the electronic nose chip. An interface circuit between the nose chip and the digital circuits is designed. Of course the future goal for the wearable electronic nose is to implement the memories on chip, such as analog memory cells. Throughout the dissertation, analog VLSI is used much more extensively than digital. The advantages of using analog VLSI are to reduce power dissipation, to speed up the signal processing by performing parallel computation, and to save chip area so that more channels of sensors can be implemented on the same chip.

Chapter 2 serves as a summary for the background knowledge of the carbon black-organic polymer sensor. This polymer sensor is utilized as the olfactory cell in the human nose. Its characteristics, such as temporal response, reproducibility, and linearity are discussed. A typical sensor array is presented. An array of different polymer sensors is used to generate a unique odor signature for each odor. These odor signatures form the basis of the electronic nose. Percolation theory, which explains the way polymer sensor works, is introduced. Finally, two of the important non-ideal characteristics, sensor noise and sensor drift, are discussed.

In chapter 3, the floorplan of the electronic nose chip is presented, and four of the stages which compose of the electronic nose chip are introduced: sensor stage, signal processing stage, database

stage, and classifier stage. The sensor stage adapts the polymer sensor to a preset baseline value, takes the AC signal voltage, then outputs a current proportional to the signal voltage. The output of the sensor stage is a signal current which contains information about the odor concentration. Taking the outputs from an array of sensors results in a signal vector, and this signal vector is output to the signal processing stage.

The signal processing stage normalizes the signal vector to obtain the signal pattern. This signal pattern is stored in the database stage in the LEARNING state or compared to existing odor patterns in the CLASSIFYING state. Euclidean distances between normalized signal vector and data vectors generated from the database stage are calculated through an Euclidean distance circuit. All the Euclidean distances are sent into a Loser-Take-All classifier in the classifier stage. A block diagram for the entire floorplan is presented at the end of the chapter.

In chapter 4 the sensor stage is described in detail. The need and advantage to adapt the sensor to the environment are discussed, and several different types of adaptive circuits are presented. The performance of the various adaptive electronics are shown and analyzed. A peak detector is designed to track the maximum sensor voltage, then a transconductance amplifier is used to extract the signal current (feature extraction). The overall performance of the whole sensor stage is tested and shown at the end of the chapter.

Chapter 5 discusses the circuits needed for the signal processing stage. In the beginning, the need for normalization is stated. Then a very powerful design principle called the translinear principle is introduced. Utilizing the translinear principle, a simple and compact normalization circuit using city-blocks distance is designed and tested. An absolute value circuit is built to take the absolute value of the difference between the input vector and data vector. Moreover, applying the translinear principle again, an Euclidean distance that calculates the Euclidean distance of a vector is designed and tested.

Chapter 6 is devoted to the database stage and chip interface. At first several different methods of digital storage are introduced, and SRAM is chosen to be the storage method. Then the chip interface is designed according to two different states of the signal processing: LEARNING state and CLASSIFYING state. To generate all the control signals for the SRAM and multiplexors in the database stage, a central control unit is designed. At the end of the chapter, a current copier cell is shown. It is built to memorize the current for a period of time in order to construct the data vector and the inputs of the Loser-Take-All circuit.

Chapter 7 describes the final stage of the electronic nose chip. Two pattern recognition techniques are introduced: series pattern recognition and parallel pattern recognition. Series pattern recognition is described shortly and its advantages and disadvantages are analyzed. A Loser-Take-All circuit is used to realize the parallel pattern recognition technique. Its performance is tested and its drawback is discussed.

Chapter 8 presents the conclusion of the dissertation. Eight different odor patterns are stored in three-dimensional vectors and six different odors are tested using the electronic nose chip. The performance of the electronic nose chip is presented, and future works for further improvement of the electronic nose chip are suggested.

Sensor type	Principle of operation	Availability	Sensitivity	Advantages	Disadvantages	References
Metal oxide	Conductivity	Commercial	5-500 ppm	Inexpensive	Operating at high temperature	[18, 19, 20, 21]
Conducting polymer	Conductivity	Commercial	0.1-100 ppm	Operates at room temperature	High sensitivity to humidity	[22, 23, 24, 25]
Quartz crystal microbalance (QCM)	Piezoelectricity	Commercial	1.0-ng mass change	Well-understood technology	Noisier when dimensions are scaled down, complicated interface electronics	[26, 27]
Surface acoustic wave (SAW)	Piezoelectricity	Commercial	1.0-pg mass change	Very sensitive differential devices	Complicated interface electronics	[28, 29]
MOSFET	Capacitive charge coupling	Commercial	Several parts per million	Excellent compatibility with IC fabrication processes	A window is needed to allow reaction products to interact with the gate structures	[30]
Optical-fiber	Fluorescence, chemoluminescence	Research	Low parts per billion (ppb)	High electrical noise immunity	Complexity of the instrumentation and control system, limited lifetime due to photobleaching	[31]
Gas chromatography	Molecular spectrum	Commercial	Low ppb	Potential analytical accuracy	Complex interface electronics, seldom perform in real time in the field	
Mass spectrometry	Atomic mass spectrum	Commercial	Low ppb	Potential analytical accuracy	Complex interface electronics, seldom perform in real time in the field	
Light spectrum	Transmitted light spectrum	Research	Low ppb	Sample not consumed	Requires tunable quantum-well devices	

Table 1.1: Different electronic nose sensor technologies

Manufacturer	Sensor type	No. of sensors	Size	Cost (US)
Airsense Analysis GmbH	Metal oxide semiconductor (MOS)	10	Laptop	20000-43000
Alpha MOS-Multi Organoleptic Systems	Conducting polymer (CP), MOS, quartz crystal microbalance (QCM), surface acoustic wave (SAW)	6-24	Desktop	20000-100000
AromaScan PLC	CP	32	Desktop	20000-75000
Bloodhound Sensors Ltd.	CP	14	Laptop	
Cyrano Sciences Inc.	CP	32	Palmtop	5000
EEV Ltd. Chemical Sensor Systems	CP, MOS, QCM, SAW	8-28	Desktop	
Electronic Sensor Technology Inc.	Gas chromatography, SAW	1	Desktop	19500-25000
Hewlett-Packard Co.	Quadrupole mass spectrometry		Desktop	79900
Lennartz Electronic GmbH	MOS, QCM	16-40	Desktop	55000
Nordic Sensor Technologies AB	Infrared, MOS, QCM	22	Laptop	40000-60000
Sawtek Inc.	SAW	2	Palmtop	5000

Table 1.2: Available electronic nose instruments

Chapter 2 Sensor

Sensors are the eyes and ears of modern measurement instrumentation and control systems. They can be viewed as a machine's way to "see", "hear", and "touch" the environment. They are widely used in both analog and digital instrumentation systems to provide the interface between electronic circuits and the real world. Numerous sensors have been investigated to perform many kinds of functions. For example, a microphone is a sensor that transforms an acoustic wave into an electric signal. In short, a sensor is a device that converts energy derived from a physical phenomenon into an electrical current or voltage, for purposes of measurement and control.

The electronic nose, by its name, is a machine that can smell and distinguish different smells. For the electronic nose chip, sensors that can transform different smells into measurable current or voltage are needed. Carbon black-organic polymer has been proven to be one of the candidates for odor sensing. In this chapter we will give a brief summary about the carbon black-organic polymer sensor. Its characteristics, theory, and application as the front end of the electronic nose chip will be discussed.

2.1 Introduction

To construct an approach to chemical sensing, one of the ideas is to reference and mimic the mammalian sense of olfaction [38, 39]. For a mammalian, instead of one single sensor in the nose, over 1000 receptor genes have been discovered in the olfactory system. Learning from the mammalian, an array of different sensors is used for odor identification, with every sensor chosen to respond to a number of different chemicals [40, 41, 42, 43]. In such an array, no individual sensor responds solely to a specific odor, but the collective response of the entire array produces a unique pattern for the odor of interest (Figure 2.1). Ideally, in order to respond to the largest cross section of analytes, the elements of the sensor array should show as much chemical diversity as possible. Then the response of the sensor array produces a distinct pattern, like a signature or fingerprint, that can be utilized for odor classification and identification.

Carbon black-organic polymers are used to form the sensor array. The sensor element is constructed by dispersing a film consisting of carbon black particles into different insulating organic polymers. Carbon black particles offer very stable electrical conductivity, while different organic polymers offer chemical diversity throughout the sensor array. When a sensor is exposed to vapor,

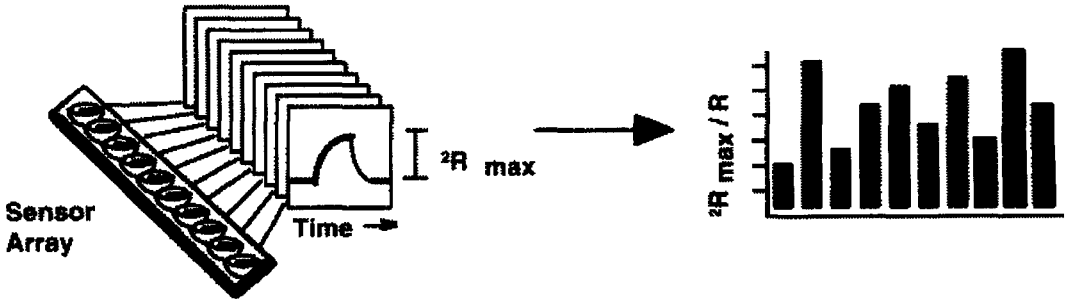


Figure 2.1: An array of broadly reactive sensors in which each individual sensor responds to a variety of odors, but the pattern of differential responses across the array produces a unique pattern for each odorant.

the polymeric phase of the composite swells while carbon black is unaffected, and forms a longer conduction path, i.e., an increased resistance. This is a very simple but great means for monitoring the presence of a vapor [44, 45]. By constructing an array of carbon black-organic polymers, a pattern showing resistance changes among different sensors forms a unique signature for the vapor of interest.

2.2 Temporal response

A typical sensor response is shown in Figure 2.2 [46]. Before being exposed to vapor, the sensor resistance maintains its baseline value R_b . The sensor responds at the time an odor vapor is applied to its surface, and its resistance increases rapidly in the rise time. The rise time is defined from the time the sensor resistance reaches 10% of its equilibrium to the time the sensor resistance reaches 90% of its equilibrium. After the rise time, the sensor resistance increases gradually to reach its equilibrium state R_{max} .

The sensor resistance maintains its equilibrium state R_{max} as long as the vapor exists. When the vapor is removed, the sensor resistance drops dramatically during its fall time, then decreases slowly toward the original baseline R_b . Similar to the rise time, the fall time is defined from the time the sensor reaches its 10% decrease to 90% decrease. The sensor resistance basically goes back to its original baseline value as time goes on.

We define the difference between the maximum sensor resistance when reaching equilibrium R_{max} and the baseline resistance R_b as

$$\Delta R_{max} = R_{max} - R_b \quad (2.1)$$

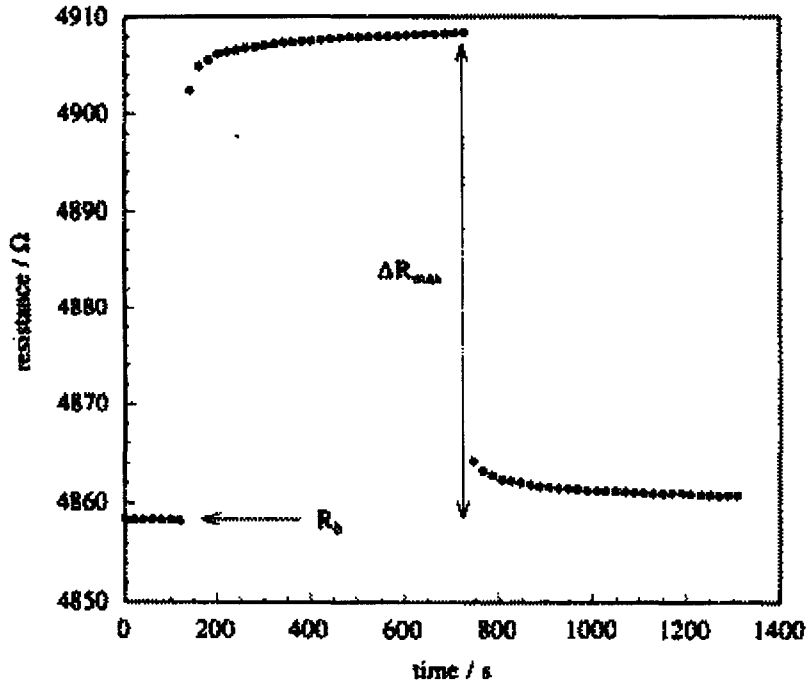


Figure 2.2: Temporal resistance response of a typical polymer composite chemiresistor detector

This differential resistance ΔR_{max} is called differential sensor resistance and is very important as we will see very soon in section 2.4.

2.3 Reproducibility

One of the important requirements for a usable sensor is its reproducibility. In the real world, a circuit designer can not tolerate a sensor that can only be used once, except in some special applications. Moreover, the sensor should be able to "return" to its initial state every time after a measurement is done. If the sensor itself cannot return to the initial state, its usefulness depends on whether the circuit designer can implement a circuit to bring the whole circuit back to initial state.

Figure 2.3 shows the resistance changes of two carbon black-polymer films during repeated, periodic exposures to two test solvent vapors[47]. The resistances of the films increased when the solvent vapor was present and then returned to their original baseline values after the vapor flow was discontinued. The reproducibility of the sensor is very good, making the sensor able to be used multiple times.

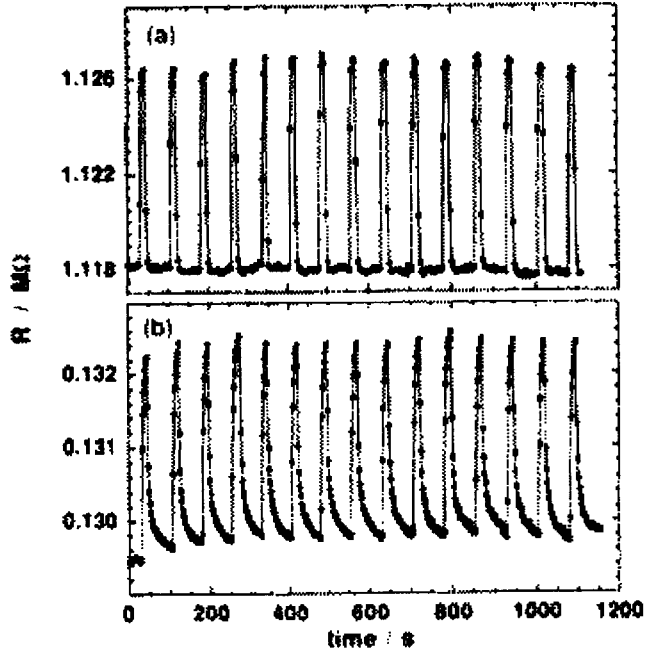


Figure 2.3: Resistances of carbon black composites of (a) PEVA and (b) PVP upon 15 repeated exposures to benzene and methanol, respectively

2.4 Linearity

For an arbitrary sensor, it would respond to the physical phenomenon in several possible ways. Some sensors relate their output voltage or current exponentially to the extent of the physical event, and some sensors have a quadratic relationship between its input and output. Many sensors exhibit more complicated relationships. But there is a kind of sensor that its output voltage or current shows a simple linear dependence to the "amount" of physical event. This linearity characteristic makes the sensor very easy to use. Because of the linearity property, the output voltage or current contains quantitative information of the physical event, i.e., it enables the machine to quantify the physical event directly.

One of the attractive properties of the carbon black-organic polymer sensor is its linearity. Many tests have shown a linear steady-state dc resistance response to analyte concentration[47, 48]. Therefore, the pattern itself forms an odor signature which allows odor classification, and the steady-state pattern height enables quantification of the odor concentration. We can describe the linearity by writing down an equation:

$$\Delta R_{max}/R_b = \lambda C \quad (2.2)$$

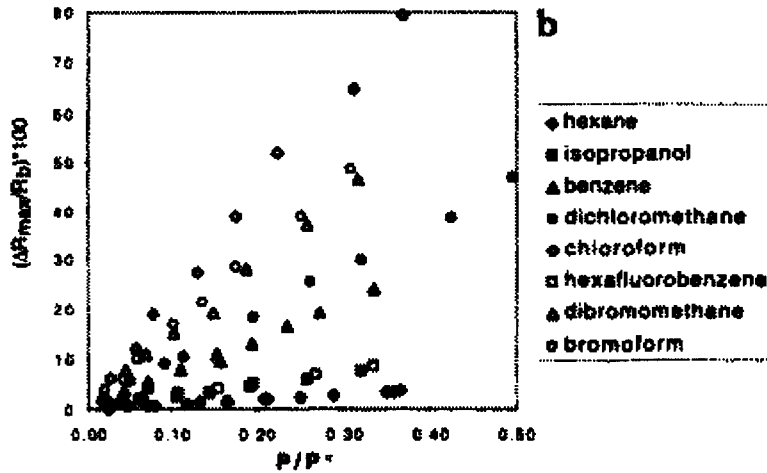


Figure 2.4: Differential relative resistance increase in a PEO-carbon black composite vs. fraction of analyte vapor pressure exposed to the film

where λ is a polymer-related constant, and C represents the odor concentration. Therefore, the relative differential resistance $\Delta R_{max}/R_b$ contains the odor concentration through the constant λ .

Figure 2.4 depicts the steady-state relative differential resistance response $\Delta R_{max}/R_b$ of carbon-black filled poly(ethylene oxide) film as a function of the analyte concentration[49]. Over the concentration range in the experiment, the data is well-fit by straight lines passing through the origin, showing great linearity characteristics. This linearity property is very useful for the use of normalization in section 2.6.

2.5 Noise

Sensors are the eyes, ears, and noses of a machine to contact the outside world. They translate the characteristics of the physical world into some measurable electrical signals. An engineering problem often related is the level of electrical noise generated in the sensor and electronic system. Since the useful information does not depend on the signal information itself, but instead on the signal-to-noise ratio (SNR), noise plays an important role in the discussion. Shurmer et al. have discussed the ultimate sensitivity attainable with resistive-based vapor sensors in the limit of Johnson or white noise[50]. The main noise source of the resistive carbon black-organic polymer sensors is also thermal noise.

Thermal noise is the most often encountered noise in resistive elements. It is caused by the

random thermally excited vibration of the charge carriers in a conductor. This kind of carrier motion is very similar to the Brownian motion of particles. When the temperature is above absolute zero, the electrons in a resistor are in random motion, and this kind of electron motion has a relationship with temperature. When the electrons move randomly in the resistor, there are many little current surges randomly in the resistor material. Of course the average current of these currents in the resistor is zero. But instantaneously there is a current fluctuation in the resistor, and these current fluctuation induces noise in the resistor.

Thermal noise is also called Johnson noise, Nyquist noise, or white noise, and the noise power can be shown as

$$N_t = kT\Delta f \quad (2.3)$$

where N_t is the thermal noise power, k is Boltzmann's constant (1.38×10^{-23} W-s/K), T is the temperature of the resistor in kelvins (K), and Δf is the noise bandwidth of the measuring system in hertz (Hz).

Another way to get a sense of the noise is to use rms thermal noise voltage E_t :

$$E_t = \sqrt{4kTR_b\Delta f} \quad (2.4)$$

For a typical sensor resistance $100k\Omega$ and $1kHz$ noise bandwidth, the rms thermal noise voltage is $1.27\mu V$. A lower limit can be set for the measurable voltage to be ten times the rms thermal noise voltage, which is $12.7\mu V$. Assume V_{ref} is $2V$, the bias current is $2V/100k\Omega=20\mu A$. So the corresponding sensor resistance change ΔR_{max} is 0.635Ω , which is $6.35 \times 10^{-4}\%$ resistance change.

In chapter 4 we will see the carbon black-organic polymer is biased by a current source, which outputs a constant current I decided by a reference voltage V_{ref} divided by the sensor resistance R_b . Assume the sensor resistance changes by ΔR_{max} , since the output remains constant, the signal voltage can be determine as

$$\Delta V = I\Delta R_{max} = \frac{V_{ref}}{R_b}\Delta R_{max} \quad (2.5)$$

So the signal-to-noise ratio can be obtained from equation 2.4 and 2.5

$$\frac{S}{N_t} = \frac{\Delta V^2}{E_t^2} = \frac{V_{ref}^2(\Delta R_{max}/R_b)^2}{4kTR_b\Delta f} = \frac{V_{ref}^2\Delta R_{max}^2}{4kTR_b^3\Delta f} \quad (2.6)$$

According to equation 2.6, there are several ways to enhance the signal-to-noise ratio. First of

sensor no.	Polymer
1	poly(4-vinylphenol)
2	poly(α -methylstyrene)
3	poly(vinyl acetate)
4	poly(sulfone)
5	poly(caprolactone)
6	poly(ethylene-co-vinyl acetate), 82% ethylene
7	poly(ethylene oxide)
8	poly(ethylene)
9	poly(butadiene)
10	poly(vinylidene fluoride)
11	poly(n-butyl methacrylate)
12	poly(epichlorohydrin)
13	poly(ethylene glycol)

Table 2.1: 13-element carbon black-organic polymer sensor array

all, decrease the temperature, i.e., cool off the sensor. This intuitively makes sense because thermal noise is proportional to temperature. Another parameter proportional to thermal noise is the noise bandwidth Δf . Secondly, raising the reference voltage V_{ref} helps the SNR. This is because V_{ref} is proportional to the output current I of the biasing current source. The higher the bias current, the greater the signal power while not affecting the noise power. Moreover, of course when the resistance change ΔR_{max} becomes larger, the signal power is larger as well. Finally, a smaller baseline resistance improves the signal-to-noise ratio.

2.6 Sensor array

Instead of using one single sensor for odor classification, an array of carbon black-organic polymer sensors is constructed for the task. Several different sensor arrays have been investigated [47, 48, 51, 34, 52, 53]. One typical sensor array is listed in Table 2.1.

Figure 2.5 [51] is a typical response for the 13-sensor array exposed to methanol, 1-butanol, and 1-octanol at partial pressure P , corresponding to 10% of the vapor pressure P^0 of the odorant. The response is shown in the form $\Delta R_{max}/R_b$ for the reason we have seen in section 2.4. The fingerprints for the three odors are very different, demonstrating the ability of the array to classify these three different odors.

The vapor pressures of the test odors in the above experiment are the same. But in the real world one can not guarantee that the vapor pressure would be the same for each unknown vapor. According to the linearity that has been discussed in section 2.4, one of the ways to resolve this is

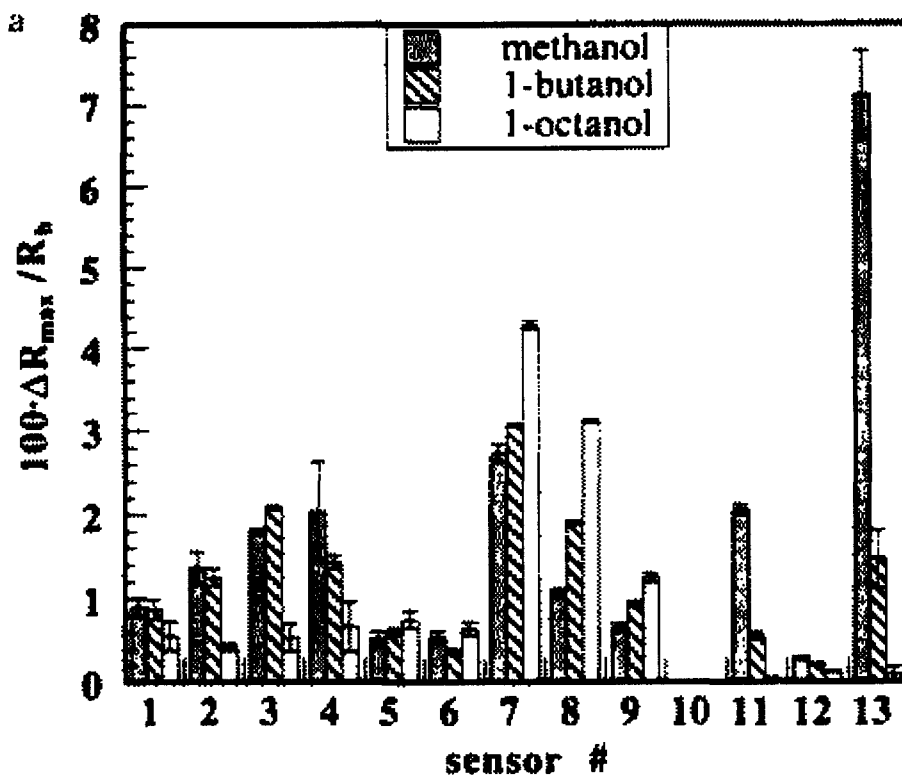


Figure 2.5: Histograms showing the response patterns of a 13-detector array of carbon black-polymer detectors exposed in air to methanol at 11 torr, 1-butanol at 0.57 torr, and 1-octanol at 5.8×10^{-3} torr.

to normalize the signals from the sensor array before comparison.

For example, in a sensor array which contains s different sensors, the normalized signal would be

$$S_j = \frac{\Delta R_{j,max}/R_{j,b}}{\sum_{j=1}^s \Delta R_{j,max}/R_{j,b}} \quad (2.7)$$

where j is the sensor number, $R_{j,b}$ is the baseline resistance of sensor j before exposure to the vapor, and $\Delta R_{j,max}$ is the largest differential resistance change observed for the j th sensor during the exposure to the vapor.

This kind of normalization uses the city-blocks distance as the denominator, and is very easy to be implemented in analog VLSI using a standard bipolar circuit, as we will see in Chapter 5.

2.7 Percolation theory

The relationship between the resistivity and carbon black content of carbon black-organic polymer composites can be explained by percolation theory[54, 55, 56]. When the carbon black concentration is low, the composites are insulators since no connected pathway of conductive particles exists across the material. As more carbon black is added gradually, there is a point when the resistivity of the composite can decrease dramatically with a small variation in the carbon black concentration. This resistance change can go up to 10 orders of magnitude. The reason for this sharp transition in the resistivity is because a connected pathway of carbon black particles is formed across the material, and this point is designated as the percolation threshold.

When an odor vapor is applied to the carbon-black organic polymer sensor, the polymer composite swells, causing disruption of the conduction pathway and increase of the resistance. Therefore, a differential resistance response is observed when odor vapors are applied to the sensor.

Percolation theory can be displayed more quantitatively by the equations given by[56, 57]

$$\rho = \frac{(z-2)\rho_c\rho_m}{A+B+[(A+B)^2+2(z-2)\rho_c\rho_m]^{1/2}} \quad (2.8)$$

$$A = \rho_c[-1 + (z/2)(1 - (\nu_c/f))] \quad (2.9)$$

$$B = \rho_m[(z\nu_c/2f) - 1] \quad (2.10)$$

where ρ is the resistivity of a carbon black-organic polymer composite, ρ_c is the resistivity of the carbon black, ρ_m is the resistivity of the polymer matrix, ν_c is the volume fraction of carbon black in the composite, z is the coordination number of the carbon black particles, and f is their total packing fraction ($\nu_c \leq f$). The volume fraction of carbon black in the composite at the percolation threshold, ν_p , is given by $2f/z$.

Setting $\nu_p = 0.33$ and $\rho_m/\rho_c = 10^{11}$ a theoretical prediction of equations 2.8 to 2.10 is shown in Figure 2.6[47]. An assumption is made that swelling does not affect the volume of the conductive element but changes only the total volume, V . So swelling of the insulating polymer matrix produces a relative volume change, $\Delta V/V$, of the film.

Two primary regions can be identified in Figure 2.6. When volume change is small enough that the carbon black volume fraction in the swollen composite ν_c^{sw} remains greater than ν_p , the con-

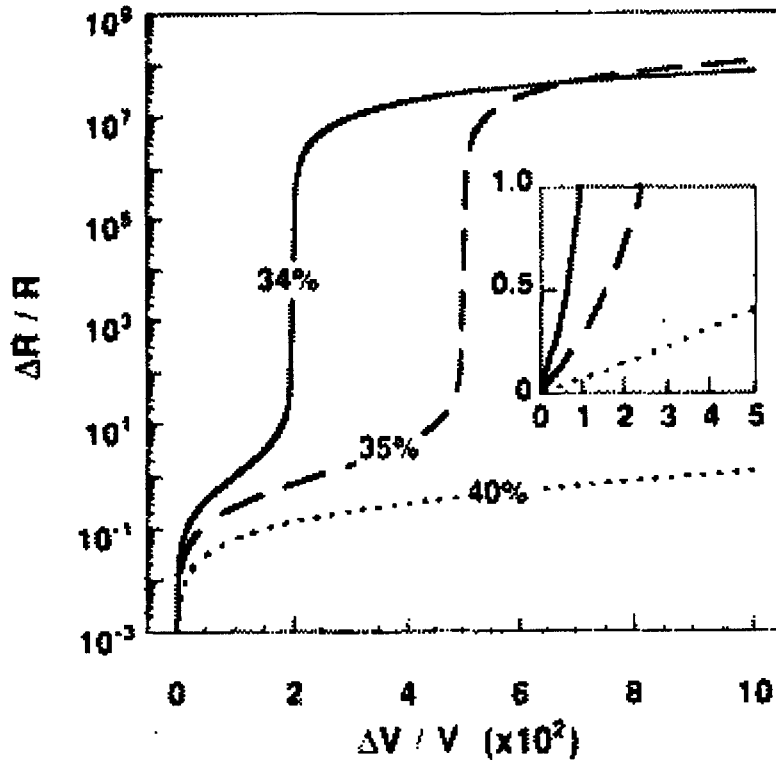


Figure 2.6: Relative differential resistance change, $\Delta R/R$, predicted by percolation theory as a function of the relative volume change, $\Delta V/V$, of a carbon black-polymer composite upon swelling

nection pathway is reduced but not eliminated by swelling. Thus the relative differential resistance response is pseudolinear (cf. Figure 2.6 inset). When $\nu_c > \nu_p > \nu_c^{sw}$, the resistivity becomes much larger.

This is basically how far we will discuss the percolation theory. Interested readers can refer to the references [54, 55, 56, 57, 58, 59].

2.8 Drift

In a real environment (for example, in a classroom), even if there are not any odor vapors being applied to the polymer sensor, the baseline resistance would not maintain the same value forever. In other words, the sensor resistance drifts from time to time.

There are several sources of sensor drift. The first reason is the background odors. Although no odors are applied to the sensor by us, there are still very many odor molecules in the air. Those are

the background odors, and their concentrations change from time to time. This background odor can not be controlled unless we keep the sensors in a well-controlled environment in the laboratory. But remember we are building a "nose" that can smell things in the real world. So the ideal environment is not taken into consideration and the background odors generate a source of sensor drift.

Another source of sensor drift is temperature variation. Since the resistance is decided by the length of the conduction pathway in the polymer, temperature drift would cause the volume of the polymer to change, resulting in a different length of the conduction pathway, i.e., different resistance. Since the sensors are openly exposed during operation, without a constant temperature environment, the sensor drifts as the temperature drifts.

One more source of sensor drift is the water vapor in the air. The effect of water vapor is to cause the sensor material to swell. So when the water vapor pressure in the air varies, the volume of the sensor changes, hence the sensor resistance changes as well.

Chapter 3 Chip Floorplan

To construct an electronic nose chip, the carbon black-organic sensors serve as the olfactory cells in a real nose. To sense and distinguish a smell, the signals received from the cells are transmitted to the brain through olfactory neurons in the olfactory bulb. In a similar way, the signals obtained from the polymer sensors have to be processed through some circuitry before being sent into the final classifier (brain) to make the final decision. The circuits needed for olfactory signal processing are introduced in this chapter and are discussed thoroughly in the next chapters.

3.1 Introduction

We have already learned from Chapter 2 that an array of carbon black-organic polymer sensors is very suitable for the task of odor classification. The polymer sensor functions as a normal resistor, and its resistance changes according to odor concentration. To measure the resistance of the sensor, a constant current is applied to the sensor, then the voltage across is measured. From the well-known ohm's law $R = V/I$ the resistance can be obtained. For this dissertation an array discrete polymer sensors will be used.

Adaptive electronics are built to adapt the voltage across the sensor¹ to some preset baseline value by adjusting a current source through a feedback loop. This current source provides a constant bias current for the sensor after adaption is done. Then the sensor voltage changes as long as the sensor resistance varies corresponding to the odor environment. The differential sensor voltage² which encodes the odor concentration information is sent to a peak detector to catch its maximum variance, and then input to a transconductance amplifier to produce a current³ proportional to the signal voltage, i.e. the output current encodes the odor concentration information.

Normalization throughout the signal currents from the sensor array⁴ is performed for further signal processing. Then Euclidean distances between the signal vectors and data vector from database are calculated. Finally, all the Euclidean distance currents are sent into a Loser-Take-All classifier to perform pattern recognition.

¹sensor voltage

²signal voltage

³signal current

⁴signal vector

A central control unit is designed to control the time sequence of all the control signals. An SRAM, an A/D converter, and a D/A converter are used to store and output the odor patterns. Finally, at the end of the chapter, an overall chip floorplan will be given.

3.2 Stages

To illustrate the whole electronic nose chip, we divide the whole circuit into four main stages: sensor stage, signal processing stage, database stage, and classifier stage. Each stage has its name given by the function of that stage.

3.2.1 Sensor stage

The sensor stage, as its name suggests, deals with the polymer sensor directly. The function of the sensor stage is to adapt the resistive sensor to a preset baseline value, take the AC signal voltage, then output a current proportional to the signal voltage. So the sensor stage outputs a signal current which contains information about the odor concentration, according to equation 2.2.

- Adaptive electronics are implemented to adapt the sensor to be within a proper working range of the circuit while tuning out the environment background. The adaption is done by constructing an adjustable current source. After adaption is done, the bias current value is held, so the sensor voltage at this time contains two different information: baseline value and signal value.
- A peak detector traces the input signal to its maximum value V_{max} , then holds the value for further signal processing. This is needed because the signal voltage is defined as the difference between the maximum sensor voltage and the baseline sensor voltage.
- A transconductance amplifier converts voltage to current linearly while functioning as a high pass filter. The output current I_{out} is equal to the difference between the two input voltage $V_p - V_n$ multiplying by some gain (called transconductance). The output of the peak detector, the maximum sensor voltage, is used as the noninverting input V_p , while the baseline sensor voltage is used as the inverting input V_n . By the differential input characteristic of the transconductance amplifier, the baseline information is cancelled, and only the signal information is remained. Thus, the output current from the transconductance amplifier contains the signal information, i.e., odor concentration.

3.2.2 Signal processing stage

The signal processing stage performs two important tasks for further signal processing. First, normalization throughout the signal array is realized. Then the Euclidean distance between the signal

vector and data vector is calculated.

- The normalization circuit using city-blocks distance is implemented to generate a normalized signal vector. This normalized signal vector is stored in a SRAM through an A/D in the LEARNING state. On the other hand, in the CLASSIFYING state, Euclidean distance between the normalized signal vector and data vector is calculated.
- The Euclidean distance circuit is implemented to calculate the Euclidean distance between signal vector and data vector. The Euclidean distance is output in the form of a current. This distance measure is utilized for classification.

3.2.3 Database stage

The database stage stores the signal vector in the data storage device (LEARNING state) or outputs the data vector from the data storage device (CLASSIFYING state). This stage also takes care of the interface between the electronic nose chip and the outside world. A central control unit is designed to generate all the control signals and arrange the time sequence.

- 8-bit Static Random-Access Memory (SRAM) is used for data storage.
- A/D converter is used to convert the signal vector into a digital word. This happens during the LEARNING process.
- D/A converter is used to convert the data from SRAM into data vector. This happens during the CLASSIFYING process.
- Current copier cell is designed to maintain the value of data current. Several current copier cells are used to form a data vector.
- Central control unit is designed to generate all the control signals needed and their time sequence.

3.2.4 Classifier stage

The classifier stage receives all the Euclidean distances between signal vector and data vectors, raises the output corresponding to the shortest Euclidean distance, while inhibiting all the other outputs. The raised output is denoted as the answer to the pattern recognition problem.

- Current copier cell in the database stage is used to maintain the value of Euclidean distance current. Several current copier cells are used to generate inputs for the LTA circuit.
- Loser-Take-All (LTA) is used for parallel classification. Global prohibition can be done by using an LTA circuit.

3.3 Floorplan

A complete floorplan is shown in Figure 3.1. Three different polymer sensors are used at the front end, so three sensor stages are constructed. Thus a three-dimensional signal vector is generated from the sensor stages, and the data vector is three dimensional as well. For this reason three current copier cells (CC) are implemented in the database stage. Eight different odor data are stored in the database, so eight current copier cells are used in the classifier stage. All the four stages are shown in the floorplan, and they will be discussed in detail in the following chapters.

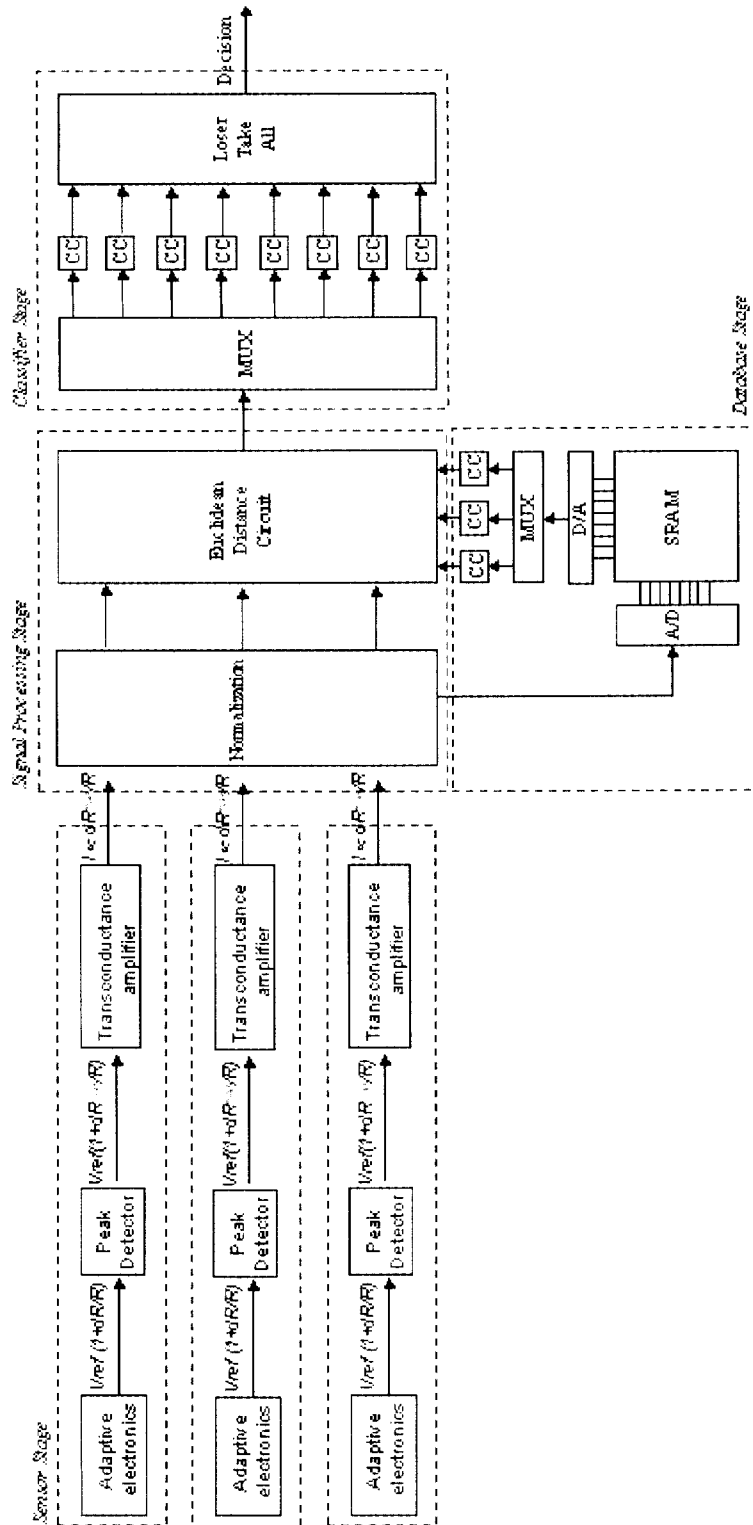


Figure 3.1: Chip floorplan for electronic nose chip

Chapter 4 Sensor Stage

A sensor is useful because it transforms a physical event into some signal data that we can read, process, and analyze. But usually output from a sensor needs to be manipulated so that useful data can be extracted from the raw data. This is what we call feature extraction. For the carbon black-organic polymer sensor we discussed in chapter 2, several things need to be done before useful data can be obtained. First, since the resistance of any given sensor is not necessarily the same, adaptive circuitry is needed to bias the sensor to an appropriate preset value before reading. Adaptive circuitry also needs to have the ability to adapt out signals with long time constants while responding to quick changes. It is very similar to human olfaction. For example, if someone enters a garden full of flowers, he smells the flavors generated from the flowers as soon as he steps in the garden. But if this person stays in the garden for a few hours, he does not feel the wonderful smell he had experienced when he just got in. It is not because the flavors are not there. It is just because the person would get used to them as time goes on.

From chapter 2, we know that the relative differential resistance $\Delta R_{max}/R_b$ is proportional to the odor vapor concentration. So our goal is to extract a voltage or current containing information about $\Delta R_{max}/R_b$, then we would have information about the odor concentration. Since the adaptive circuit sets the sensor voltage to some baseline value (reference voltage), the differential voltage (signal voltage) is obtained by subtracting the original sensor voltage from the responded sensor voltage. By doing this an AC signal voltage is extracted. Finally, since it is easier to process signals for mathematical calculation in current mode than in voltage mode for our purposes which will be discussed in chapter 5, AC signal voltage is converted into AC signal current through the use of a transconductance amplifier.

Figure 4.1 shows the block diagram for the sensor stage. In this chapter, all of the three building blocks of the sensor stage will be discussed: *adaptive electronics*, *peak detector*, and *transconductance amplifier*. For each building block, circuits will be described and their performance will be reported, analyzed, and discussed.

4.1 Adaptive electronics

Adaptive electronics comprise the first building block of the sensor stage. In this section, the need and advantage will be discussed first, then several different adaptive circuits will be presented.

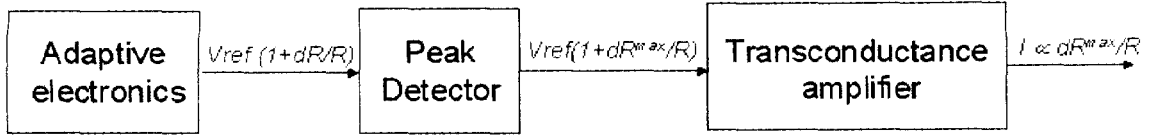


Figure 4.1: Sensor stage block diagram

4.1.1 Need and advantage

From chapter 2 we have known that the resistivity of the carbon black-organic sensor is determined by the concentration of carbon black in the polymer composite. Therefore, the resistance of the sensor depends on the doping of carbon black. Unless the doping concentration is under very good control, the resistance of the sensor would vary from one to the other. But from the point of view of a circuit designer, a good circuit should not depend on the value of the sensor resistance. One way to solve this problem is to bias the sensor to a certain preset voltage before reading its response. By this means the exact sensor resistance does not affect the way circuit works, and we can concentrate on how to extract the signal of interest.

Since the sensor responds to odor vapors, it responds as soon as it is brought into a new environment. But usually we are interested in detecting existence of a particular odor instead of the change of environment background. So it is necessary to employ adaptive signal processing techniques to tune out the environment background. Moreover, if the sensor is applied with the same odor with the same concentration for a long time, we would like the sensor not respond to that odor but respond to some newly applied odors instead. Thus circuits are developed to ignore changes on a long time scale, but react to quick changes.

Several generations of adaptive circuits have been built and experiments have been performed on all of them. They will be described thoroughly in the following subsections.

4.1.2 Discrete adaptive circuit

The first generation of the adaptive circuit is built by discrete electronics. The discrete adaptive circuit has been built on PCB and tested. Figure 4.2 shows the schematic. To analyze the circuit, first realize that the top op-amp¹, PMOS transistor, and sensor together form a standard noninverting amplifier whose output voltage is determined by

$$V_{out} = V_{ref} \left(1 + \frac{R_b}{R_{PMOS}} \right) \quad (4.1)$$

¹op-amp 1

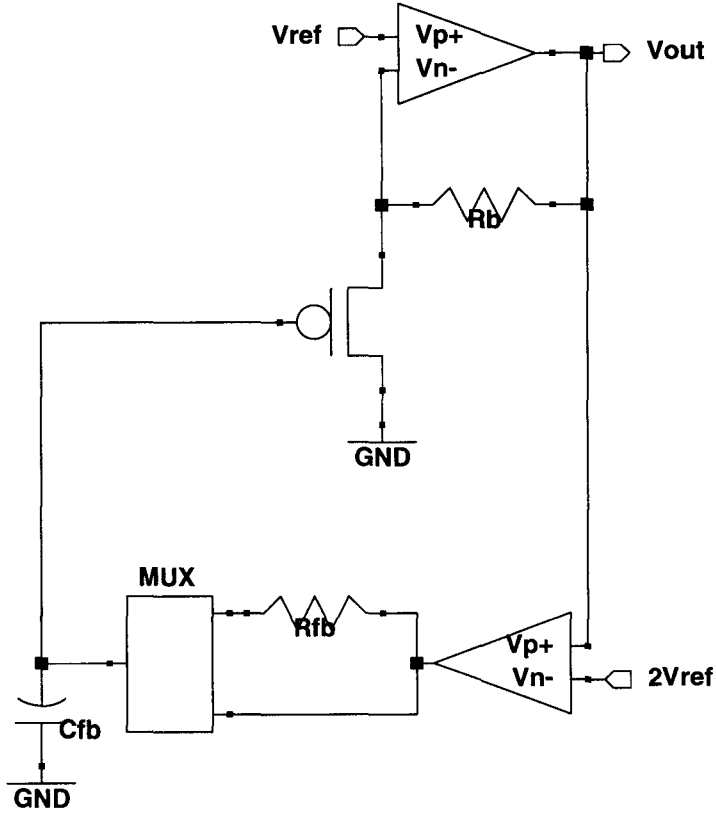


Figure 4.2: Schematic of the discrete adaptive circuit

where V_{ref} is the voltage at the noninverting terminal, R_b is the baseline sensor resistance, and R_{PMOS} is the effective PMOS resistance. This noninverting amplifier configuration forms the forward part of the adaptive circuit.

Then taking the MUX, the feedback resistor and capacitor out of consideration, we can identify that the bottom op-amp² and PMOS transistor form the feedback part of the adaptive circuit. Op-amp 2 basically serves as a comparator. If $R_b > R_{PMOS}$, according to 4.1, $V_{out} > 2V_{ref}$, so the output of op-amp 2 goes up. Since the gate of the PMOS is biased by the output of op-amp 2, the effective PMOS resistance R_{PMOS} is raised. A negative feedback loop is then formed. The circuit does not reach steady state until $R_{PMOS} = R_b$. For the same reason, if $R_b < R_{PMOS}$, according to 4.1, $V_{out} < 2V_{ref}$, so op-amp 2 outputs low, R_{PMOS} decreases until $R_{PMOS} = R_b$.

²op-amp 2

Now taking the MUX, feedback resistor and capacitor back into analysis: When the circuit is in adaption mode, the bottom pathway of the MUX is connected while the upper pathway is left open. The output of op-amp 2 charges the feedback capacitor and changes the PMOS effective resistance R_{PMOS} quickly. The gate voltage that biases the PMOS to cause $R_{PMOS} = R_b$ is stored in the feedback capacitor. The adaption is done because the output voltage V_{out} has been adapted to the preset voltage V_{ref} . When the circuit is in sensing mode, the bottom pathway of the MUX is open while the upper pathway is connected. The output of op-amp 2 charges the feedback capacitor through the huge feedback resistor according to the large time constant. In our case the resistor is $10M\Omega$ and the capacitor is $47\mu F$. So the time constant is 470 seconds! Thus, in sensing mode the adaptive circuit responds to quick sensor resistance changes but tunes out changes on a long time scale.

A simple RC high pass filter is constructed following the adaptive circuit to extract the sensor signal. The corner frequency is set to 1Hz, since we are only interested in quick signal changes. According to equation 4.1, when there is a slight increase at the sensor resistance ΔR_b , the output voltage becomes

$$V_{out} = V_{ref} \left(1 + \frac{R_b + \Delta R_b}{R_{PMOS}} \right) = V_{ref} \left(1 + \frac{R_b}{R_{PMOS}} \right) + V_{ref} \frac{\Delta R_b}{R_{PMOS}}$$

And remember $R_b = R_{PMOS}$ after adaption, so the output voltage can be rewritten as

$$V_{out} = 2V_{ref} + V_{ref} \frac{\Delta R_b}{R_b}$$

Since $2V_{ref}$ is a DC voltage, the output of the high pass filter would be

$$V_{ref} \frac{\Delta R_b}{R_b}$$

So the output contains the $\Delta R_b/R_b$ information we want. The circuit is tested to work for baseline resistance ranging from $10k\Omega$ to $1M\Omega$. 1% resistance changes can be detected.

4.1.3 Digital adaptive circuit

The second generation of the adaptive circuit is a digital adaptive circuit implemented in VLSI. Figure 4.3 shows the schematic. The circuit is constructed by several parts: an up/down counter, a current output digital to analog converter (DAC), two amplifiers, and a control clock generator.

The up/down counter together with the DAC can be viewed as a controllable constant current source. The counter outputs an 8-bit digital word, and this digital word controls the current output

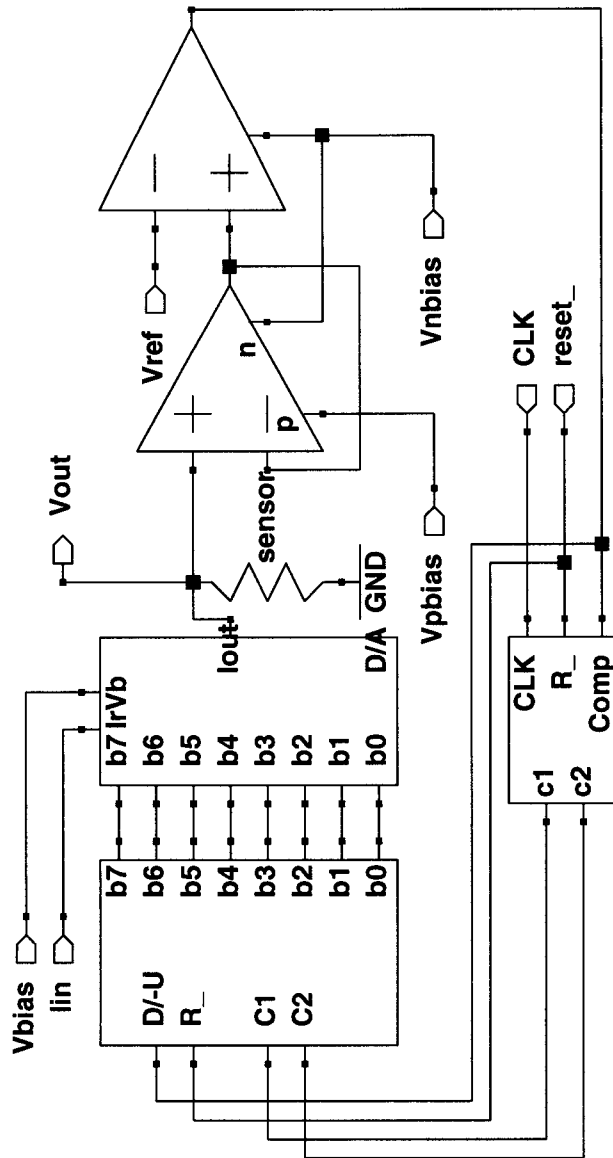


Figure 4.3: Schematic of the digital adaptive circuit

of DAC. When the output of the counter goes up, the output current goes up correspondingly. Therefore, by adjusting the output of the up/down counter, the current output can be controlled. The output current is used to bias the sensor and output the sensor voltage V_{out} . V_{out} is then compared to a reference voltage V_{ref} by a comparator through the use of a follower, and outputs a signal *comp*.

Another important circuit block is the control clock generator at the bottom of the figure. It has three inputs, *clock*, *reset*, *comp*, and two outputs *c1* and *c2*. The function of the clock generator is to generate two nonoverlapping clock signals for the counter. At startup, *comp* is low, *c1* and *c2* have the same frequency as the input *clock*. Once *comp* goes high, *c1* and *c2* are reduced to 256 times slower, no matter whether *comp* is high or low in the future.

The way to reduce the output clock frequency is to have another 8-bit counter for frequency reduction and a register for memorizing the status. When *comp* is low at the startup, the output of register is low, and the original clock is sent to a standard clock generator circuit. Once *comp* becomes high, the register outputs high and stays there no matter what value *comp* is in the future, the original clock is sent to the counter and the most significant bit is used as clock for the standard clock generator and slower *c1* and *c2* are generated.

At startup, the counters are reset, so the output of the counter is 00000000. The DAC outputs zero current, thus the sensor voltage V_{out} is close to GND, and the output of comparator *comp* is low. Notice that *comp* is also used to control the counter to count up or down. Since *comp* is low, the up/down counter is set to count up with the original clock. This is the adaption mode of the circuit. As the output of counter goes up, the output current of current source goes up as well. At some point when $V_{out} > V_{ref}$, *comp* goes high and reduces the clock frequency for the up/down counter. The circuit enters its sensing mode. In the sensing mode, if V_{out} is larger than V_{ref} , *comp* is high, the counter counts down, the output of DAC goes down, and V_{out} goes back toward V_{ref} . The counter keeps counting down until $V_{out} < V_{ref}$, then *comp* goes low again, causing the counter to count up until $V_{out} > V_{ref}$. The circuit would only respond to quick changes.

The circuit has been implemented and tested. It works for sensor resistance ranging from 10k Ω to 1M Ω . Resistance change about 0.5% can be detected.

One can soon realize that one of the biggest disadvantage of the digital adaptive circuit is the cost of space, especially the two counters and the digital-to-analog converter. An alternative way is to implement analog electronics for the adaption task.

4.1.4 First analog adaptive circuit

The cost of chip area in the digital adaptive circuit is mainly due to the up/down counter and the digital-to-analog converter. Realizing that the function of the counter and DAC is to implement a controllable constant current source, we can replace it by a simple PMOS transistor. By doing this we transform the adaptive circuit from digital to analog. This is the third generation of our adaptive circuit.

Circuit description

Figure 4.4 displays the schematic of the first analog adaptive circuit we built in VLSI. A PMOS transistor serves as a controllable constant current source that outputs a current to bias the sensor. Then sensor voltage is compared with a given voltage V_{ref} by the comparator. The output of the comparator is sent to a feedback capacitor through an NMOS switch. The switch turns on (low impedance) in the adaption mode, forms a negative feedback loop with a small time constant, and adapts the sensor voltage to be the same as the reference voltage V_{ref} . In the sensing mode, the switch turns off (high impedance), a negative feedback loop with a large time constant is formed to tune out the environment background, and now circuit responds to quick changes.

The analog adaptive circuit is very similar to the discrete and digital adaptive circuits in some phases. As mentioned earlier, the PMOS transistor functions as the combination of the up/down counter and digital-to-analog converter in the digital adaptive circuit. Moreover, the switch together with the feedback capacitor works as the multiplexer and feedback capacitor and resistor in the discrete adaptive circuit.

The greatest advantage for the analog adaptive circuit is its usage of chip area can be so compact and small. Since there will be an array of sensors at the front end of the electronic nose chip, the space cost by the sensor stage should be as small as possible, since there will be one sensor stage for each single sensor. Analog adaptive circuit certainly serves one of the best solutions in terms of chip area.

Performance and analysis

Figure 4.5 shows the ability for the first analog adaptive circuit to adapt the sensor voltage to V_{ref} by sweeping V_{ref} from 0V to 5V while measuring the sensor voltage. In the figure we can see the adaption works from $0.1V < V_{ref} < 3.5V$. So two boundaries are observed for the first analog adaptive circuit.

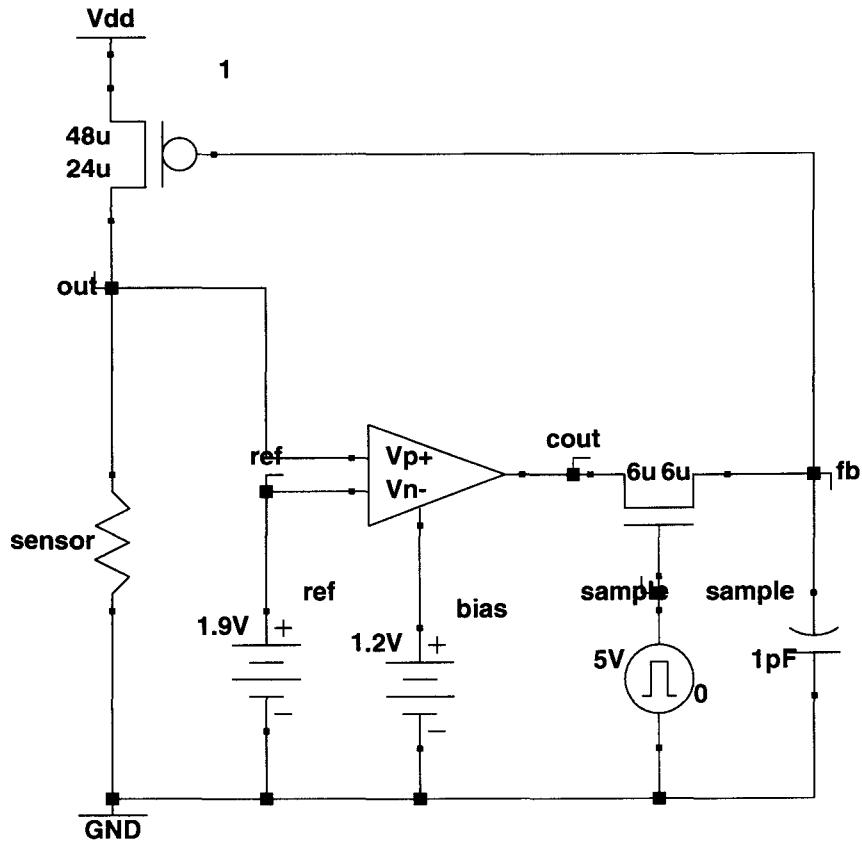


Figure 4.4: Schematic of the first analog adaptive circuit

The upper boundary is caused by the maximum output of the current source PMOS transistor. A PMOS transistor outputs its maximum output current when its gate is applied by the most negative voltage, i.e., 0V in our case. When the current output reaches its maximum value, the sensor voltage remains at that value times the resistance. If the reference voltage goes even higher, the comparator output stays zero, and the current cannot go higher. This is the upper boundary of the adaptive circuit.

As the upper boundary, the source of the lower boundary is the minimum output current of the PMOS transistor. Ideally the minimum current should be zero, when the voltage applied to the gate is V_{dd} . But since the ability of a NMOS transistor to pass high voltage is poor, V_{fb} cannot really go rail to rail. Thus a small current still flows out from the PMOS current source, and results in the

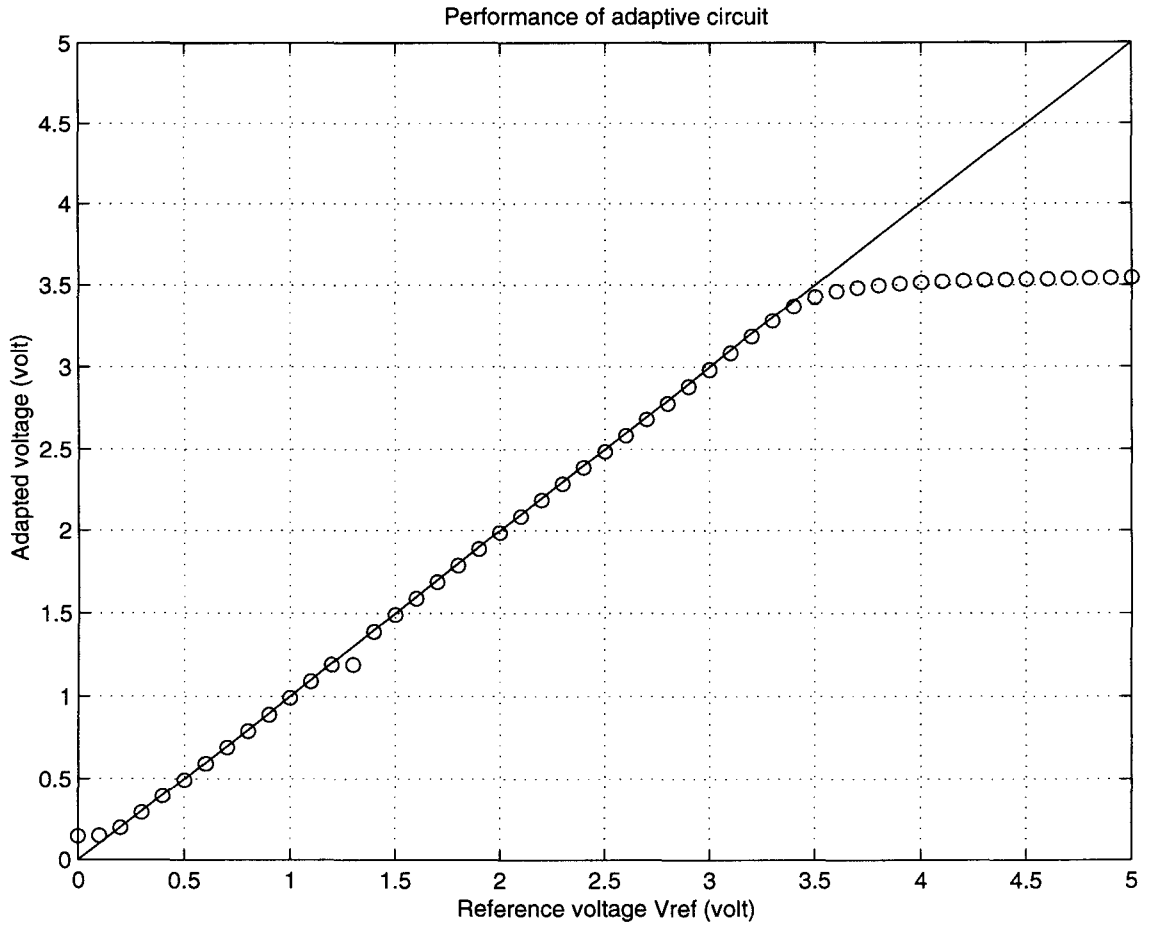


Figure 4.5: Performance of the first analog adaptive circuit

lower boundary of the adaptive circuit.

For purposes we will see later in this chapter, the sensor is biased so that the sensor voltage is 2V, i.e., we set the baseline at 2V. This falls almost at the center of the working range. So the first analog adaptive circuit is well-suited for the job so far.

Although the first analog adaptive circuit works very well in terms of the ability to adapt the sensor voltage to the baseline we need, a severe drawback is noticed. When the circuit works in the sensing mode, the switch is off, and the capacitor is supposed to hold the voltage that controls the current source. But in the real case the capacitor discharges as time goes on, so the voltage on the capacitor decreases. Since the voltage across the feedback capacitor is used to control the current source, the output current from PMOS and the sensor voltage increase as the gate voltage decreases without the presence of odors. This is apparently a severe drawback that needed an immediate

solution.

The main source of the voltage discharge on the feedback capacitor is the leakage current of the NMOS switch when the switch is turned off. By using a PMOS switch instead of NMOS the leakage current should be reduced. Also the switch is made small to reduce the effect of charge injection. Moreover, since the PMOS current source displays exponential (sub-threshold) or square (above-threshold) relationship between source current and gate voltage, a slight variation at the gate would result in huge difference of the source current. A way to reduce the "sensitivity" of the current source is to implement a current source that has a linear gate voltage vs. source current relationship. A temperature-insensitive voltage-to-current converter is one of the options[60].

4.1.5 Improved analog adaptive circuit

To eliminate the discharging problem which occurred in the first analog adaptive circuit, a PMOS switch is used to reduce the leakage current instead of NMOS switch, and a linear voltage to current source is used instead of the simple PMOS transistor. This improved analog adaptive circuit is the fourth generation of the adaptive circuit.

Circuit description

Figure 4.6 shows the schematic of the improved adaptive circuit. The sensor is biased by a linear V/I source formed by two PMOS transistors M_1, M_2 and two NMOS transistors M_3, M_4 . M_1, M_2 form a standard current mirror, and M_3, M_4 provide a linear voltage to current relationship as the following:

For a standard NMOS transistor, the relationship between the drain current and the gate voltage, ignoring the channel length modulation effect, can be stated as:

$$I_d = \begin{cases} K(V_{GS} - V_t)^2 & \text{if } V_{DS} > V_{GS} - V_t \\ 2K \left[(V_{GS} - V_t)V_{DS} - \frac{V_{DS}^2}{2} \right] & \text{if } V_{DS} < V_{GS} - V_t \end{cases}$$

where I_d is the drain current, V_{GS} is the gate-source voltage, V_{DS} is the drain-source voltage, and V_t is the threshold voltage of NMOS. Both equations apply only when $V_{GS} > V_t$. When $V_{GS} < V_t$, I_d is considered zero, as we neglect subthreshold region.

For transistor M_3 , since its gate and drain are connected, $V_{D3} = V_{G3}$, the transistor sources a current as long as its gate voltage exceeds threshold voltage. So for a working linear V/I current source,

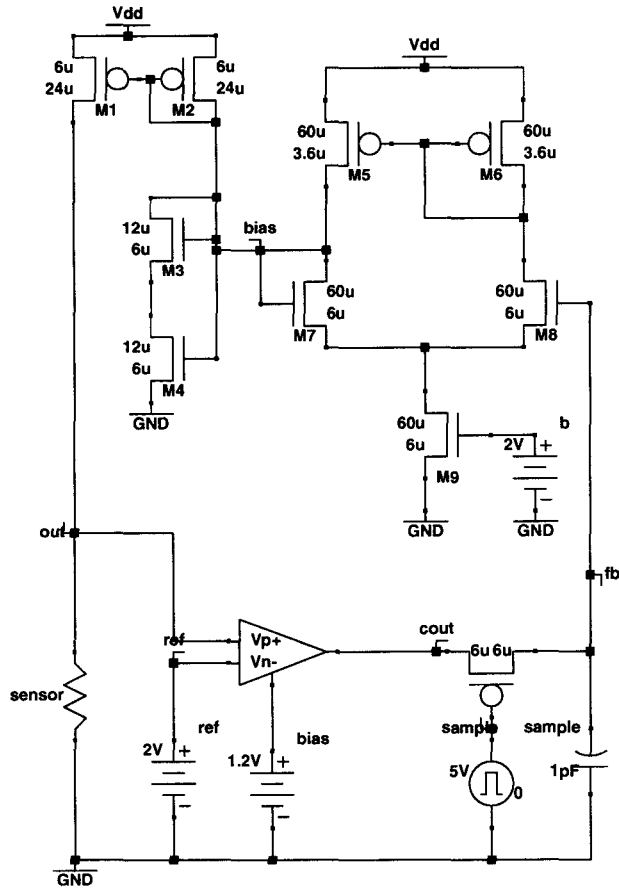


Figure 4.6: Schematic of the improved analog adaptive circuit

$$V_{G3} - V_{S3} > V_t \quad (4.2)$$

Equation 4.2 can be rearranged as

$$V_{S3} < V_{G3} - V_t \quad (4.3)$$

From transistor M_4 , since its gate is connected to the gate of transistor M_3 , and its drain is connected to the source of M_3 , equation 4.3 can be rewritten as

$$V_{D4} < V_{G4} - V_t \quad (4.4)$$

According to equations above, the output drain current I_{d4} should have a linear relationship with

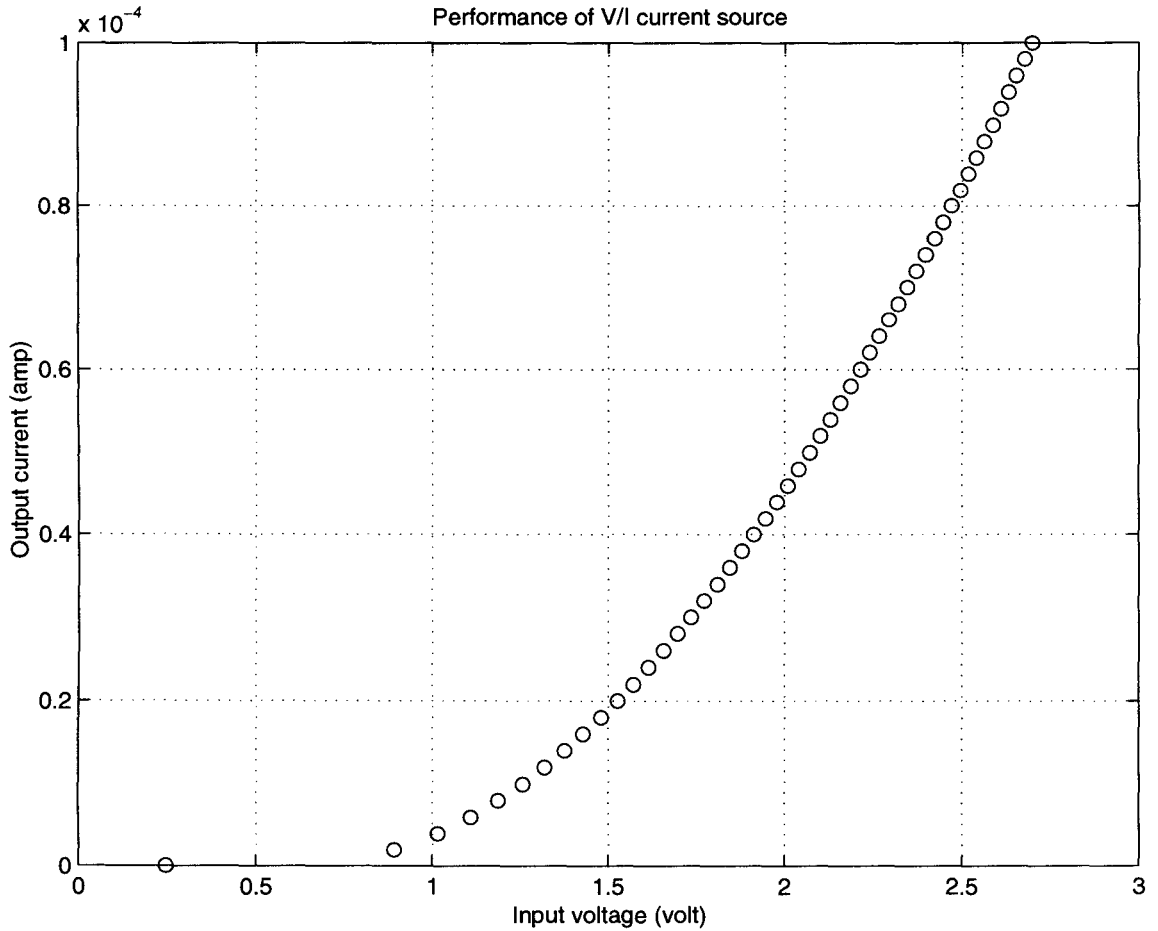


Figure 4.7: Performance of the linear V/I current source

the gate voltage V_{G4} that is applied. Since $I_{d3} = I_{d4}$, and $V_{G3} = V_{G4}$, transistors M_3 and M_4 form a linear V/I current source.

Figure 4.7 shows performance of the linear V/I current source. The linear V/I current source turns on when its input voltage $V_{in} = V_{G3} = V_{G4}$ is greater than the transistor threshold voltage V_t , which is approximately 0.8V. From the figure we can see a linear relationship with a little deviation. To analyze the deviation first rewrite the transistor equation to be

$$I_{out} = 2KV_{D4}V_{in} - 2KV_tV_{D4} - KV_{D4}^2 \quad (4.5)$$

From equation 4.5 the output current of the linear V/I source has a linear dependence with its input voltage as long as V_{D4} and V_t are constants. V_t is the threshold voltage of transistor and is a process dependent constant, so the source of deviation comes from V_{D4} not being a constant.

Notice the drain current of M_3 and M_4 are the same, from transistor M_3 we can write down another equation:

$$I_{out} = K(V_{in} - V_{D4} - V_t)^2 \quad (4.6)$$

So combine equation 4.5 and 4.6 we can write down

$$\begin{aligned} I_{out} &= 2KV_{D4}V_{in} - 2KV_tV_{D4} - KV_{D4}^2 \\ &= K(V_{in} - V_{D4} - V_t)^2 \\ &= KV_{in}^2 + KV_{D4}^2 + KV_t^2 - 2KV_{D4}V_{in} - 2KV_tV_{in} + 2KV_tV_{D4} \end{aligned} \quad (4.7)$$

Arrange equation 4.7 we can obtain the relationship between V_{D4} and V_{in} to be

$$2V_{D4}^2 + (4V_t - 4V_{in})V_{D4} + (V_{in} - V_t)^2 = 0 \quad (4.8)$$

By solving equation 4.8 the dependence of V_{D4} on V_{in} can be written down as

$$V_{D4} = \frac{2 \pm \sqrt{2}}{2}(V_{in} - V_t)$$

For transistor M_3 to turn on, its gate-source voltage needs to be larger than the threshold voltage.

If $V_{D4} = \frac{2+\sqrt{2}}{2}(V_{in} - V_t)$, the gate-source voltage of M_3 is

$$\begin{aligned} V_{GS3} &= V_{in} - V_{D4} \\ &= V_{in} - \frac{2 + \sqrt{2}}{2}(V_{in} - V_t) \\ &= -\frac{1}{\sqrt{2}}V_{in} + \left(1 + \frac{1}{\sqrt{2}}\right)V_t \end{aligned}$$

To compare V_{GS3} and V_t , we simply subtract the threshold voltage from V_{GS3} we get

$$\begin{aligned} V_{GS3} - V_t &= -\frac{1}{\sqrt{2}}V_{in} + \left(1 + \frac{1}{\sqrt{2}}\right)V_t - V_t \\ &= -\frac{1}{\sqrt{2}}(V_{in} - V_t) \end{aligned}$$

For transistor M_4 to turn on, $V_{in} - V_t > 0$. So we can conclude that

$$V_{GS3} - V_t = -\frac{1}{\sqrt{2}}(V_{in} - V_t) < 0$$

So we can conclude that $V_{D4} = \frac{2+\sqrt{2}}{2}(V_{in} - V_t)$ can not be the solution. To examine the other solution $V_{D4} = \frac{2-\sqrt{2}}{2}(V_{in} - V_t)$, first we check transistor M_3

$$\begin{aligned} V_{GS3} - V_t &= V_{in} - \frac{2-\sqrt{2}}{2}(V_{in} - V_t) - V_t \\ &= \frac{1}{\sqrt{2}}(V_{in} - V_t) > 0 \end{aligned}$$

So transistor M_3 is turned on. Also compare V_{DS4} and V_{GS4} :

$$\begin{aligned} V_{DS4} - (V_{GS4} - V_t) &= \frac{2-\sqrt{2}}{2}(V_{in} - V_t) - (V_{in} - V_t) \\ &= -\frac{1}{\sqrt{2}}(V_{in} - V_t) < 0 \end{aligned}$$

So transistor M_4 is in the triode region. Notice that V_{D4} is a function of the input voltage V_{in} , according to equation 4.5, the output current of the linear V/I current source is not a pure linear function of V_{in} . This is the source of deviation for the linear V/I current source. But remember the reason we need a linear V/I current source is to reduce the dependence of the feedback voltage on the feedback capacitor to the current source from exponential or square to a lower dependence. So the current source does reduce the dependence.

A problem appears that, to form a negative feedback loop, the current source output needs to decrease when its input control voltage increases, and vice versa. The linear V/I current source we just analyzed actually works the other way³. Moreover, the voltage on the feedback capacitor cannot apply to the current source input directly, since it is not a high impedance node. To overcome these problems we insert a simple five-transistor transconductance amplifier between the feedback capacitor and the inverse linear V/I current source.

To analyze the circuit, first rewrite the transistor equation to be

$$I_d = \alpha V_{GS} - \beta \quad (4.9)$$

where $\alpha = 2KV_{DS}$, $\beta = 2KV_tV_{DS} + KV_{DS}^2$. Since V_{DS4} in the inverse linear V/I current source changes only slightly, first assume α and β as constants. Moreover, for a transconductance amplifier,

$$I_{out} = G_m(V_+ - V_-) \quad (4.10)$$

³So we call it "inverse" linear V/I current source.

where G_m is the transconductance of the amplifier, V_+ is the noninverting input voltage and V_- is the inverting input voltage.

Given V_{in} as the gate voltage of M_8 , the input voltage at the noninverting terminal of the transconductance amplifier, and V_G as the input voltage for the inverse linear V/I current source, we can write down by KCL

$$I_p + G_m(V_{in} - V_G) = \alpha V_G - \beta \quad (4.11)$$

where I_p is the input current I_{d2} of the PMOS current mirror. By rearranging the equation

$$I_p = (\alpha + G_m)V_G - \beta - G_m V_{in} \quad (4.12)$$

Also we can obtain the relationship between I_p and V_G through the PMOS transistor

$$I_p = K_p(V_{dd} - V_G - |V_{tp}|)^2 \quad (4.13)$$

Hence we can write down the relationship between I_p and V_G according to equation 4.13

$$V_G = V_{dd} - |V_{tp}| - \sqrt{\frac{I_p}{K_p}} \quad (4.14)$$

Substitute equation 4.14 into equation 4.12

$$I_p = (\alpha + G_m)(V_{dd} - |V_{tp}| - \sqrt{\frac{I_p}{K_p}}) - \beta - G_m V_{in} \quad (4.15)$$

Finally, we can get the expression showing the relationship between the input voltage V_{in} and the output current I_p as

$$I_p + \epsilon\sqrt{I_p} = \gamma - G_m V_{in} \quad (4.16)$$

where*

$$\epsilon = \frac{\alpha + G_m}{\sqrt{K_p}}$$

$$\gamma = (\alpha + G_m)(V_{dd} - |V_{tp}|) - \beta$$

From equation 4.15 I_p is linearly dependent on V_{in} when $I_p \gg \epsilon\sqrt{I_p}$, i.e., $I_p \gg \epsilon^2$. As long as this criteria is met, the desired linear V/I current source is obtained.

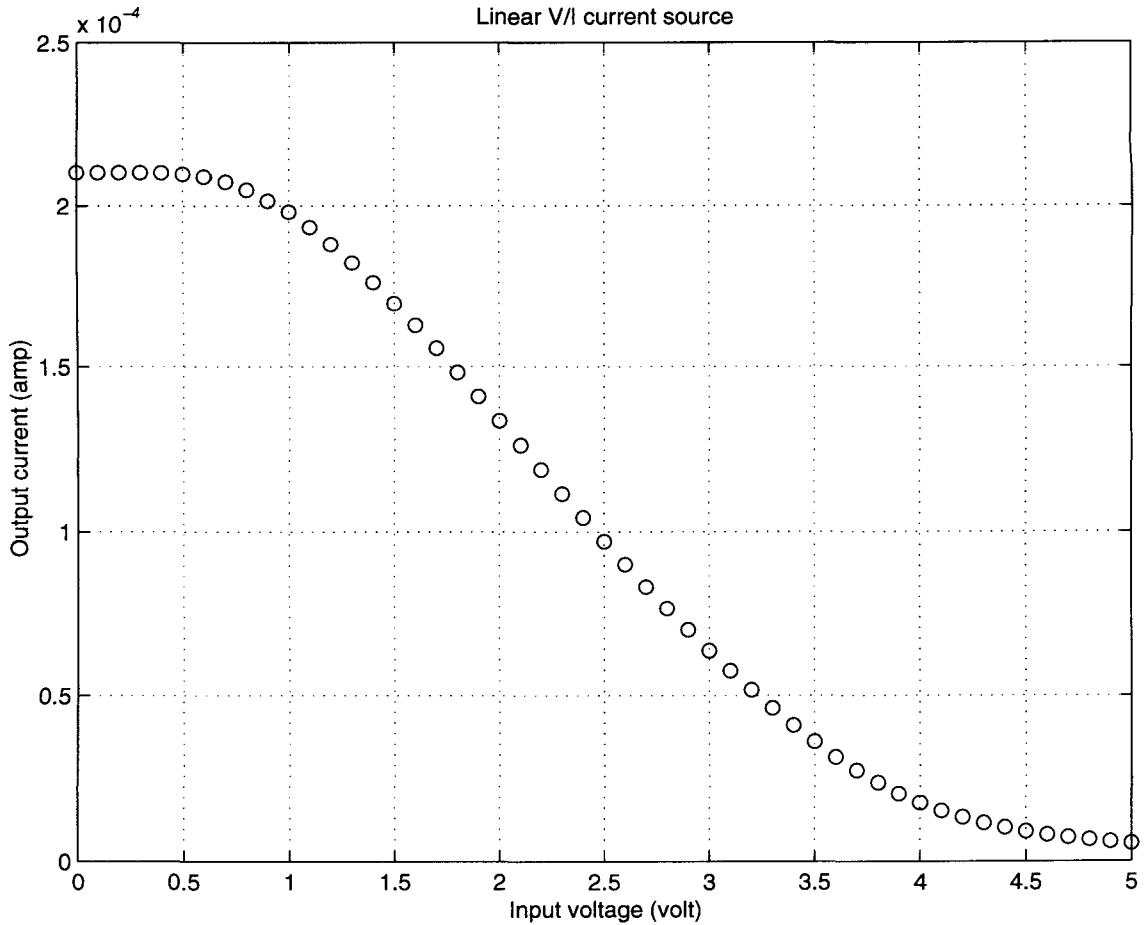


Figure 4.8: Output performance of linear V/I current source

Sensor voltage is obtained by connecting the current output to the sensor. The sensor voltage is then applied to the comparator to compare with reference voltage V_{ref} . The output charges the feedback capacitor through a PMOS switch instead of NMOS to reduce the leakage current caused by NMOS switch.

Performance and analysis

Figure 4.8 shows the performance of the linear V/I current source. The circuit shows good linearity when the input voltage is between 1V and 3.5V. The output current decreases when the input voltage increases, as we expected. The output current clips at both end, ranging from 5uA to 210uA. The maximum output current happens when the input voltage of the inverse linear V/I current source reaches zero. In this condition $V_{G1} = V_{G3} = V_{G4} = 0$, M_3 and M_4 are off, so there is no current flowing in the linear V/I current source. I_{d1} reaches its maximum value since V_{G1} is GND. This is the source of the upper clipping boundary. The output current starts decreasing as currents start

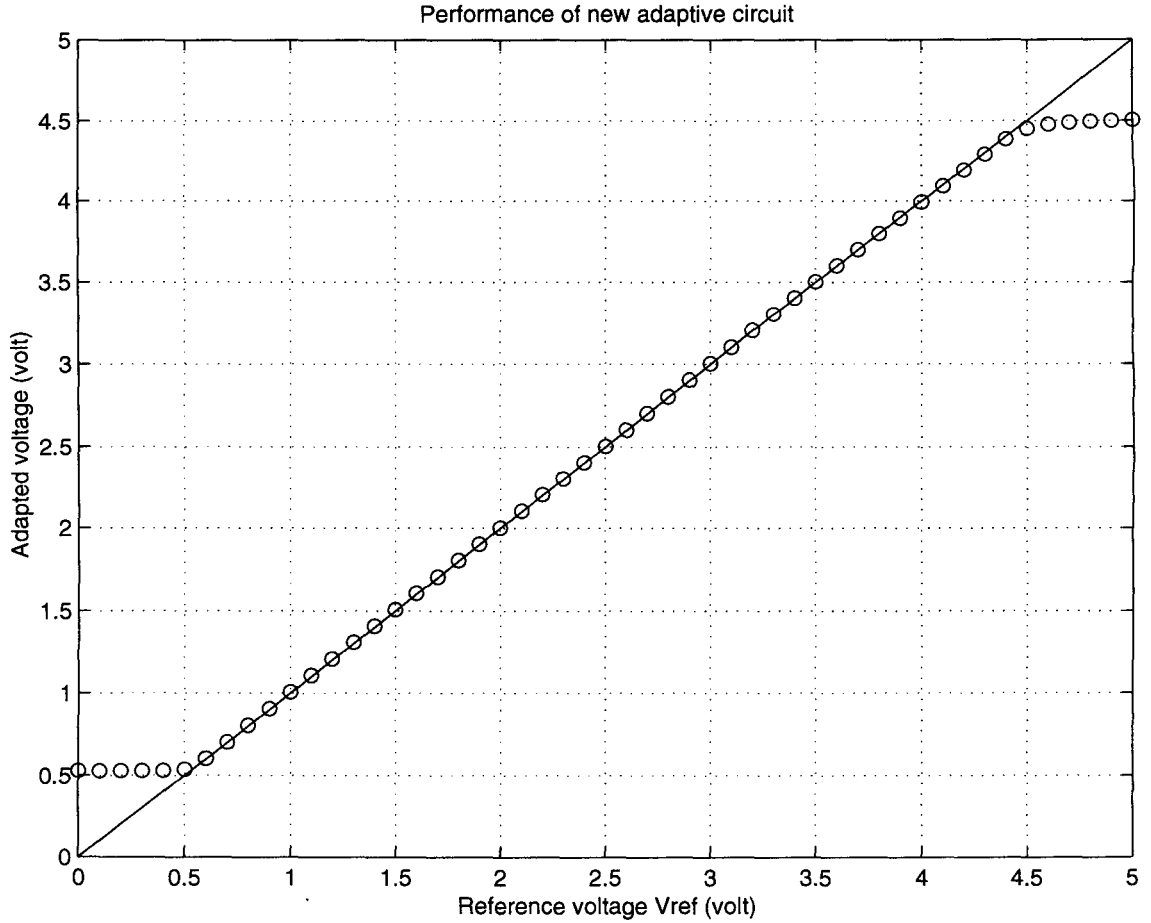


Figure 4.9: Performance of improved analog adaptive circuit

to flow in transistors M_3 and M_4 .

The lower clipping boundary of the linear V/I current source happens when the input voltage of the inverse linear V/I current source, V_G , biases the transistors M_3 and M_4 so that the current flowing through the transistors I_{d3} is almost equal to the output current I_{out} from the transconductance amplifier. Since $I_p = I_{d3} - I_{out}$, when $I_{d3} \approx I_{out}$, I_p is very small, resulting in the lower clipping boundary of the current source.

Since the reference voltage is set to 2V, the sensor resistance the circuit can adapt ranges from 10k Ω to 400k Ω . Although it seems that adaptability of the range of resistance is decreased, the overall performance is improved because the effect of leakage of the feedback capacitor decreases dramatically by changing the current source.

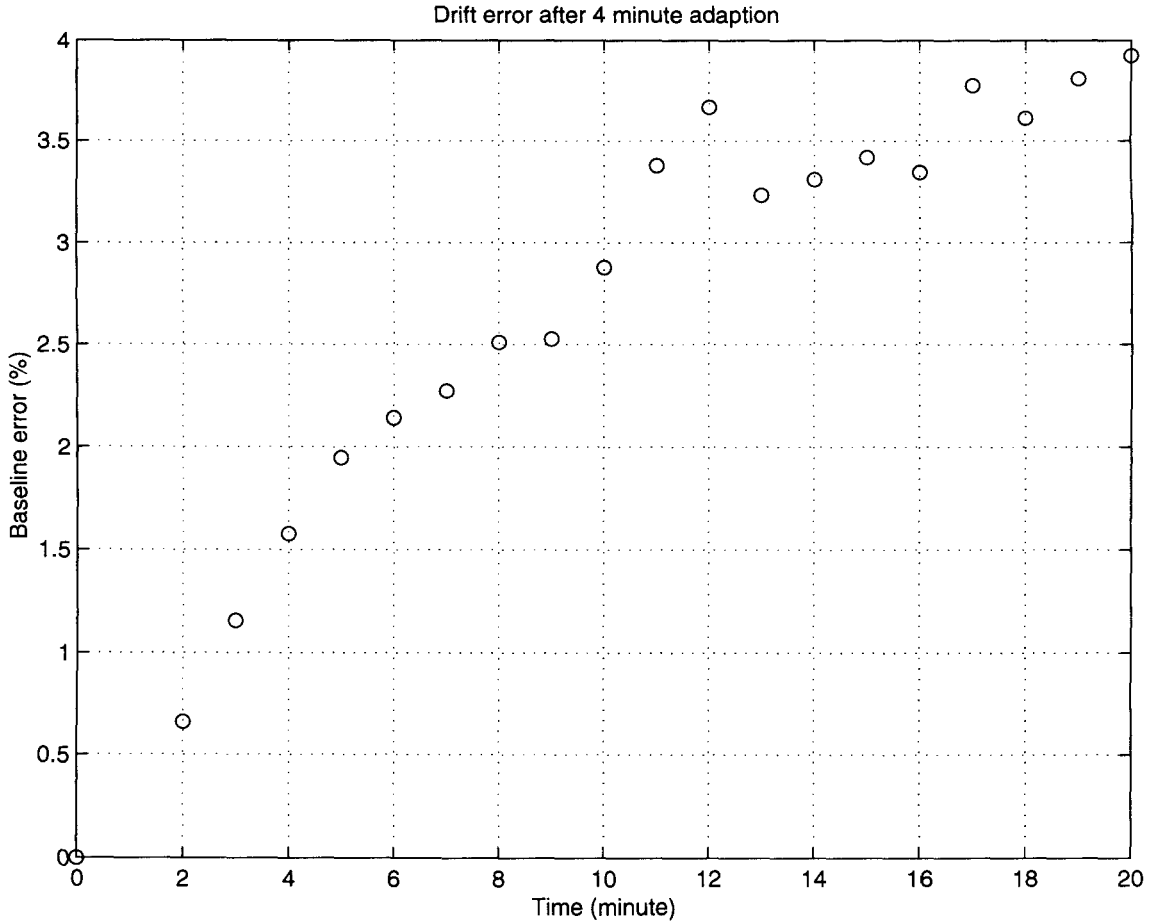


Figure 4.10: Drift of the sensor voltage

Figure 4.9 shows the adaptability of the improved analog adaptive circuit. The circuit is able to adapt the sensor voltage from 0.5V to 4.5V. The upper bound and lower bound are due to the maximum and minimum output currents from the current source. In our application we usually adapt the sensor voltage to 2V, which sits right at the middle of the working range. Therefore the circuit works properly for our requirements.

Figure 4.10 shows baseline drift after turning off the adaption switch. The main source of the baseline drift is the leakage current from the switch, I_{leak} . To analyze the dependence between the leakage current and the baseline drift, first note the feedback capacitor,

$$I_{leak} = C_{fb} \frac{dV_{fb}}{dt} \quad (4.17)$$

According to Figure 4.8, the voltage change on the feedback capacitor results in a current change

from the current source. So

$$\frac{dI_{out}}{dt} = f\left(\frac{dV_{fb}}{dt}\right) = f\left(\frac{I_{leak}}{C_{fb}}\right) \quad (4.18)$$

where $f(\cdot)$ can be determined from equation 4.15. So the baseline drift can be found as

$$\frac{dV_{drift}}{dt} = \frac{dI_{out}}{dt} R_{sensor} = f\left(\frac{I_{leak}}{C_{fb}}\right) R_{sensor} \quad (4.19)$$

From equation 4.19 the relationship between switch leakage current and baseline is stated. The larger the leakage current is, the more serious the baseline deviation is. Less than 4% deviation from the baseline in 20 minutes is observed after 4 minutes adaption. This is pretty good for the purpose of our circuit.

4.1.6 Summary

Table 4.1 summarizes the four generation of adaptive circuits that have been developed and tested. All adaptive circuits show good adaptability to the preset baseline voltage. The discrete adaptive circuit, of course, costs a large amount of space for the electronics. The digital adaptive circuit uses a large amount of chip area. The first analog adaptive circuit saves chip area but still has a drawback because of its severe baseline drift. The improved analog adaptive circuit resolves the baseline drift problem significantly at the cost of a little more chip area than the first analog adaptive circuit.

4.2 Peak detector

The signal voltage is defined as the maximum voltage change when an odor is applied to the sensor. In other words, the signal voltage is the maximum sensor voltage minus the baseline sensor voltage. The analog adaptive circuit has been built to adapt the sensor to some baseline voltage in the adaption mode, then read the sensor voltage using a constant current source in the sensing mode. In order to obtain the signal voltage, a circuit that can extract the maximum sensor voltage is needed.

The peak detector basically traces its input voltage to its maximum value and stays at the value. So the sensor voltage coming from the analog adaptive circuit is sent to the peak detector as its

Adaptive circuit	Performance	Advantage and Disadvantage
Discrete adaptive circuit	10k Ω to 1M Ω	Big space (discrete)
Digital adaptive circuit	10k Ω to 1M Ω	Big chip area
First analog adaptive circuit	10k Ω to 10M Ω	Small chip area and severe baseline drift
Improved analog adaptive circuit	10k Ω to 400k Ω	Small chip area and low baseline drift

Table 4.1: Summary of adaptive circuits

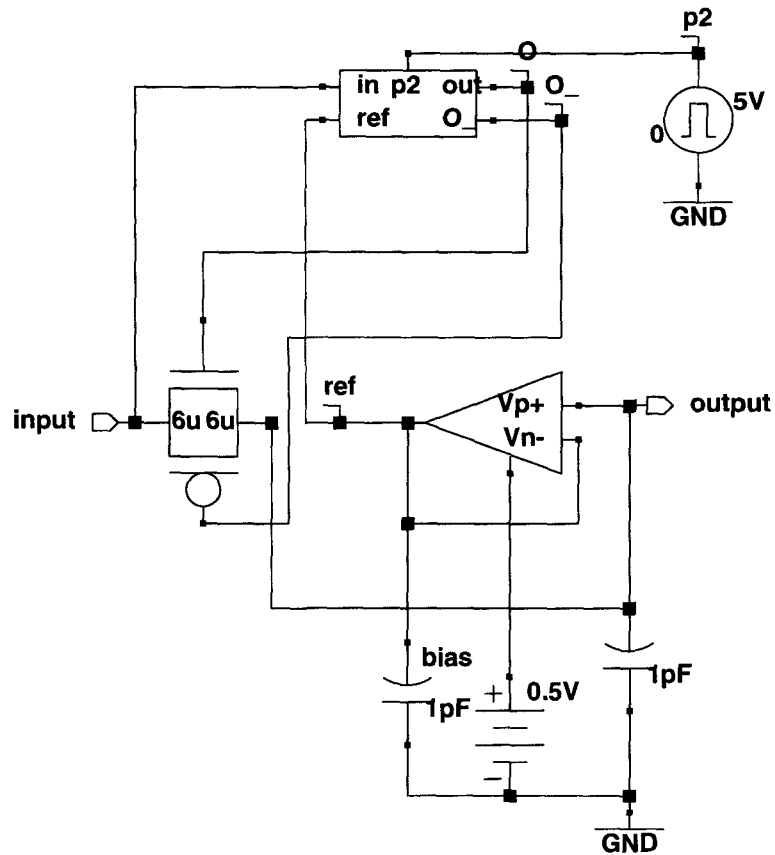


Figure 4.11: Schematic of the peak detector circuit

input. The peak detector outputs the maximum sensor voltage to the transconductance amplifier. Figure 4.11 shows the schematic of the peak detector.

4.2.1 Circuit description

A peak detector is designed to extract the maximum value of an input signal. This is done by tracing the input signal to its maximum value then maintaining that value. So a comparator is needed to decide if the peak detector needs to "trace" the input signal or not. Unlike the traditional comparator, a latched comparator is used to maintain the speed as well as ensuring that the comparator output is either high or low.

The peak detector is composed of a regenerative latch, a CMOS transmission gate, a buffer and

two capacitors. The input of the regenerative latch $V_{in,latch}$ is connected to the signal input, while the reference voltage $V_{ref,latch}$ of the regenerative latch is connected to the output of buffer, whose input is the voltage of the output capacitor.

A schematic of the regenerative latch is shown in Figure 4.12. It has two compliment outputs, out and \overline{out} . out and \overline{out} together serve the control signal for the CMOS transmission gate. It works as a comparator when $p2$ is high. Thus, out is high and \overline{out} is low as long as $V_{in,latch} > V_{ref,latch}$ when pulse $p2$ is high, while out is low and \overline{out} is high as long as $V_{in,latch} < V_{ref,latch}$. On the other hand, when $p2$ is low, because of the SR flip-flop at the output of the latch, the output remains at the same value as long as power is on.

The performance of the regenerative latch is shown in Figure 4.13. The reference voltage $V_{ref,latch}$ is set at 2.5V(4). The input voltage $V_{in,latch}$ is an $1V_{p-p}$ sine wave with 2.5V DC bias(2). Input pulse $p2$ (1) and latch output out (3) are also shown in the figure. When $p2$ is high, the latch works as a comparator, and out is high or low if $V_{in,latch}$ is larger or smaller than $V_{ref,latch}$. When $p2$ goes low, out remains until the next time $p2$ raises.

One thing we should pay attention to is the limit of the regenerative latch. Notice M_1 and M_4 are in diode connected configuration and their gates and drains are connected to each other. So M_1 and M_4 are working in the saturation region. Neglecting channel-length modulation effects we can write down their equations:

$$\begin{aligned} I_{d1} &= K_n(V_{G1} - V_{tn})^2 \\ I_{d4} &= K_p(V_{dd} - V_{G4} - |V_{tp}|)^2 \end{aligned}$$

Also notice that $I_{d1} = I_{d4}$, we can rewrite the above equation to be

$$K_n(V_{G1} - V_{tn})^2 = K_p(V_{dd} - V_{G4} - |V_{tp}|)^2$$

Assume that $K_n = K_p$, and also notice that $V_{G1} = V_{G4} = V_G$ we can obtain

$$\begin{aligned} V_G - V_{tn} &= V_{dd} - V_G - |V_{tp}| \\ \Rightarrow V_G &= \frac{V_{dd} - |V_{tp}| + V_{tn}}{2} \end{aligned} \tag{4.20}$$

For convenience, we assume that $V_{tn} = |V_{tp}| = V_t$, from equation 4.20 $V_G = V_{dd}/2$. So $V_{G5} =$

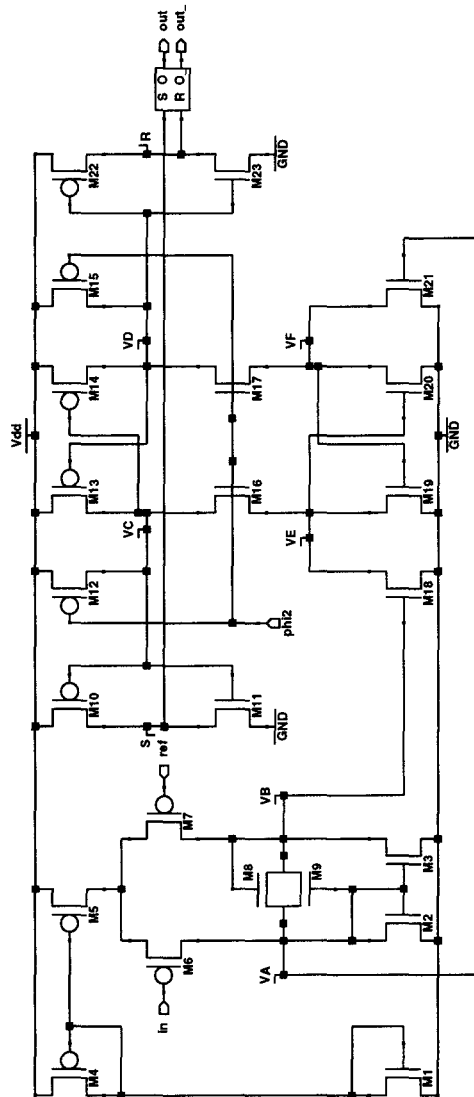


Figure 4.12: Schematic of regenerative latch

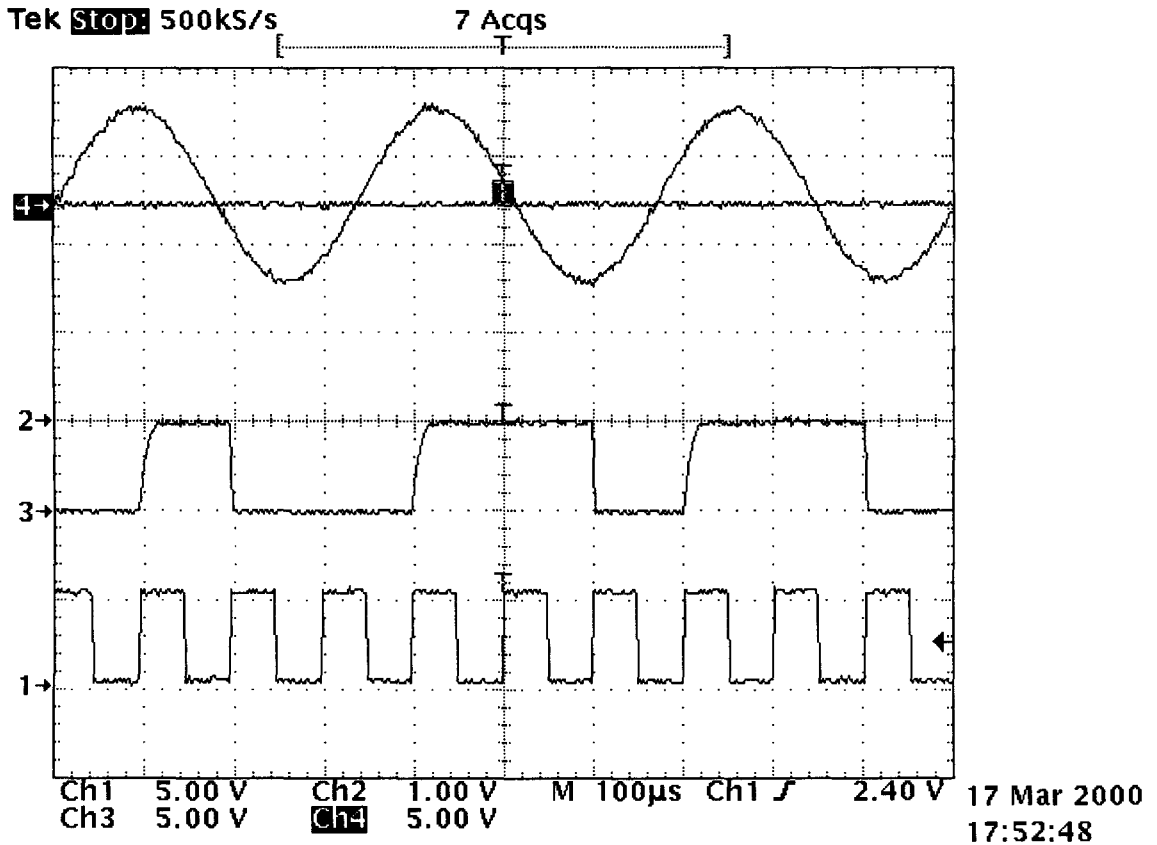


Figure 4.13: Performance of regenerative latch

$V_{D5}/2$. V_{D5} is decided by the two input voltages, V_{in} and V_{ref} . The transistor associated with the smaller input voltage takes all the current from M_5 , while turning off the other transistor. For example, if V_{ref} is smaller than V_{in} , M_7 takes all the current from M_5 and M_6 is turned off. Therefore, $V_{Dd} - V_{G5} = V_{D5} - V_{ref}$. Remember that $V_{G5} = V_{Dd}/2$,

$$V_{D5} = V_{ref} + \frac{V_{Dd}}{2} \quad (4.21)$$

The regenerative latch starts deviating from its normal function when M_5 leaves its saturation region, i.e.,

$$\begin{aligned}
V_{dd} - V_{G5} - |V_{tp}| &> V_{dd} - V_{D5} \\
&\Rightarrow V_{D5} > V_{G5} + |V_{tp}| \\
\Rightarrow V_{ref} + \frac{V_{dd}}{2} &> \frac{V_{dd}}{2} + |V_{tp}| \\
&\Rightarrow V_{ref} > |V_{tp}|
\end{aligned} \tag{4.22}$$

From equation 4.22 the regenerative latch does not function properly when the lower input voltage is higher than a certain voltage, which is the PMOS threshold voltage in this case. In other words, if the two inputs are greater than $|V_{tp}|$, the regenerative latch does not work properly. In the real case this voltage is much higher than $|V_{tp}|$, since $K_n \neq K_p$, $V_{tn} \neq |V_{tp}|$. But this is a good example to show us that there is an upper bound voltage for the regenerative latch to function properly.

The capacitors are discharged initially before the input signal comes in. As the input signal is applied to the peak detector, $V_{in} = V_{in,latch}$, and $V_{ref,latch} = 0$, the output of the regenerative latch out is high while its complement \overline{out} is low. out and \overline{out} together turn on the CMOS transmission gate, and the input signal charges the output capacitor so that $V_{out} = V_{in}$. Then the output voltage is used as the reference voltage of the regenerative latch through the use of a buffer. This buffer is configured as a follower integrator so that the change at the output voltage does not affect the reference voltage immediately. The output of the peak detector now traces its input voltage.

When the input voltage is smaller than the output voltage, i.e., $V_{in} = V_{in,latch} < V_{ref,latch}$, the latch output is low while its complement goes high, thus the latch turns off the CMOS transmission gate and holds the maximum input value at the output. The time constant of how long the peak detector can hold the voltage depends on the leakage current of the CMOS transmission gate and the size of the output capacitor by the equation

$$\frac{dV}{dt} = \frac{I_{leak}}{C} \tag{4.23}$$

Since the output of the peak detector is connected to the noninverting input of the transconductance amplifier whose input impedance, ideally, is infinite, an output buffer is not needed.

4.2.2 Performance and analysis

Figure 4.14 shows the performance of the peak detector when the maximum input voltage is smaller than 4V. The DC bias of the input sine wave is 2.5V, and the peak to peak voltage is 3V. In the figure the tracking part of the peak detector is not shown. Instead only the holding part is shown.

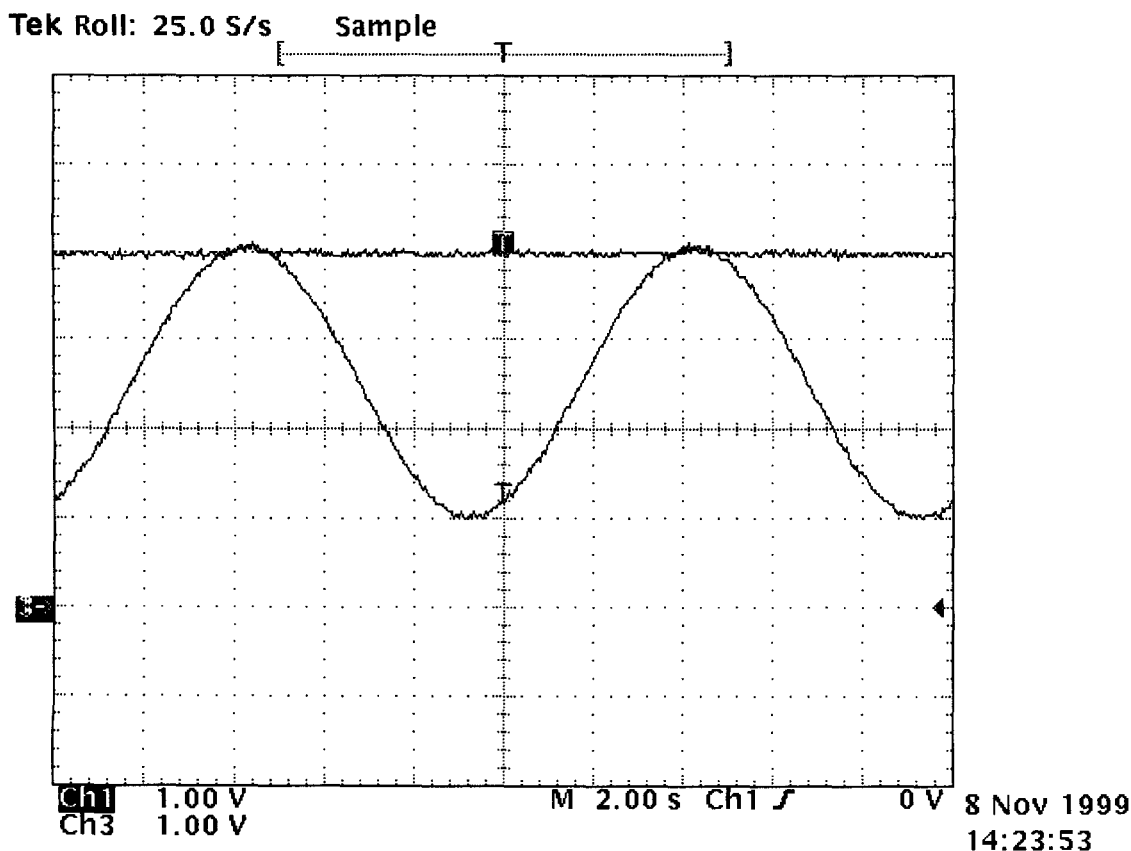


Figure 4.14: Performance when maximum voltage is less than 4 V

The frequency of the input sine signal is 0.1Hz. The peak detector functions properly and holds the maximum voltage at 4V.

Figure 4.15 shows the performance of the peak detector when the maximum input voltage is larger than 4V. The DC bias of the input sine wave remains at 2.5V, but the peak to peak voltage is increased to 4V. The frequency of the input sine signal is still 0.1Hz. Figure 4.15 shows that the peak detector has a limit on the maximum input voltage. When the input voltage is smaller than 4.3V, the peak detector functions properly as we expected. But when the input voltage is larger than 4.3V, the peak detector traces the input signal all the time. The source of this failure is because of the regenerative latch. When the input voltage $V_{in,latch}$ and the reference voltage $V_{ref,latch}$ are both high, say 4.3V, the regenerative latch deviates from its normal function. So as figure 4.15 shows, out is always high and \overline{out} is always low, then the CMOS transmission gate is always turned on, resulting in the error of peak detector.

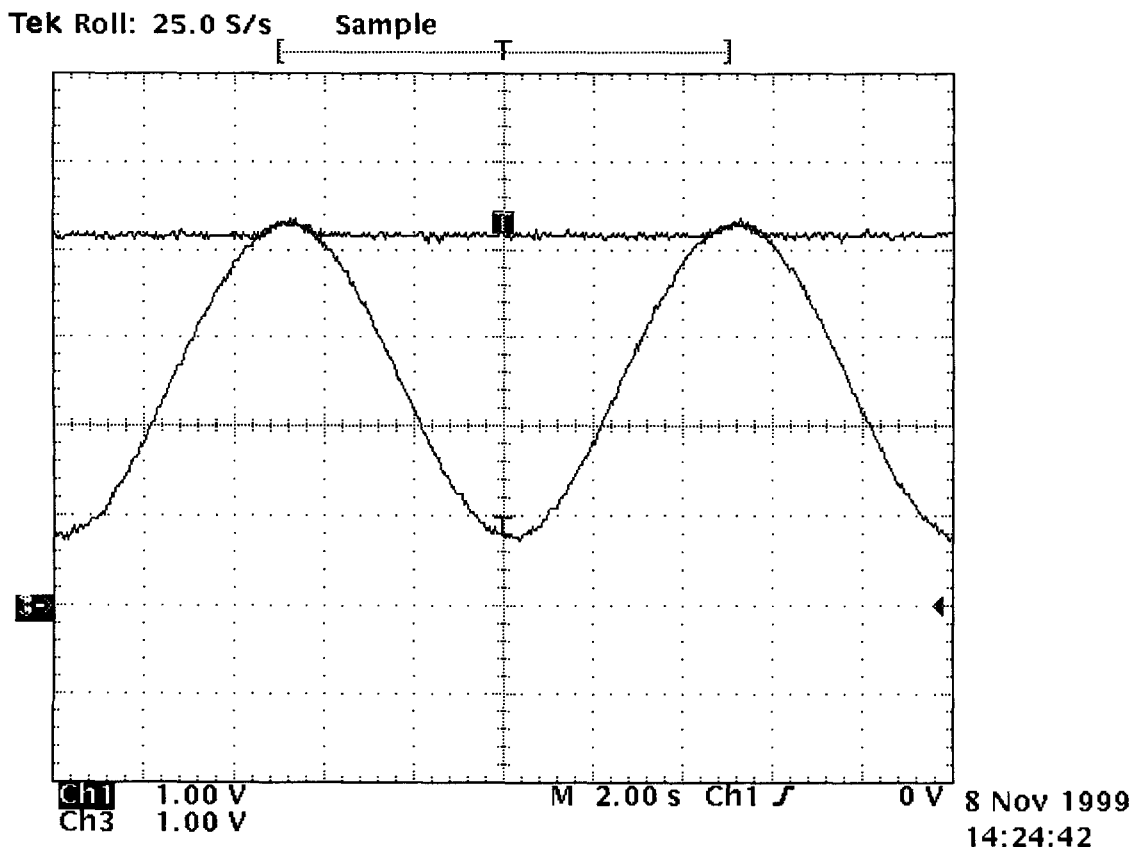


Figure 4.15: Performance when maximum voltage is larger than 4 V

The adaptive circuits bias the sensors so that their baseline sensor voltage are all 2V. The circuit is designed to be able to detect 100% sensor resistance change, i.e., the circuit needs to be able to detect the maximum sensor voltage up to 4V. The peak detector designed is suitable for the job.

4.3 Transconductance amplifier

From chapter 3, the output of the sensor stage is sent into the signal processing stage. Two main functions of the signal processing stage are to perform normalization and calculate Euclidean distance. These two math calculations can be very easily done in current mode analog circuitry, as we will soon discuss in the next chapter.

Since the output of the peak detector is the maximum sensor voltage when some odor source is applied to polymer sensor, a circuit that can extract the signal voltage and transform it into signal current is needed. A transconductance amplifier transforms a differential voltage input into

a current output proportional to the differential input voltage. Thus, high pass filtering can be achieved through the differential input characteristics of the transconductance amplifier by feeding the baseline sensor voltage to the inverting terminal of the transconductance amplifier. At the same time, voltage to current transformation can also be done.

One thing crucial when performing the voltage-to-current transformation in our case is the linearity of the transconductance amplifier. Since the signal voltage contains information about the odor concentration, the V/I transformation should not lose any information that the signal voltage contains. Thus a highly linear transconductance amplifier is required to meet the demand. Much research has been devoted to design transconductance amplifier with extremely high linearity [61, 62, 63, 64, 65, 66, 67, 68].

4.3.1 Circuit description

Figure 4.16 is the schematic of our transconductance amplifier. The amplifier is based on Wang's circuit[68] with slight modifications. This circuit exhibits a very good linear characteristic that we need to preserve the sensor signal. The ideal constant current source in Wang's paper is removed to eliminate the need to build a ideal source on chip. Current mirrors are added to obtain a single-ended output.

Circuit operation can be described as the following: the circuit can be divided into two main parts: transistors $M_1 \dots M_8$ form the nucleus of the transconductance amplifier, while transistors $M_9 \dots M_{14}$ serve as current mirrors to obtain the output current we want. When all transistors work in the saturation region, the currents of $M_2, M_3, M_5,$ and M_6 can be expressed as

$$I_{d2} = K_2(V_p - V_T)^2 \quad (4.24)$$

$$I_{d3} = K_3(V_n - V_T)^2 \quad (4.25)$$

$$I_{d5} = K_5(V_A - V_T)^2 \quad (4.26)$$

$$I_{d6} = K_6(V_B - V_T)^2 \quad (4.27)$$

where $V_A = V_{GS5} = V_{G5}$, and $V_B = V_{GS6} = V_{G6}$. To determine the intermediate voltage V_A , notice that the drain current flowing through transistor M_1 and M_7 are the same. Therefore, the gate-source voltage V_{GS1} is equal to the gate-source voltage V_{GS7} , i.e., $V_p - V_A = V_{bias}$. Thus we

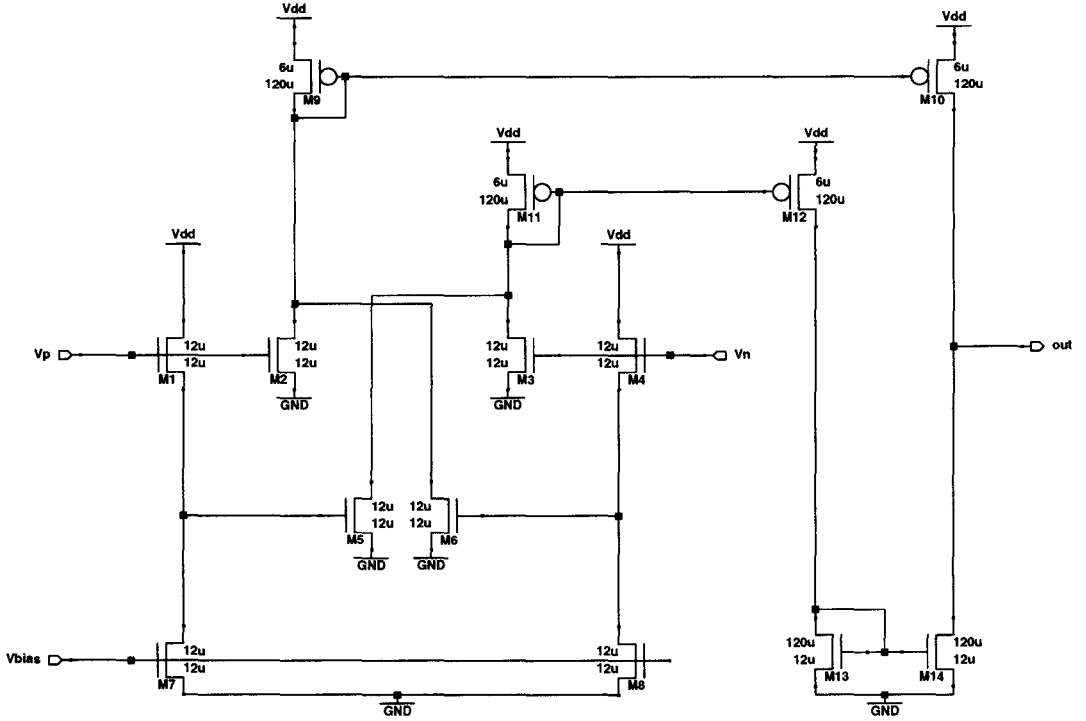


Figure 4.16: Schematic of the transconductance amplifier circuit

know:

$$V_A = V_p - V_{bias} \quad (4.28)$$

By substituting equation 4.28 into equation 4.26, we can obtain

$$I_{d5} = K_5(V_p - V_{bias} - V_T)^2 \quad (4.29)$$

By the same means we can rewrite equation 4.27 as

$$I_{d6} = K_6(V_n - V_{bias} - V_T)^2 \quad (4.30)$$

First, set the dimension of transistors $M_1 \dots M_8$ to be the same $K_1 = K_2 = \dots = K_8 = K$.

The dimension of transistors is chosen such that the maximum transconductance amplifier current output reaches $150\mu\text{A}$ in SPICE simulation. From SPICE simulation the value of K is chosen to be one. To reduce channel-length modulation effect of the transistors, the lengths are chosen as $12\mu\text{m}$, thus the dimensions of $M_1 \dots M_8$ are designed as $12\mu\text{m}/12\mu\text{m}$.

The current mirrors $M_9 \dots M_{14}$ are used to obtain a single-ended output from the transconductance amplifier. Therefore, the dimension of the mirrors are designed to be able to load the amount of currents of $I_{d2} + I_{d6}$ and $I_{d3} + I_{d5}$. From SPICE simulation dimensions of the mirrors are designed as $120\mu\text{m}/6\mu\text{m}$. By using current mirrors, the output current can be arranged as

$$I_{out} = I_{d2} - I_{d3} - I_{d5} + I_{d6} = 2KV_{bias}(V_p - V_n) \quad (4.31)$$

The transconductance amplifier thus has a tunable constant transconductance

$$g_m = 2KV_{bias} \quad (4.32)$$

which is independent of the transistor parameter V_T and can be adjusted by changing the DC bias voltage V_{bias} . From equation 4.31 not only the DC offsets but also higher-order nonlinearities are cancelled in I_{out} by arranging the transistors symmetrically. Thus extremely high linearity over a wide input range can be obtained.

4.3.2 Performance and analysis

The transconductance amplifier works only when all the transistors function in the saturation region. Suppose the threshold voltage of all the transistors is V_T , the gate voltage V_{bias} of the current source transistors M_7 and M_8 needs to be larger than V_T to turn on the transistors. Moreover, to keep the transistors M_7, M_8 in saturation,

$$V_A, V_B \geq V_{bias} - V_T \quad (4.33)$$

But also notice that V_A and V_B are also the gate voltages for transistors M_5, M_6 , respectively. To turn on transistors M_5 and M_6 :

$$V_A, V_B > V_T \quad (4.34)$$

According to equation 4.28, $V_p = V_A + V_{bias}$, $V_n = V_B + V_{bias}$, we can state the minimum criteria for the input voltages:

$$\begin{cases} V_p, V_n > 2V_{bias} - V_T & \text{if } V_{bias} > 2V_T \\ V_p, V_n > V_{bias} + V_T & \text{if } V_{bias} < 2V_T \end{cases}$$

The maximum criteria for the input voltages is when transistors M_2 and M_3 leave the saturation region. Since the sources of transistors M_2 and M_3 are connected to GND, the transistors leave saturation when their drain voltages are less than $V_p, V_n - V_T$, respectively. In fact, their drains are loaded by current mirror transistors M_9 and M_{11} . Suppose the input voltages V_p and V_n are the same, we can analyze transistors M_2 and M_9 first. Transistors M_3 and M_{11} work in the same way.

Transistor M_2 works in saturation when $V_{D2} > V_p - V_T$. Its drain is connected to the drain of transistor M_6 and M_9 . Since $V_{G6} = V_B = V_A < V_p$, as long as M_2 works in saturation, M_6 would be in the saturation region. So we can neglect the effect of M_6 . Since the current mirror transistor M_9 loads the summation current $I_{d2} + I_{d6}$, its gate voltage, V_{D2} , needs to be small enough to source this summation current. As we increase the input voltage V_p , it would reach some point that the summation current forces V_{D2} to be too small that transistor M_2 leaves saturation. This sets the maximum input voltage criteria.

Figure 4.17 shows the performance of the transconductance amplifier. We sweep the noninverting input voltage from 0 to 5V while setting the inverting input at 2.5V. The bias voltage V_{bias} is set to be 1V. The threshold voltage V_T of the NMOS transistor is roughly 0.8V. The transconductance amplifier works for input voltage between 1.8V and 4.5V. Since $V_{bias} = 1V < 2V_T = 1.6V$, according to what we have discussed, the input voltage needs to be larger than $V_{bias} + V_T = 1.8V$ to keep all the transistors in saturation. The inverting input voltage V_n fulfills the requirement while the noninverting input voltage V_p needs to fulfill the requirement for the circuit to function properly. This is the source of the minimum input voltage for the transconductance amplifier. Moreover, the maximum input voltage 4.5V is due to the loading effect of current mirror transistor as we have discussed. So the transconductance amplifier works in a certain range of input voltage. This is what we need to keep in mind when designing the circuit.

The transfer function of the transconductance amplifier can be written as

$$I_{out} = G_m(V_{in} - V_{ref}) \quad (4.35)$$

From figure 4.17 $G_m = 67.5\mu A/V$. When the differential input voltage is zero, i.e., $V_{in} = V_{ref}$, the output current is almost zero as well. And since the transconductance is a constant when $1.8V < V_{in} < 4.5V$, the output current contains the same information as the differential input

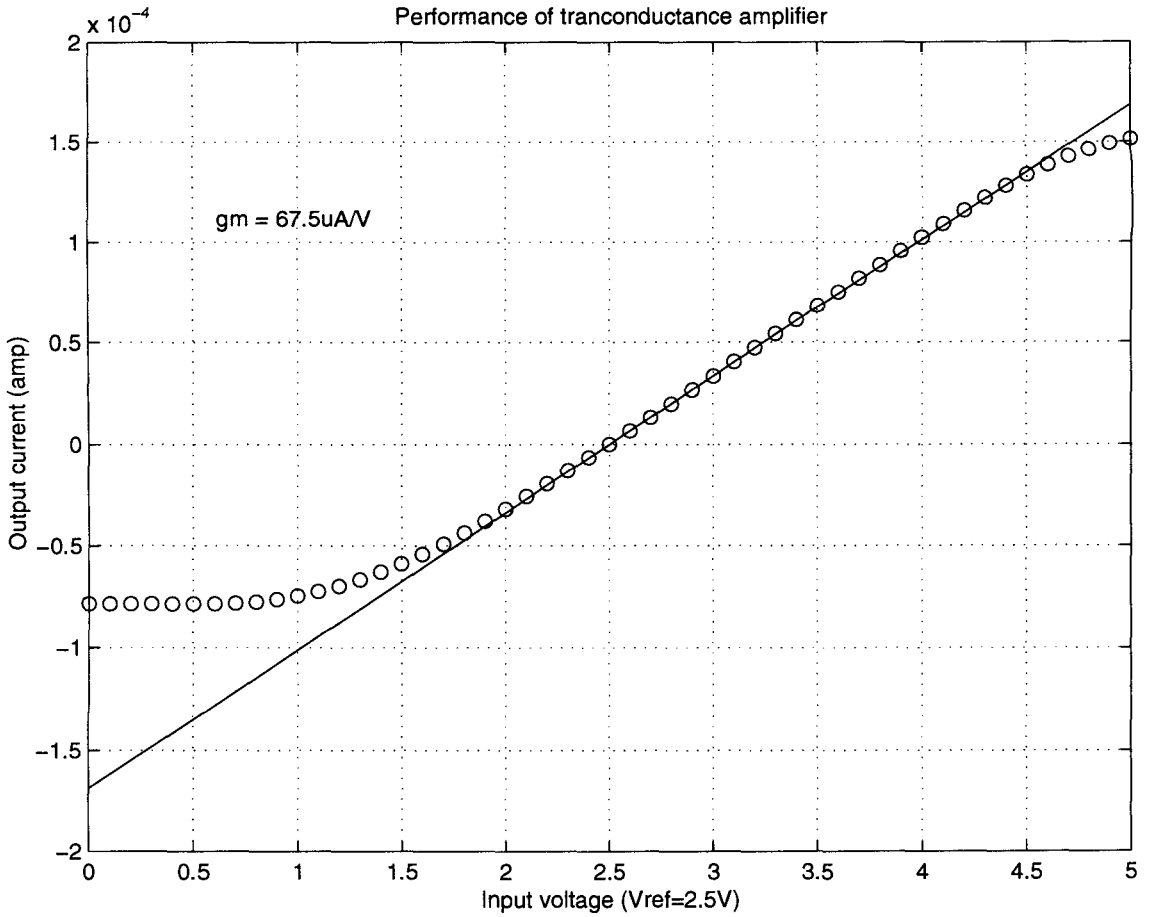


Figure 4.17: Performance of transconductance amplifier

voltage, and this current can be sent to the signal processing stage.

To examine the dependence of V_{bias} to transconductance the output current with different bias voltages are measured and shown in figure 4.18. The inverting terminal is set to 2V and the non-inverting terminal voltage is swept from 0 to 5V. When V_{in} is smaller than 2V the output current is almost the same for all the curves. When $V_{in} > V_{ref}$ the output current responds to the input voltage with different slopes according to different bias voltages. The lowest curve is biased by 0.8V, the second lowest curve is biased by 1V, the middle curve is biased by 1.2V, the second highest curve is biased by 2V, and the highest curve is biased by 2.2V. The higher the bias voltage, the larger the transconductance (slope), according to equation 4.32.

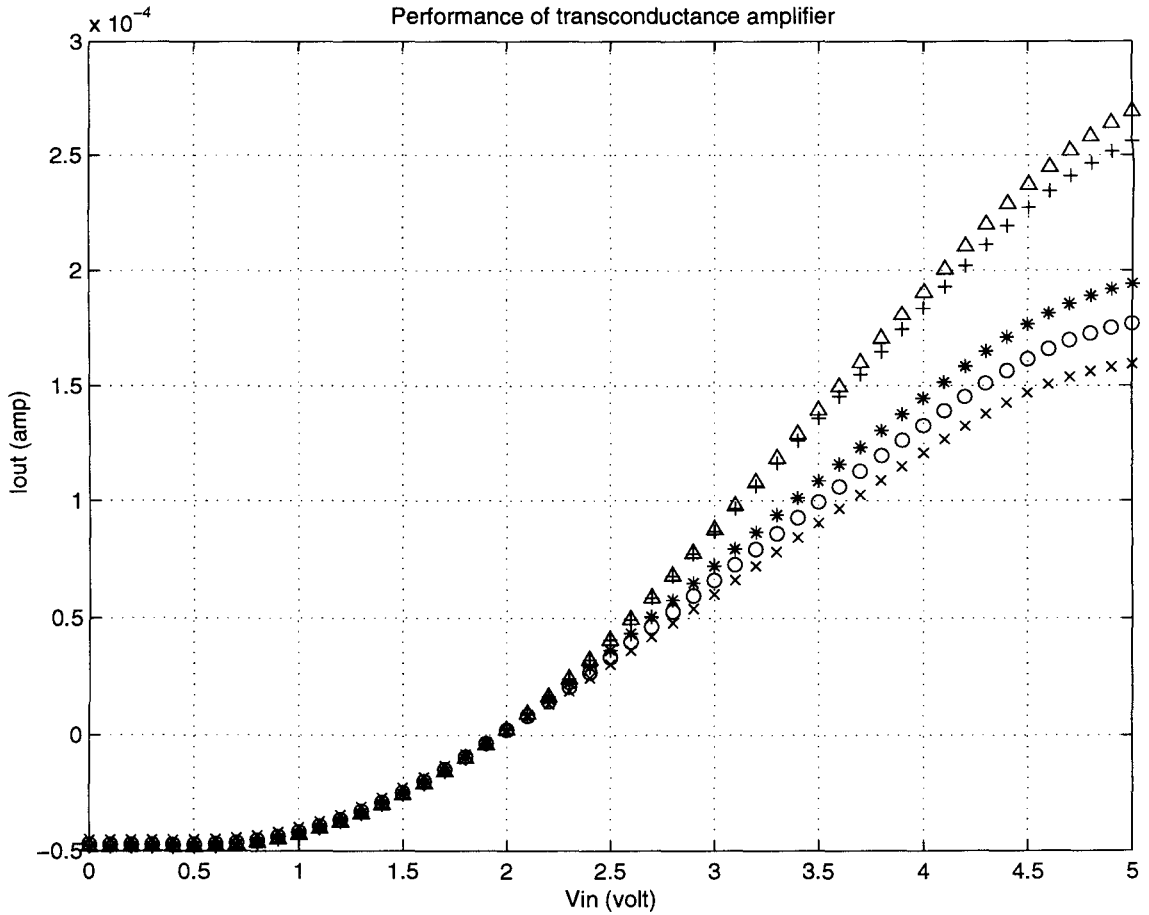


Figure 4.18: Performance of transconductance amplifier with different bias voltages

4.4 Overall performance

Figure 4.19 shows the overall performance of the sensor stage. Initially the whole circuit is not turned on, so the output current is zero. At 10 seconds, the circuit turns on and the sensor is adapted to the baseline voltage 2V, the output voltage from the peak detector is 2V, and the current from the transconductance amplifier is about 1 μ A. After 50 seconds an odor is applied to the sensor, the sensor resistance changes 100%, and the sensor voltage changes from 2V to 4V. The output voltage from the peak detector now is also 4V, resulting in a current output 112 μ A from the transconductance amplifier. After 100 seconds the odor is taken away. The sensor resistance goes back to baseline, but the output from the peak detector still remains at 4V though decreasing slowly. The corresponding output current decreases from 112 μ A slowly as well. The whole sensor stage functions properly as designed.

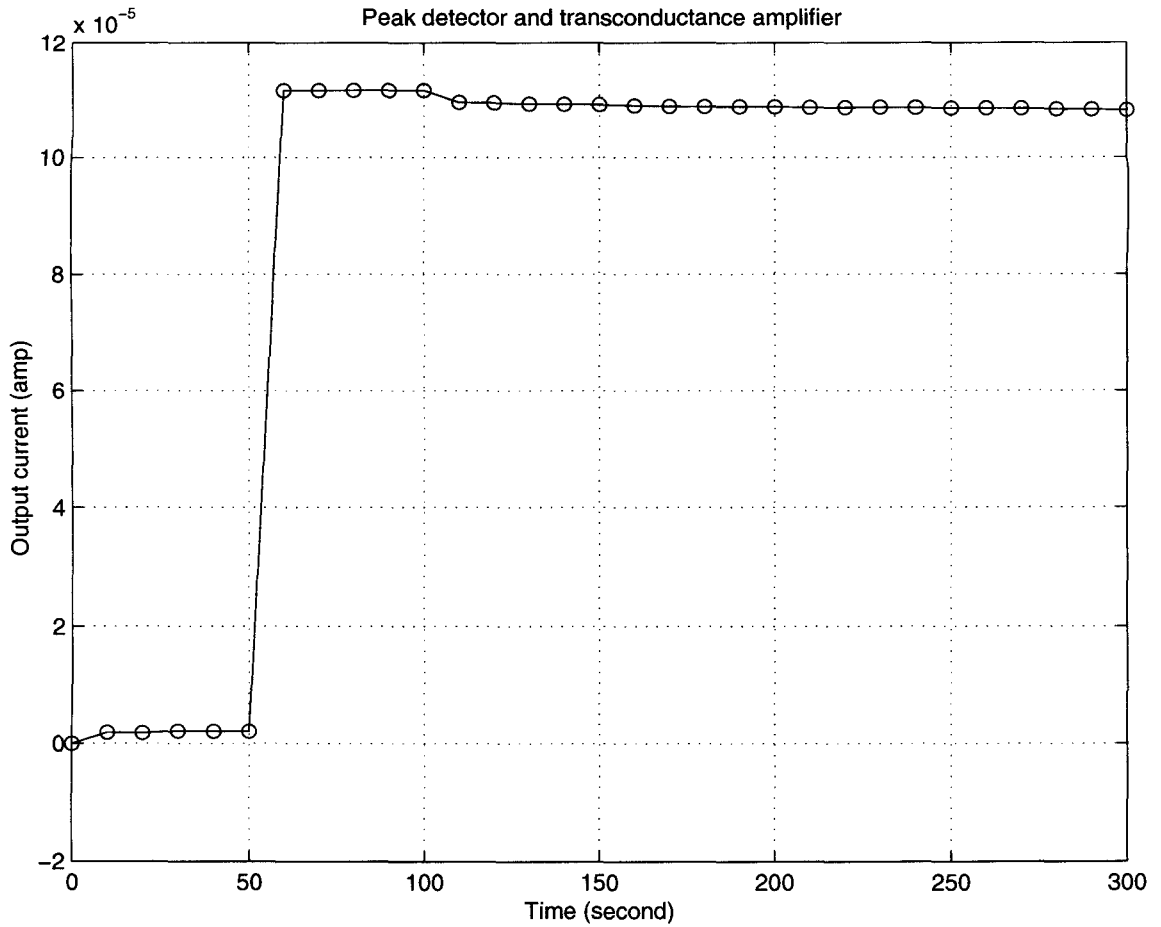


Figure 4.19: Overall performance of the sensor stage

We have already built the adaptive electronics, peak detector, and transconductance amplifier to complete the sensor stage. This stage adapts the sensor voltage to 2V and then outputs a current proportional to $\Delta R_{max}/R_b$, which is proportional to odor concentration. The output current contains the information that we need for odor classification. Since there is an array of different sensors, an array of sensor stages are needed. If the sensor array is constructed by n different carbon black-organic polymer sensors, n sensor stages are needed. These n sensor stages output n currents, and these n output currents form an n -dimensional signal vector. This n -dimensional signal vector is sent to the signal processing stage either for learning or for classification.

Chapter 5 Signal Processing Stage

As it has been shown in chapter 4, an n -dimensional signal vector from the sensor stages is sent to the signal processing stage. This n -dimensional signal vector represents an odor fingerprint obtained from the n carbon black-organic polymer sensor array. Unfortunately, this signal vector cannot be used directly for odor classification. Before feeding this signal vector into the classifier stage, some signal processing needs to be done. First of all, notice that the magnitude of the signal vector is proportional to the odor concentration. So even if two signal vectors represent the same odor with different concentrations, they are different in magnitude. Of course we can not classify them as different odors by using these signal vectors directly. This is a very important point that odor classification is determined by the "shape" of the odor fingerprint instead of its absolute value. Therefore, the signal vector needs to be normalized in some means before its further use.

There are many kinds of classifiers. Among them, the nearest neighbor classifier is used because of its simplicity and feasibility in VLSI circuits. The nearest neighbor classifier chooses the pattern that is closest to the signal template, i.e., the pattern which has the shortest distance to the pattern of interest. Since the nearest neighbor requires distances to compare, a kind of distance measure is needed. Euclidean distance is one of the distance measures that is frequently used in the nearest neighbor classifier, so a circuit that does Euclidean distance calculation is built.

Figure 5.1 is a block diagram of the signal processing stage. A three-dimensional signal vector (I_1, I_2, I_3) is from the sensor stages. Each dimension is a signal current proportional to $\Delta R_{max}/R_b$. This signal vector is sent into a normalization circuit to perform city-blocks distance normalization. The normalized signal vector (I_{n1}, I_{n2}, I_{n3}) still contains the same information of odor fingerprint that the signal vector has, and it is sent into the Euclidean distance circuit to calculate the Euclidean distance to a data vector (I_{d1}, I_{d2}, I_{d3}) from the database stage. The output is a current containing the distance information, and it is sent into the classifier stage.

In this chapter two kinds of signal processing are discussed: *Signal normalization* and *Distance measurement*. To implement these two kinds of signal processing, three kinds of circuits are presented: *Normalization circuit*, *Absolute value circuit*, and *Euclidean distance circuit*.

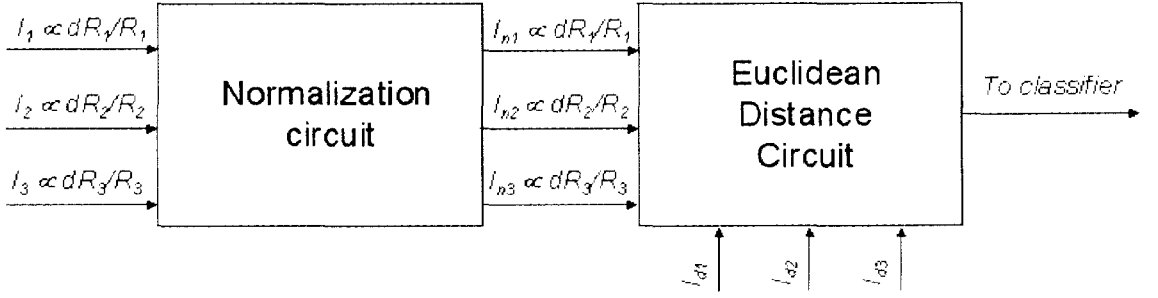


Figure 5.1: Block diagram of the signal processing stage

5.1 Signal normalization

The first signal processing block is to perform normalization to the signal vector. In this section, the necessity of normalization is discussed. Two different ways for normalization are introduced, and the circuit used for the normalization task is presented.

5.1.1 Need

The signal vector is composed of signal currents from the sensor stage. Each current is proportional to the relative resistance change $\Delta R_{max}/R_b$. We can write down the relationship:

$$I_{in} = \mu \frac{\Delta R_{max}}{R_b} \quad (5.1)$$

where I_{in} is the signal current, and μ is a constant. According to section 2.4, the relative resistance change is proportional to the odor concentration:

$$\frac{\Delta R_{max}}{R_b} = \nu C \quad (5.2)$$

where ν is a constant, and C is the odor concentration. Combine equation 5.1 and equation 5.2 together:

$$I_{in} = \lambda C \quad (5.3)$$

where $\lambda = \mu\nu$. The magnitude of the signal current is linearly dependent on the odor concentration by the constant λ .

There are different ways to perform the classification task. The nucleus of the task is to obtain variant data patterns (data vectors), and compare the similarity of the data patterns with the input

pattern (input vector). A way to get a measure of the similarity is to use the Euclidean distance. The data pattern that has the most similarity to the input pattern would have the shortest Euclidean distance between its data vector and signal vector.

Moreover, the data vectors and the signal vector need a common basis in order for comparison. Let us take a very simple example:

Student A is taking Algebra under professor M in school X, and student B is taking the same course under a different professor N in school Y. Student A got 90 for midterm, and student B got 85. Since the school and the professor for student A and B are different, one can not claim that student A learned better in Algebra simply because he got a better grade than student B. They need to compete on the same basis. This is why the schools need the SAT, GMAT, or GRE score when a student wants to apply for college or graduate school. Only in this way can students be compared on the same basis.

So right now the question becomes: *What is the basis for the data vectors and the signal vector?* One guess would be getting the data vector and the signal vector on the same concentration. Let us look at another example:

Suppose that a data vector $\vec{A} = (a_1, a_2, a_3)$ represents odor class A with concentration C_A for a three-dimensional carbon black-organic polymer sensor array. Also suppose that another data vector $\vec{B} = (b_1, b_2, b_3)$ represents odor class B with concentration C_A . Suppose that $b_1 = 1.5a_1, b_2 = 2.5a_2, b_3 = 1.5a_3$. If the array is exposed to odor A with concentration $2C_A$, the signal vector would be $(2a_1, 2a_2, 2a_3)$, according to equation 5.3. The Euclidean distance of the signal vector to data vector \vec{A} is

$$D_{Eu1} = \sqrt{(2a_1 - a_1)^2 + (2a_2 - a_2)^2 + (2a_3 - a_3)^2} = \sqrt{a_1^2 + a_2^2 + a_3^2}$$

and the Euclidean distance of the signal vector to data vector \vec{B} is

$$D_{Eu2} = \sqrt{(2a_1 - 1.5a_1)^2 + (2a_2 - 2.5a_2)^2 + (2a_3 - 1.5a_3)^2}$$

$$\Rightarrow D_{Eu2} = 0.5\sqrt{a_1^2 + a_2^2 + a_3^2}$$

If we just simply classify the input signal to the class that has the shortest Euclidean distance to the signal vector, we would get the wrong answer class B . The point shown in this example is, in the real world we do not know the odor concentration beforehand

when an odor is applied to the sensor array. So odor concentration cannot be the basis of comparison.

Instead of using odor concentration as the basis of comparison, normalization is used to form the basis of comparison. There are two kinds of normalization that are frequently used, one is Euclidean distance normalization, and the other is city-blocks distance normalization. Euclidean distance normalization uses Euclidean distance from the vector to the origin as denominator in the formula, while city-blocks distance normalization uses city-blocks distance as denominator.

For an n -dimensional vector (I_1, I_2, \dots, I_n) , its Euclidean distance normalization is

$$I_{n1} = \frac{I_1}{\sqrt{I_1^2 + I_2^2 + \dots + I_n^2}} \quad \dots \quad I_{nn} = \frac{I_n}{\sqrt{I_1^2 + I_2^2 + \dots + I_n^2}} \quad (5.4)$$

One can easily examine that the length of the normalized vector is

$$\sqrt{I_{n1}^2 + I_{n2}^2 + \dots + I_{nn}^2} = 1 \quad (5.5)$$

By performing Euclidean distance normalization, the length of all the data vectors and the signal vector are normalized to unity. Thus all the normalized data vectors and normalized signal vector can be viewed as a point in a unit length circle centering at the origin. Because of the linearity characteristics of the carbon black-organic polymer sensor, signal vectors with different odor concentrations can be normalized to the same point if they are generated from the same odor. We can take another example to illustrate this point:

Suppose that a Euclidean distance normalized data vector $\vec{A} = (a_1, a_2, a_3)$ represents odor class A for a three-dimensional carbon black-organic polymer sensor array. Also suppose that another Euclidean distance normalized data vector $\vec{B} = (b_1, b_2, b_3)$ represents odor class B . From equation 5.5, $\sqrt{a_1^2 + a_2^2 + a_3^2} = 1$, $\sqrt{b_1^2 + b_2^2 + b_3^2} = 1$. If the array is exposed to odor A with some concentration C_A , the signal vector \vec{S} would be $(\alpha a_1, \alpha a_2, \alpha a_3)$, according to equation 5.3. To classify the signal vector, first normalize the signal vector \vec{S}

$$S_{n1} = \frac{\alpha a_1}{\sqrt{(\alpha a_1)^2 + (\alpha a_2)^2 + (\alpha a_3)^2}} = a_1$$

$$S_{n2} = \frac{\alpha a_2}{\sqrt{(\alpha a_1)^2 + (\alpha a_2)^2 + (\alpha a_3)^2}} = a_2$$

$$S_{n3} = \frac{\alpha a_3}{\sqrt{(\alpha a_1)^2 + (\alpha a_2)^2 + (\alpha a_3)^2}} = a_3$$

The normalized signal vector $\vec{S} = (S_{n1}, S_{n2}, S_{n3}) = (a_1, a_2, a_3)$. So the normalized signal vector is the same as data vector \vec{A} , though the odor concentration is unknown. Unlike using odor concentration as the basis of comparison, Euclidean distance normalization is more suitable for odor classification application because odor concentration is usually unknown when classification is performed.

One of the setbacks of Euclidean distance normalization is the complexity of an implementation in a VLSI circuit. In order to perform normalization while keeping the circuit simple, city-blocks distance normalization is used instead.

5.1.2 City-blocks distance normalization

Instead of performing Euclidean distance normalization, city-blocks distance normalization is used. For an n -dimensional vector (I_1, I_2, \dots, I_n) , its city-blocks distance normalization is

$$I_{n1} = \frac{I_1}{I_1 + I_2 + \dots + I_n} \quad \dots \quad I_{nn} = \frac{I_n}{I_1 + I_2 + \dots + I_n} \quad (5.6)$$

One can soon verify that $I_{n1} + I_{n2} + \dots + I_{nn} = 1$. Therefore the summation of all the components in the normalized vector is unity. Similar to Euclidean distance normalization, signal vectors with different odor concentrations can be normalized to the same point if it is generated from the same odor by city-block distance normalization. We can take a similar example to illustrate this point:

Suppose that a city-blocks distance normalized data vector $\vec{A} = (a_1, a_2, a_3)$ represents odor class A for a three-dimensional carbon black-organic polymer sensor array. Also suppose that another city-block distance normalized data vector $\vec{B} = (b_1, b_2, b_3)$ represents odor class B . $a_1 + a_2 + a_3 = 1$, $b_1 + b_2 + b_3 = 1$. If the array is exposed to odor A with some concentration C_A , the signal vector \vec{S} would be $(\alpha a_1, \alpha a_2, \alpha a_3)$, according to equation 5.3. To classify the signal vector, first normalize the signal vector \vec{S}

$$S_{n1} = \frac{\alpha a_1}{\alpha a_1 + \alpha a_2 + \alpha a_3} = a_1$$

$$S_{n2} = \frac{\alpha a_2}{\alpha a_1 + \alpha a_2 + \alpha a_3} = a_2$$

$$S_{n3} = \frac{\alpha a_3}{\alpha a_1 + \alpha a_2 + \alpha a_3} = a_3$$

The normalized signal vector $\vec{S} = (S_{n1}, S_{n2}, S_{n3}) = (a_1, a_2, a_3)$. So again the normalized signal vector is the same as data vector \vec{A} , without knowing the actual odor concentration. Compared to Euclidean distance normalization, the difference that city-blocks distance normalization makes is only the denominator in the normalized components. City-blocks distance normalization is simpler mathematically than Euclidean distance normalization since summation is easier than calculating Euclidean distance. Moreover, by applying the translinear principle, city-blocks distance normalization can be very easily implemented in VLSI circuit.

5.1.3 Translinear principle

The term "translinear" was first coined in 1975[69] by Barrie Gilbert. The word *translinear*, by his recommendation, is reserved exclusively for those cells invoking *exponential* device behavior, which applies to all bipolar transistors, including heterojunction types, and to MOS transistors operated in the subthreshold domain[70, 71]. We would use bipolar transistors in our design to realize the translinear principle in this chapter. The advantage to use bipolar transistor over subthreshold MOS is its ability to work in higher current, resulting in a larger signal and a much better signal-to-noise ratio than subthreshold MOS. The process we fabricated all the chips allows us to fabricate good quality npn bipolar transistors. Therefore, bipolar transistors are used in the signal processing stage because the simplicity of circuitry while MOS transistors are used for the other circuits to achieve a smaller chip area.

In a bipolar transistor, the relationship between I_C and V_{BE} is the most important:

$$I_C = A_E J_S(T) \exp(V_{BE}/nV_T) \quad (5.7)$$

where A_E is the emitter area and $J_S(T)$ is the saturation current density. $I_S(T) = A_E J_S(T)$ is defined as the saturation current. The factor n is the emission coefficient generally close to unity (typically 1.001 to 1.01) for 'analog-quality' bipolar transistors operated in their normal forward active mode at moderate currents. We can assume n is constant over the working current range. By differentiating equation 5.7

$$\frac{\partial I_C}{\partial V_{BE}} = g_m = \frac{I_C}{V_T} \quad (5.8)$$

From equation 5.8, the transconductance of an ideal bipolar transistor is a linear function of its collector current. This is the origin of the term "trans-linear" (or TL). Moreover, by rearranging

equation 5.7

$$V_{BE} = nV_T \ln I_C / A_E J_S(T) \quad (5.9)$$

Now we are ready to state the principle[72]:

In a closed loop containing an even number of ideal junctions, arranged so that there are an equal number of clockwise-facing and counterclockwise-facing polarities, with no further voltage generators inside this loop, the product of the current densities in the clockwise direction is equal to the product of the current densities in the counterclockwise direction.

A brief proof can be based on the analysis of a general closed loop containing N junction devices. Assume the junctions are biased into forward conduction by the associated currents. The junction voltages, V_{Fk} , must sum to zero by KVL:

$$\sum_{k=1}^N V_{Fk} = 0 \quad (5.10)$$

For our purpose, these junctions represent the base-emitter terminals of the bipolar transistors in the loop. So V_{Fk} can be replaced by the base-emitter voltage V_{BE} and the associated currents can be replaced as the collector currents I_{Ck} . From substituting equation 5.9 into equation 5.10

$$\sum_{k=1}^N nV_T \ln \frac{I_{Ck}}{I_{Sk}} = 0 \quad (5.11)$$

Assume that nV_T is the same for all the junctions. Also notice the summation of a series of logarithmic terms can be written as a product, and zero may be written as $\ln 1$. Equation 5.11 can be rewritten as

$$\prod_{k=1}^N \frac{I_{Ck}}{I_{Sk}} = 1 \quad (5.12)$$

Notice that any practical circuit operates only when $I_C / I_S \gg 1$. So equation 5.12 holds only when two conditions are met:

1. There must be an even number of junctions in a TL loop.
2. There must be an equal number of clockwise-facing (CW) and counterclockwise-facing (CCW) junctions.

According to this need for symmetry, equation 5.12 can be stated as

$$\prod_{CW} \frac{I_{Ck}}{I_{Sk}} = \prod_{CCW} \frac{I_{Ck}}{I_{Sk}} \quad (5.13)$$

I_{Sk} in equation 5.13 can be replaced by $A_{Sk}J_{Sk}$. And since the saturation current density J_{Sk} equally weights the LHS and RHS of the equation,

$$\prod_{CW} \frac{I_{Ck}}{A_{Sk}} = \prod_{CCW} \frac{I_{Ck}}{A_{Sk}} \quad (5.14)$$

Notice that I_{Ck}/A_{Sk} is the current density in the device. So equation 5.14 can be rewritten as

$$\prod_{CW} J = \prod_{CCW} J \quad (5.15)$$

Hence the proof of translinear principle is done.

One more thing which is useful. When all the emitter areas are the same, equation 5.14 can be rewritten as

$$\prod_{CW} I_{Ck} = \prod_{CCW} I_{Ck} \quad (5.16)$$

5.1.4 Circuit description

Figure 5.2 is the circuit diagram based on Gilbert's paper[72] for the city-blocks distance normalization. To analyze how the circuit functions, instead of writing down complicated equations, we can apply the translinear principle:

$$\frac{I_{out1}}{I_1} = \frac{I_{out2}}{I_2} = \frac{I_{out3}}{I_3} \quad (5.17)$$

By equation 5.17 we can do some mathematics

$$\frac{I_{out1}}{I_1} = \frac{I_{out2}}{I_2} = \frac{I_{out3}}{I_3} = \frac{I_{out1} + I_{out2} + I_{out3}}{I_1 + I_2 + I_3} \quad (5.18)$$

And notice that the summation of the output currents $I_{out1} + I_{out2} + I_{out3}$ is equal to the reference current I_{ref} , equation 5.18 can be rewritten as

$$\frac{I_{out1}}{I_1} = \frac{I_{out2}}{I_2} = \frac{I_{out3}}{I_3} = \frac{I_{ref}}{I_1 + I_2 + I_3} \quad (5.19)$$

So the circuit performs city-blocks distance normalization:

$$I_{out1} = \frac{I_1}{I_1 + I_2 + I_3} I_{ref}$$

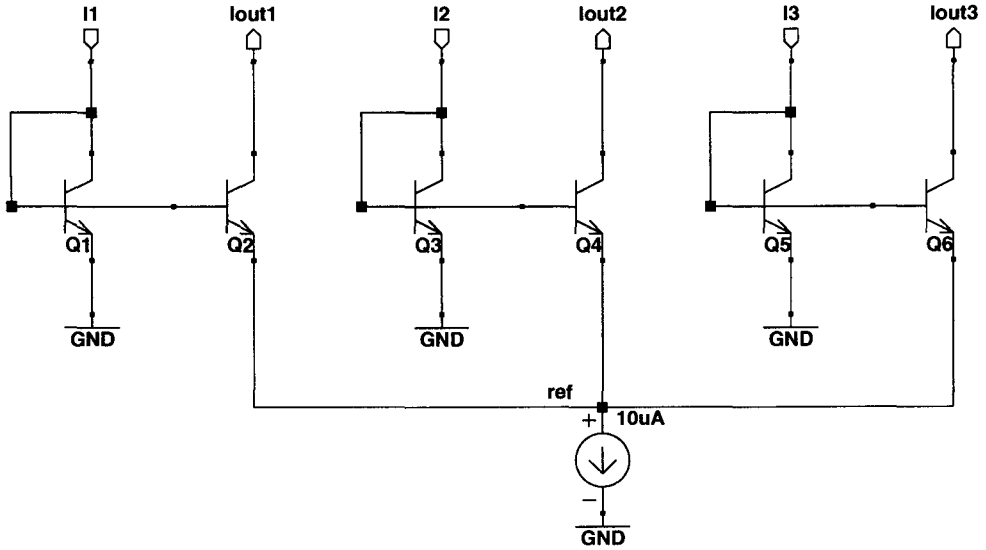


Figure 5.2: Schematic of the city-blocks distance normalization circuit

$$I_{out2} = \frac{I_2}{I_1 + I_2 + I_3} I_{ref}$$

$$I_{out3} = \frac{I_3}{I_1 + I_2 + I_3} I_{ref}$$

The circuit continuously computes the ratio of each input in the array to the sum of all the inputs, and then multiplies the result by the output scaling current I_{ref} . This circuit demonstrates the remarkable processing power which can be accomplished within the confines of a very rudimentary circuit. The entire circuit is built by bipolar transistors to result in very simple and compact hardware implementation.

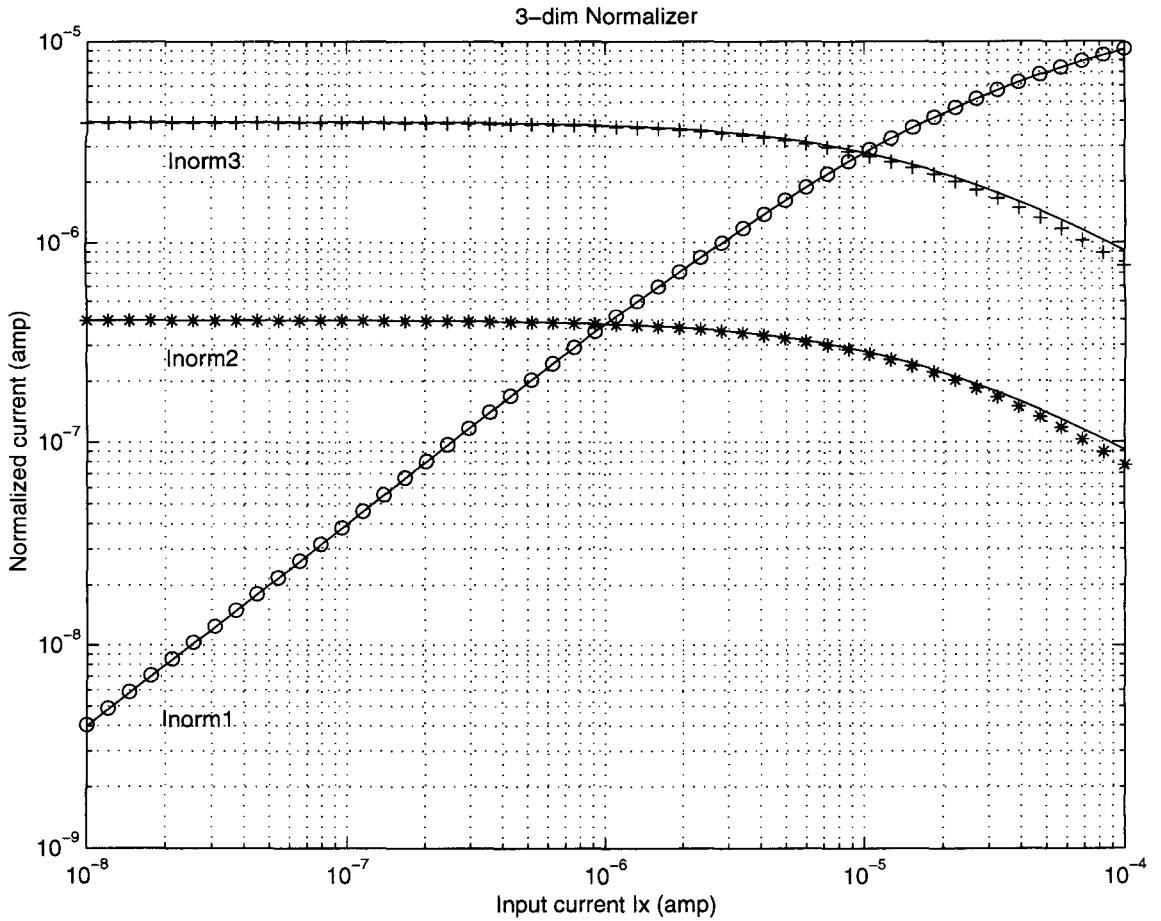


Figure 5.3: Performance of city-blocks distance normalization circuit

One point that is very valuable to notice: to add another dimension to the circuit, only two bipolar transistors are needed. So the bipolar city-blocks distance normalization circuit can be very easily extended to multiple dimensions.

5.1.5 Performance and analysis

Figure 5.3 displays the performance of the city-blocks distance normalization circuit. I_1 is swept from 10nA to 100uA while I_2 is set as 1uA and I_3 is set as 10uA. Very good performance is achieved by the simple bipolar circuit, and the circuit works at least for 4 orders of magnitude. The error is within 5% throughout the sweep, which is very reasonable in analog VLSI.

One more thing needs to be mentioned before closing this section. In Gilbert's city-blocks distance normalization circuit, assume the voltage at the emitter of the bipolar Q_1 with input current I_1 as V_{E1} , and the voltage at the emitter of the bipolar Q_2 with output current I_{out1} as V_{E2} . According

to equation 5.9

$$V_{BE1} = nV_T \ln \frac{I_1}{I_S} \quad V_{BE2} = nV_T \ln \frac{I_{out1}}{I_S}$$

Notice that $V_{E1} = 0$. The voltage V_S across the reference current source would be

$$V_S = V_{E2} = V_{E2} - V_{E1} = V_{BE1} - V_{BE2} = nV_T \ln \frac{I_1}{I_{out1}} \quad (5.20)$$

Remember n is close to unity, and V_T is approximately 0.0259V under room temperature. In order to have a 1V voltage across the reference current source, I_1/I_{out1} would need to be at least 5.86×10^{16} ! This is apparently impractical. For a more practical ratio $I_1/I_{out1} = 100$, the voltage across the reference current source is 0.12V. In the real world, the current source is usually realized by a transistor. For example, if we use a NMOS transistor whose gate is biased at 0.8V as the reference current source, its drain voltage would need to be higher than 0.8V in order to keep the transistor functioning in pinch-off region. But since the voltage across the current source, which is the drain voltage, is very small (usually close to GND), the NMOS transistor works in triode region and deviates from its current source characteristics. Although the circuit still performs city-blocks distance normalization continuously, I_{ref} is not a constant current and the normalized output currents lose the signal information.

To overcome this deviation from the ideal characteristics, the emitters of all the input currents are connected together to some biased voltage instead of being connected to ground. According to equation 5.20

$$V_{E2} = V_{E1} + nV_T \ln \frac{I_1}{I_{out1}}$$

Since the voltage across the reference current source V_S is equal to V_{E2} , this voltage can be set well above the gate voltage of the NMOS transistor by controlling V_{E1} . Take our old NMOS current source example, if the gate is biased at 0.8V, and V_{E1} is set at 1V, the drain voltage would be larger than 1V, and the transistor is working in the pinch-off region. In this way the problem with the non-ideal current source characteristic is solved.

5.2 Distance measurement

The nearest neighbor classifier is the classifier we use to perform the pattern recognition task. In order to determine which class is the nearest to the input signal pattern, a kind of distance measurement is needed. One kind of distance measurements is to use Euclidean distance as distance measure. So the nearest neighbor classifier would classify the input signal pattern to the class which

has the shortest Euclidean distance to the input signal vector. In this section, two circuits which can be used to perform Euclidean distance calculation are presented: *Absolute value circuit* and *Euclidean distance circuit*.

5.2.1 Absolute value circuit

For a three-dimensional input signal vector $\vec{x} = (x_1, x_2, x_3)$ and a data vector $\vec{A} = (a_1, a_2, a_3)$ representing odor class A, the Euclidean distance between them is

$$|\vec{x}\vec{A}| = \sqrt{(x_1 - a_1)^2 + (x_2 - a_2)^2 + (x_3 - a_3)^2} \quad (5.21)$$

For the Euclidean distance circuit, $(x_1 - a_1), (x_2 - a_2), (x_3 - a_3)$ are the input signals to the circuit. Mathematically the value of $(x_1 - a_1)^2$ and that of $(a_1 - x_1)^2$ are the same, since for a real number its square is always positive. But as we will soon come to in section 5.2.2, the real Euclidean distance circuit only accepts positive current as its inputs. So the inputs to the Euclidean distance circuit need to be positive, i.e., we need to take the absolute value of the input currents before they are sent into the distance calculating circuit. Therefore, an absolute value circuit is implemented to take the absolute value of the input currents.

Figure 5.4 displays a schematic for the absolute value circuit. The absolute value circuit is composed of five bipolar transistors. The sign of the current is defined as positive when the current goes into the circuit and negative when the current goes out from the circuit. The circuit takes the input current I_{in} and outputs its absolute value $|I_{in}|$. The output current can be loaded by a PMOS current mirror and subsequently measured.

Figure 5.5 shows the performance of the absolute value circuit. The input current I_{in} ranges is swept from two directions: from 10nA to 100uA and from -10nA to -100uA. The circuit shows very good performance, and the error is within 3%.

5.2.2 Euclidean distance circuit

Many efforts have been made to design a circuit that can calculate Euclidean distance, or in other words, vector summation[73, 74, 75]. The translinear principle in section 5.1.3 can also be used to design and analyze the circuit. Figure 5.6 displays the schematic of Euclidean distance circuit based on Gilbert's paper[72]. First notice the output current I_{out} is composed of three currents from three different bipolar transistors, whose bases are connected to the input current I_1, I_2, I_3 separately. Denote the collector current from the bipolar transistor whose base is connected to I_1 as xI_{out} , the collector current from the bipolar transistor whose base is connected to I_2 as yI_{out} , and the collector

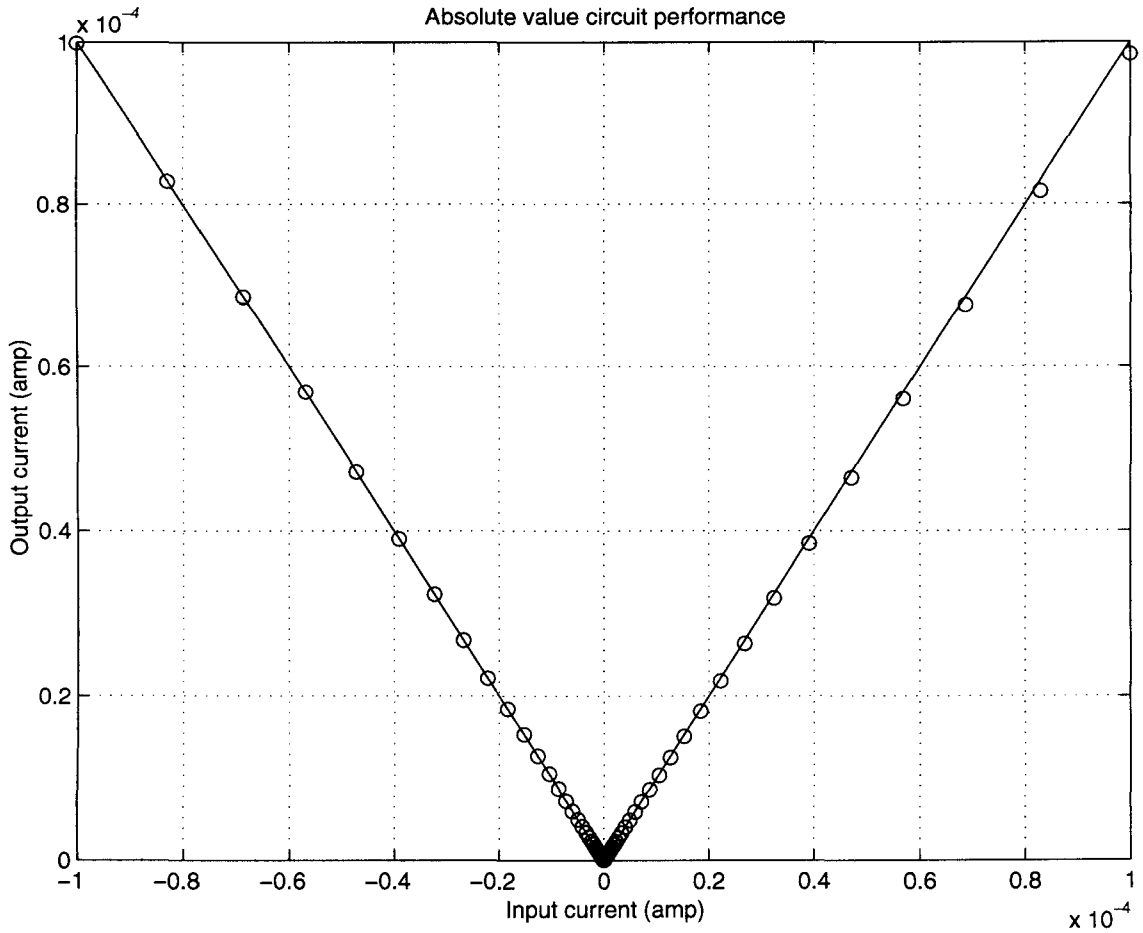


Figure 5.5: Performance of the absolute value circuit

Summation of the equations 5.22, 5.23, and 5.24 results in

$$I_1^2 + I_2^2 + I_3^2 = I_{out}^2 \quad (5.25)$$

By taking the square root LHS and RHS of the equation we can get the final form of interest:

$$I_{out} = \sqrt{I_1^2 + I_2^2 + I_3^2} \quad (5.26)$$

Hence the circuit performs Euclidean distance calculation. From the derivation of equations one can easily extend this circuit to multidimension. Every three more bipolar transistors can add another dimension to the circuit. So the circuit can be made very simple and compact.

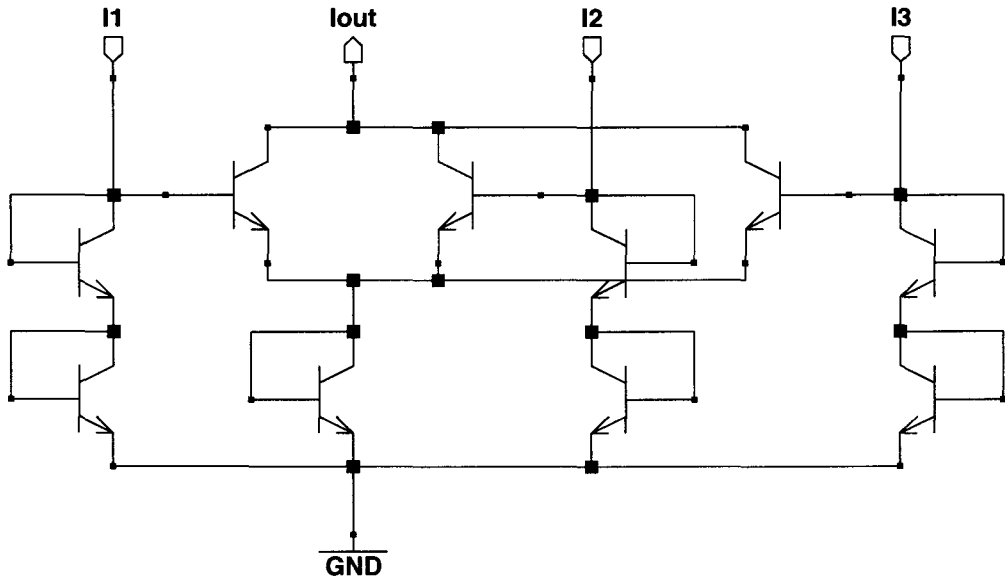


Figure 5.6: Schematic of the Euclidean distance circuit

5.2.3 Performance and analysis

Figure 5.7 displays the performance of Euclidean distance circuit. The input current one I_1 is swept from 10nA up to 100uA while I_2 is maintained at 1uA and I_3 is maintained at 10uA. The circuit works very well for at least 4 orders of magnitude. The error is within 5% throughout the sweep, showing great performance for an analog circuit.

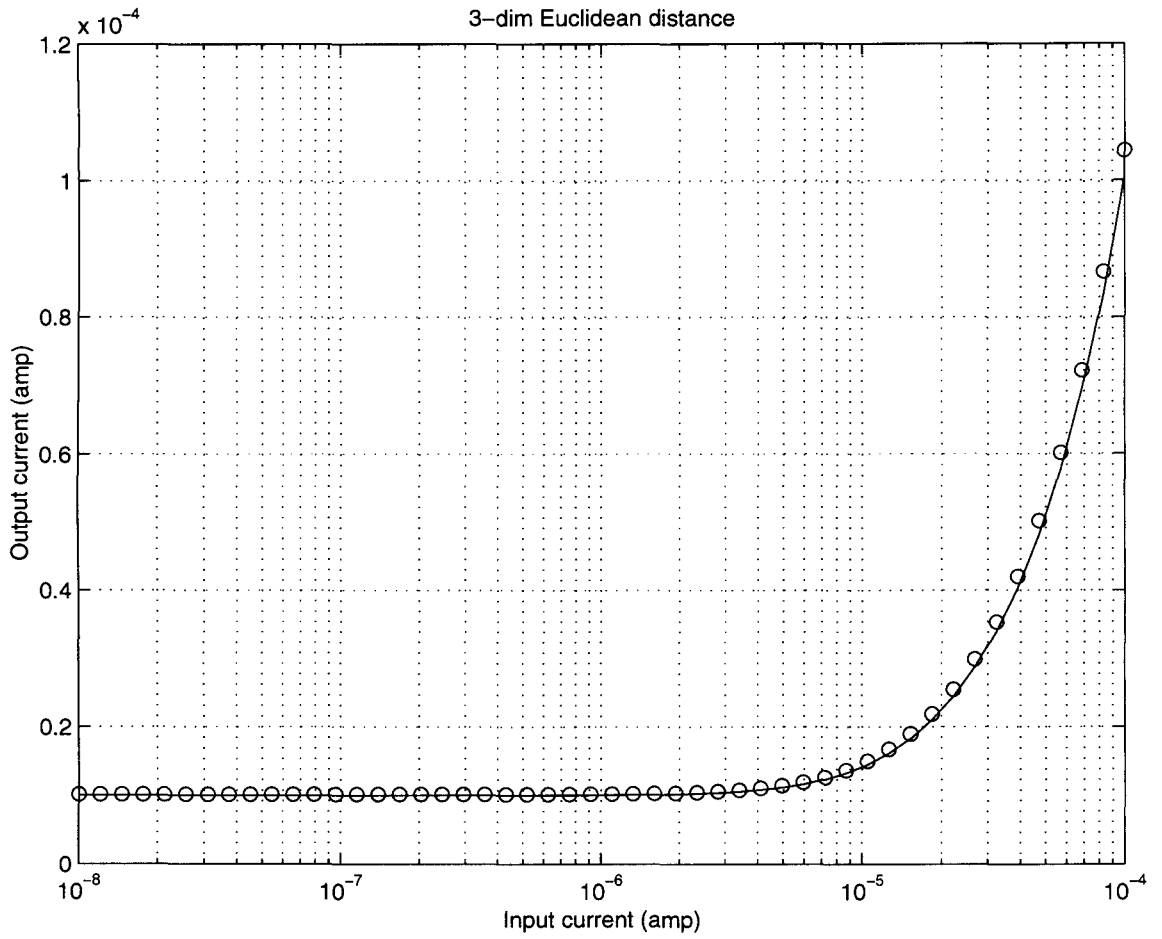


Figure 5.7: Performance of the Euclidean distance circuit

Chapter 6 Data Storage and Chip Interface

To decide to which class an input odor pattern belongs, a measure of similarity has to be obtained between the input odor pattern and the stored odor signatures. A simple way to define the similarity is to quantize the patterns into vectors, then calculate the Euclidean distances between the input odor vector and the known odor vectors. Euclidean distances between the normalized signal vector from the sensor stage and the data vectors stored in the database stage are calculated by an Euclidean distance circuit, as we proposed in the preceding chapter. But one question still remains: *What kind of storage method should be used for the electronic nose chip?*

In this chapter standard random-access memory (RAM) will be introduced for the use of data storage. The interface between the electronic nose chip and the outside world is presented, too. At the end of the chapter, a current copier cell, which can be described as a current-mode sample and hold circuit, is realized.

6.1 Data storage

Data storage has been a very important issue for pattern classification. Since the object of pattern recognition is to distinct the similarity between the input pattern and the known patterns, the question of how to store the known patterns is apparently unavoidable. Today, hardware data storage is mainly divided into two groups: analog memory and digital memory.

Memory efforts have already been devoted to find an integrable analog memory [76, 77, 78]. Many of them utilize the concept of a floating gate device [79]. This kind of floating-gate MOS device is often used in neural networks to store the synaptic weights. The analog memory is usually designed to be small, low power, and capable for fine adjustment to achieve high resolution.

Digital memory, including RAM, Read-only-memory (ROM), Programmable ROM (PROM), EEPROM, etc., are used broadly in many different areas. Each different digital memory has its distinct function and purpose. Since this dissertation is focused on the circuit cells needed to perform the odor classification task, existing digital memory is used directly to reduce the effort for building our own memory. In our case a simple 8-bit Static RAM is used for data storage of the electronic nose chip.

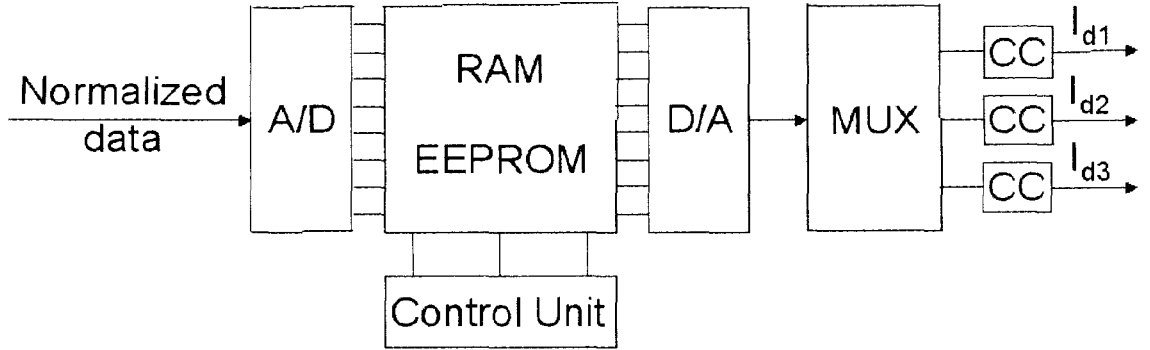


Figure 6.1: Block diagram of the database stage

MB8464 is a CMOS 8192 word by 8-bit SRAM from Fujitsu Microelectronics Inc. This SRAM is capable of storing 8192 different words with each word contains 8-bit resolution. Only a single 5V supply voltage is needed to enable the chip. There are four control lines to the chip: \overline{E}_1 , E_2 , \overline{R} , \overline{W} . The chip is disabled when \overline{E}_1 is high or E_2 is low. The chip is enabled only when \overline{E}_1 is low and E_2 is high at the same time. When MB8464 is enabled, the chip is at "READ" mode when \overline{R} is low, while at "WRITE" mode when \overline{W} is low. Output is disabled when \overline{R} and \overline{W} are both high. These four control lines are controlled by a central control circuit that will be discussed in the following section.

6.2 Chip interface and control

The electronic nose chip communicates with an analog-to-digital (A/D) converter and a digital to analog (D/A) converter directly, and uses a SRAM as its memory unit. An A/D converter is used to convert the normalized odor vector into digital information and store the information in the SRAM for the use of future classification. This is the learning state of the circuit function. After the learning state is done, the normalized input signal vector is used to calculate the Euclidean distances with the data vectors output from the SRAM through the use of D/A converter, and the distances are sent into a loser-take-all circuit to make the final decision. This is the classifying state of the circuit function.

Figure 6.1 displays a simple block diagram for the chip interface. The normalized data is sent from the normalization circuit of the signal processing stage to the SRAM through an A/D converter in the learning state. The odor patterns stored in the SRAM are converted into analog signals through a D/A converter in the classifying state. The analog data signal is sampled and held in a current

copier whose position is decided by a multiplexor. In Figure 6.1, a three-dimensional data vector is generated, so a one-to-three multiplexor and three current copiers are needed.

Moreover, the database stage is controlled by a central control unit. This control unit sets up all the control signals and their time sequence to the A/D converter, D/A converter, SRAM, and multiplexors. This control unit will be described in the subsection.

6.2.1 Learning state

The ADC0841 from National Semiconductor is chosen to convert the analog signal into digital in the database stage. It is an 8-bit microprocessor compatible A/D converter. The ADC0841 is controlled by several control lines: \overline{CS} , \overline{RD} , \overline{WR} , and \overline{INTR} . These control lines can be programmed by a microprocessor, though it is rather complicated. Fortunately in our case it only requires the A/D converter to perform continuous conversion. By simply connecting all the control lines to ground at the startup, then leaving \overline{WR} and \overline{INTR} floating, ADC0841 is in the mode of performing continuous conversion, i.e., an analog input would be converted into digital output in real time.

In the learning state, the normalized signal vector coming from the signal processing stage is converted to a digital word by the ADC0841. This is done from the first dimension of the normalized signal vector to the last dimension. For example, assume the normalized signal vector is three-dimensional, a three-to-one multiplexor in front of ADC0841 is used to extract the very dimension that is converted to a digital word. The control signal of the multiplexor is provided by the central control unit. Moreover, the output of the A/D converter is directly connected to the I/O port of SRAM. The control unit at this time outputs signals that enables the WRITE mode of the SRAM. Thus, the information from the testing odors are stored in the SRAM. The information of each odor pattern is stored in n digital words for an n -dimensional signal vector.

6.2.2 Classifying state

DAC0830 from National Semiconductor is chosen to convert the digital signal into analog in the database stage. It is an 8-bit microprocessor compatible, double-buffered D/A converter. DAC0830 is controlled by several control lines: \overline{CS} , \overline{WR} , ILE , and \overline{XFER} . These control lines can be programmed by a microprocessor, though it is rather complicated. Fortunately in our case it only requires the D/A converter to perform flow-through operation. By simply connecting all the control lines except ILE to ground and connecting ILE high, DAC0830 is in flow-through mode, i.e., the digital input directly affects the D/A converter analog output.

The input of the D/A converter is connected directly to the I/O port of SRAM. When the circuit is in the classifying state, the central control unit outputs control signals that SRAM is in its READ state, and the D/A converter outputs analog output corresponding to its digital input coming from the SRAM. The analog outputs are stored in current copiers through the use of a 1-to- n multiplexor, where n is the dimension of the data patterns. So, for example, if the odor pattern is stored as a three-dimensional vector, three digital words are required to store the information, which also requires a 1-to-3 multiplexor and three current copiers. The outputs of the current copiers altogether construct an n -dimensional data vector that is used to perform Euclidean distance calculation with the input normalized signal vector.

6.2.3 Central control unit

The central control unit provides all the control signals needed for the operation of SRAM and multiplexors. Since the A/D and D/A converter are both set in continuous conversion mode, there is no need to control the converters but simply set them to perform flow-through operation.

General description

Figure 6.2 is a simplified block diagram for the central control unit. Some assumptions are made here in the description to make it simple, and they do not affect the overall performance when extended into full-scale circuit realization. First, every odor is described by a three-dimensional vector. Second, only two different odor patterns are stored in SRAM. Since one odor pattern is composed of three different dimensions, three digital words are needed to store one odor pattern in the SRAM. So two different odor patterns require six digital words in the SRAM. Thus, 3-bit addresses in the memory need to be controlled. Third, we neglect the control of the multiplexors associated with the A/D, since its control has nothing different from those associated with the D/A. So only the control of the multiplexors associated with the D/A converter will be discussed to get the idea of how these multiplexors are controlled. Finally, only the classifying state is shown, since the learning state is just the opposite of the classifying state.

A state table is shown to display the states and the control signals generated in that state. Control signals $MUX1 \dots MUX5$ are control signals for the multiplexors. When $MUX1$ is high, the CMOS transmission gate associated with $MUX1$ turns on. When $MUX1$ is low, the CMOS transmission gate turns off. Notice that $MUX1$, $MUX2$, and $MUX3$ control three CMOS transmission gates that form an 1-to-3 multiplexor. In the same way, $MUX4$ and $MUX5$ control two CMOS transmission gates that form an 1-to-2 multiplexor. Also notice that $MUX1$, $MUX2$, $MUX3$ can not be high at the same time, since the multiplexor can only pass the signal to one channel at a time. The same thing applies to $MUX4$ and $MUX5$.

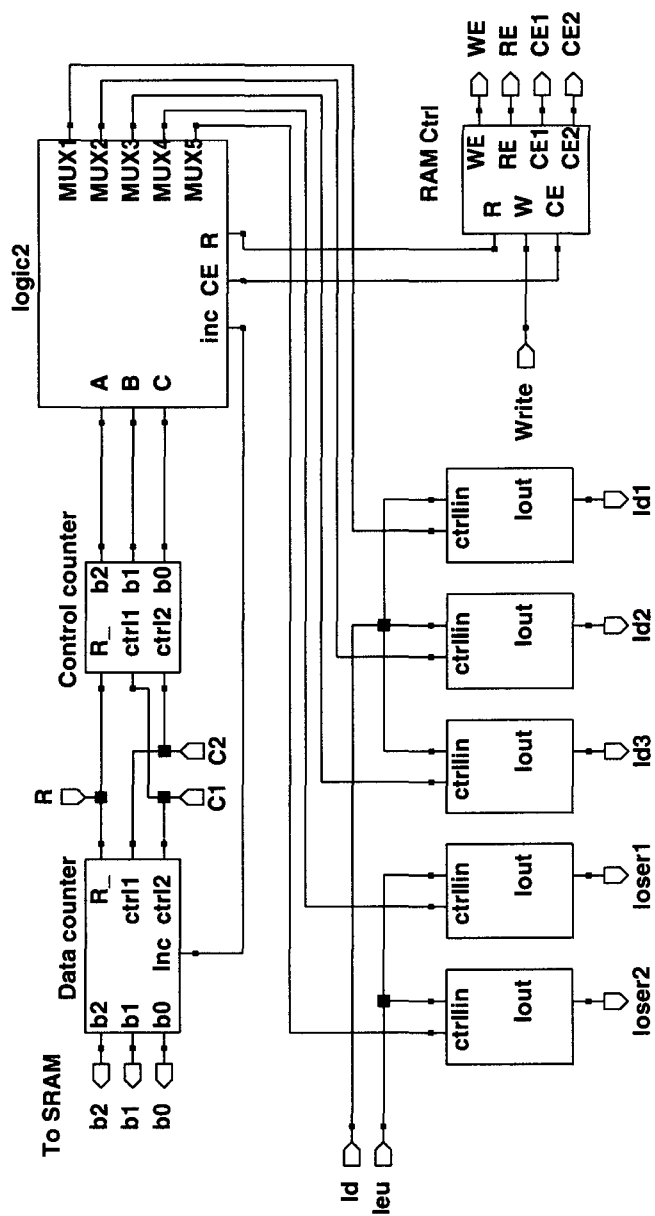


Figure 6.2: Simplified block diagram of the central control unit

Control counter

As in Figure 6.2, two counters are used in the central control unit. One is called the data counter, and the other is called the control counter. The control counter, by its name, is responsible for generating all the control signals. Actually it should be viewed as a state machine. It generates the states and uses a combinational logic circuit to generate the output signals for each stage. The control counter has three inputs and three outputs. The three inputs are R , $C1$, and $C2$. R is the compliment of the reset signal. When R is low, the counter is reset; when R is high, the counter is enabled to count up. $C1$ and $C2$ are two non-overlapping clock pulses for the counter. The output A, B, C from the control counter represent the state ABC , and is sent into a block called *logic2* to generate the control signals.

Data counter

The data counter is used to decide the address for SRAM to look at. The inputs $R, C1$ and $C2$ perform the same function as those in the control counter. The input Inc is set to decide if the counter counts up. When Inc is high, the counter is enabled to count up. When Inc is low, the counter will not count up, no matter whether $C1$ and $C2$ are applied to the counter. The outputs b_2, b_1 and b_0 are connected directly to the address lines of the SRAM. Notice that $C1, C2$ of the control counter are crossover connected to $C2, C1$ of the data counter. This makes sure that the two counters count up at the same frequency but not count at the same time. This is because when the control counter moves to a new state, it may generate a signal to read the output of the SRAM at an address. So at this very time the address line of the SRAM needs to be stable. If $C1, C2$ of the control counter and data counter are connected to each other, it is possible to cause ambiguity. So the solution is to make sure whenever the state machine goes into a new state, the data counter does not output the new address.

RAM Ctrl

RAMCtrl is a logic circuit used, as its name suggests, for the control of the SRAM. It receives three input signals W, R, CE and outputs $\overline{CE_1}, CE_2, \overline{WE}, \overline{OE}$. Table 6.1 shows the truth table or *RAMCtrl*.

The SRAM is enabled only when $\overline{CE_1}$ is low and CE_2 is high at the same time. So whenever input CE is high, $\overline{CE_1}$ is set low and CE_2 is set high, hence enables the SRAM. Then the operation of the SRAM is dependent on the other two input signals W and R . On the other hand, when CE is low, $\overline{CE_1}$ is set high and CE_2 is set low. The SRAM is disabled, and the outputs \overline{WE} and \overline{OE} are both set high. CE actually is the abbreviation for "Chip Enable".

CE	W	R	CE_1	CE_2	\overline{WE}	\overline{OE}
0	0	0	1	0	1	1
0	0	1	1	0	1	1
0	1	0	1	0	1	1
0	1	1	1	0	1	1
1	0	0	0	1	1	1
1	0	1	0	1	1	0
1	1	0	0	1	0	1
1	1	1	0	1	1	1

Table 6.1: Truth table for RAM Ctrl

Another input signal, W (Write), controls the WRITE operation of the SRAM. It affects the SRAM operation only when the SRAM is enabled, i.e., CE is high. If CE and W are both high while R is low, the SRAM functions in its WRITE mode, \overline{WE} is set low and \overline{OE} is set high. The SRAM stores the data at the I/O port to the address specified. On the other hand, when the other input signal R (Read) and CE are both high while W is low, the SRAM functions in its READ mode, \overline{WE} is set high and \overline{OE} is set low. The SRAM outputs the data at the specified address to the I/O port.

When the input signals W and R are both high or both low, we force the SRAM to do nothing to avoid any ambiguity. Therefore, \overline{WE} is set high and \overline{OE} is set high, too.

logic2

Circuit block *logic2* is a combinational logic circuit. It receives inputs from the control counter, then outputs the control signals to the data counter, RAM Ctrl, and multiplexors. In other words, *logic2* outputs control signals corresponding to the present state of the central control unit. So one can say that the combination of the control counter and *logic2* is the real "nucleus" of the central control unit. Table 6.2 is the state table of the function of *logic2*.

The input of *logic2* comes directly from the control counter. The present state is the counter output ABC . The counter is reset at the startup, so its output begins at state $a(000)$. The function of each state can be described as below:

stage a(000) CE and R are both set high, while W is set low to enable SRAM in its READ mode.

SRAM reads the data stored at the address specified by the data counter (000) and outputs the first dimension of first data vector (denoted as I_{dx1}) through the D/A converter. $MUX1$ is set high, while $MUX2 \dots MUX5$ are set low. So the output current goes through the first CMOS transmission gate controlled by $MUX1$ which stores the current in a current copier. Inc is set high for the data counter to count up for the next address.

Present State	Next State	MUX1	MUX2	MUX3	MUX4	MUX5	Inc	R	CE
000(a)	001(b)	1	0	0	0	0	1	1	1
001(b)	010(c)	0	1	0	0	0	1	1	1
010(c)	011(d)	0	0	1	0	0	1	1	1
011(d)	100(e)	0	0	0	1	0	0	0	0
100(e)	101(f)	1	0	0	0	0	1	1	1
101(f)	110(g)	0	1	0	0	0	1	1	1
110(g)	111(h)	0	0	1	0	0	1	1	1
111(h)	000(a)	0	0	0	0	1	0	0	0

Table 6.2: State table and function of *logic2*

stage b(001) *CE* and *R* are both set high, while *W* is set low to enable SRAM in its READ mode.

SRAM reads the data stored at the address specified by the data counter (001) and outputs the second dimension of first data vector (donated as I_{dx2}) through the D/A converter. *MUX2* is set high, while *MUX1*, *MUX3*, *MUX4*, *MUX5* are set low. So the output current goes through the second CMOS transmission gate controlled by *MUX2* which stores the current in a current copier. *Inc* is set high for the data counter to count up for the next address.

stage c(010) *CE* and *R* are both set high, while *W* is set low to enable SRAM in its READ mode.

SRAM reads the data stored at the address specified by the data counter (010) and outputs the third dimension of first data vector (donated as I_{dx3}) through the D/A converter. *MUX3* is set high, while *MUX1*, *MUX2*, *MUX4*, *MUX5* are set low. So the output current goes through the third CMOS transmission gate controlled by *MUX3* which stores the current in a current copier. *Inc* is set high for the data counter to count up for the next address.

stage d(011) *CE*, *R*, and *W* are all set low to disable SRAM. Thus D/A converter still reads the

address specified by the data counter (010) and outputs the third dimension of first data vector (donated as I_{dx3}). But since *MUX1*...*MUX3* are all set low, the value of I_{dx1} , I_{dx2} , I_{dx3} stored in the current copiers are not affected. At this time the Euclidean distance circuit in the signal processing stage calculates the Euclidean distance between the normalized input signal vector (I_{s1} , I_{s2} , I_{s3}) and the data vector (I_{dx1} , I_{dx2} , I_{dx3}). *MUX4* is set high while *MUX5* is set low. So the Euclidean distance current goes through the fourth CMOS transmission gate controlled by *MUX4* which stores the current in a current copier whose output goes to the loser-take-all circuit. *Inc* is set low to pause the data counter not to count up for the next address.

stage e(100) *CE* and *R* are both set high, while *W* is set low to enable SRAM in its READ mode.

SRAM reads the data stored at the address specified by the data counter (011) and outputs the first dimension of second data vector (donated as I_{dy1}) through the D/A converter. *MUX1* is set high, while *MUX2*...*MUX5* are set low. So the output current goes through the first

CMOS transmission gate controlled by $MUX1$ which stores the current in a current copier. Inc is set high for the data counter to count up for the next address.

stage f(101) CE and R are both set high, while W is set low to enable SRAM in its READ mode. SRAM reads the data stored at the address specified by the data counter (100) and outputs the second dimension of second data vector (donated as I_{dy2}) through the D/A converter. $MUX2$ is set high, while $MUX1, MUX3, MUX4, MUX5$ are set low. So the output current goes through the second CMOS transmission gate controlled by $MUX2$ which stores the current in a current copier. Inc is set high for the data counter to count up for the next address.

stage g(110) CE and R are both set high, while W is set low to enable SRAM in its READ mode. SRAM reads the data stored at the address specified by the data counter (101) and outputs the third dimension of second data vector (donated as I_{dy3}) through the D/A converter. $MUX3$ is set high, while $MUX1, MUX2, MUX4, MUX5$ are set low. So the output current goes through the third CMOS transmission gate controlled by $MUX3$ which stores the current in a current copier. Inc is set high for the data counter to count up for the next address.

stage h(111) $CE, R,$ and W are all set low to disable SRAM. Thus D/A converter still reads the address specified by the data counter (101) and outputs the third dimension of first data vector (donated as I_{dy3}). But since $MUX1 \dots MUX3$ are all set low, the value of $I_{dx1}, I_{dx2}, I_{dx3}$ stored in the current copiers are not affected. At this time the Euclidean distance circuit in the signal processing stage calculates the Euclidean distance between the normalized input signal vector (I_{s1}, I_{s2}, I_{s3}) and the data vector ($I_{dy1}, I_{dy2}, I_{dy3}$). $MUX5$ is set high while $MUX4$ is set low. So the Euclidean distance current goes through the fifth CMOS transmission gate controlled by $MUX5$ which stores the current in a current copier whose output goes to the loser-take-all circuit. Inc is set low to pause the data counter so it will not count up for the next address. At this time the loser-take-all circuit has two Euclidean distance currents of the normalized input vector to two different data vectors. The final decision is made to select the odor which has the shorter Euclidean distance.

The central control unit, as mentioned, generates the control signals in an arranged time sequence. The unit in this section is designed to classify an input signal pattern to two known odors. All the patterns are quantized into three-dimensional vectors. Higher-dimension vector and more known odor patterns can be easily realized by simply adding more bits to the data and control counters and adding more current copier cells.

6.3 Current copier cell

Since there is only one D/A converter, the digital words have to be converted into analog currents one at a time. But to calculate the Euclidean distance, n times D/A conversion have to be made to obtain an n -dimensional data vector. Therefore, a method to "hold" the D/A converter output current needs to be implemented. Moreover, the Euclidean distance current of an input vector to a data vector is calculated after the data vector is obtained. So for n odor patterns n data vectors need to be generated, and n Euclidean distance currents are calculated. Since the data vectors are generated one by one, the Euclidean distance currents are calculated one by one, too. Thus the Euclidean distance currents need to be held before the final decision is made since the loser-take-all circuit is a parallel signal processor. This also requires a way to "hold" the Euclidean distance currents.

One of the ways to sample and hold a current is to use a current copier cell. A current copier, by its name, copies the input current to the output. There are many articles discussing about how to make current copiers[80, 81, 82, 83]. Here, we just implement the standard current copier cell.

6.3.1 Circuit description

Figure 6.3 displays a standard current copier cell. It is composed of three NMOS transistors and a capacitor. Transistors M_1 and M_2 form a standard NMOS current mirror, and transistor M_3 serves as a NMOS switch. When the gate voltage of M_3 goes high, transistor M_3 turns on, and a low-impedance current path is formed. The current copier at this time can be viewed as a standard NMOS current mirror, and the input current I_{in} is copied to the output I_{out} . Moreover, the input current charges the capacitor at the gates of the current mirror when the current mirror is formed. At the steady state, there is no current flowing to the capacitor. So the voltage on the capacitor is the gate voltage that biases transistor M_1 to source the input current I_{in} . In another point of view, the input current I_{in} is stored as a voltage on the capacitor.

When the gate voltage of transistor M_3 goes low, M_3 turns off, thus disconnects the current path from the input to the capacitor. At this time the input current does not affect the output of the current copier. The gate voltage of M_2 is maintained on the capacitor, so the output current remains at the value of previous input current. This is actually a current-mode sample and hold circuit. When V_{G3} goes high, the current copier is in its SAMPLE mode. Then when V_{G3} goes low, the current copier goes to its HOLD mode.

How long can the capacitor hold the current depends on the leakage current through the switch

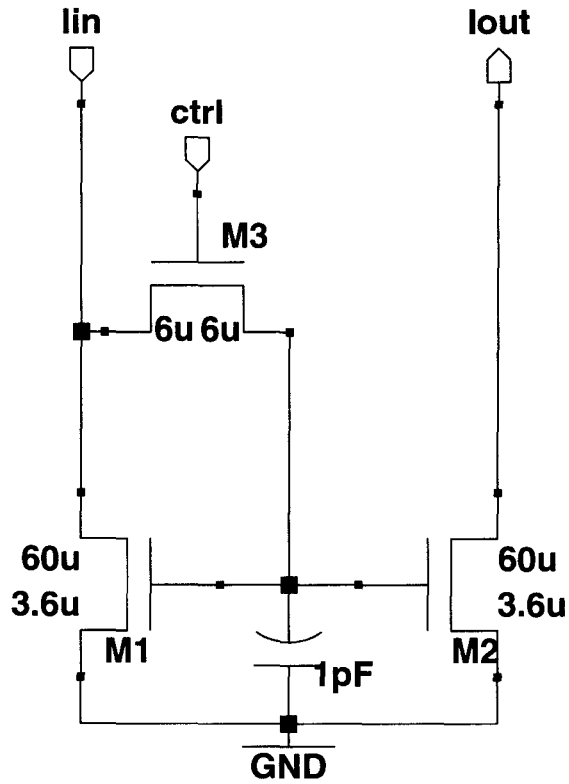


Figure 6.3: Schematic of the standard current copier circuit

M_3 . For the capacitor:

$$I_{leakage} = C \frac{dV_{cap}}{dt} \quad (6.1)$$

where $I_{leakage}$ is the leakage current, C is the capacitance of the capacitor at the gate of M_1 and M_2 , V_{cap} is the voltage across the capacitor, and t is time. Equation 6.1 can be rewritten as

$$\Delta V = \frac{I_{leakage} T}{C} \quad (6.2)$$

where ΔV is the leakage voltage, and T is the time period of leakage. Also remember that for a NMOS transistor in saturation:

$$I_d = K(V_{GS} - V_T)^2 \quad (6.3)$$

Assume the gate voltage corresponding to the output current I_{out} is V , after time T the gate voltage decreases by ΔV , then the deviated output current is

$$\begin{aligned} \Delta I_{out} &= K(V - V_T)^2 - K(V - \Delta V - V_T)^2 \\ &= K(2V - 2V_T - \Delta V)\Delta V \end{aligned} \quad (6.4)$$

The output current deviates by ΔV^2 , according to equation 6.4. Remember that in equation 6.2, ΔV is proportional to the leakage current $I_{leakage}$. So the leakage current of the NMOS switch affects the output current in a square relationship. There are many ways to reduce this effect. First, one can always use a PMOS switch instead of a NMOS. This is because the leakage current of a PMOS switch is smaller than a NMOS. One thing to keep in mind is that a PMOS switch is good at passing high voltage but poor at passing low voltage, while an NMOS switch is good at passing low voltage but poor at passing high voltage. So one needs to make sure that PMOS switch can pass the gate voltage needed to load the input current.

Another way to reduce the leakage current is to reduce the dependence of the output current to the gate voltage. According to equation 6.3, we know that the output current of a NMOS transistor is affected by the square of its gate voltage in saturation region. From equation 6.2 we also know the gate voltage is affected linearly by the leakage current. So if we can reduce the output current dependence so that it is linearly dependent to the gate voltage instead of a square relationship, output current will be affected by the leakage current linearly, hence the deviation is dramatically improved. The inverse linear V/I converter in section 4.1.5 can be one of the options.

6.3.2 Performance and analysis

Figure 6.4 shows the performance of the current copier cell. The input current is set to 100uA initially. The current copier is at its SAMPLE mode at the startup. After taking the data for one second the current copier switches to its HOLD mode and lasts for another 29 seconds. The initial output current is about 107uA, due to the channel-length modulation effect of transistor M_2 , since the drain voltage of M_1 and M_2 are not the same. The output current decreases slowly as time goes on, which makes a pretty good current copier for our use.

From figure 6.4, a linear dependence of the deviated output current to time is observed. From

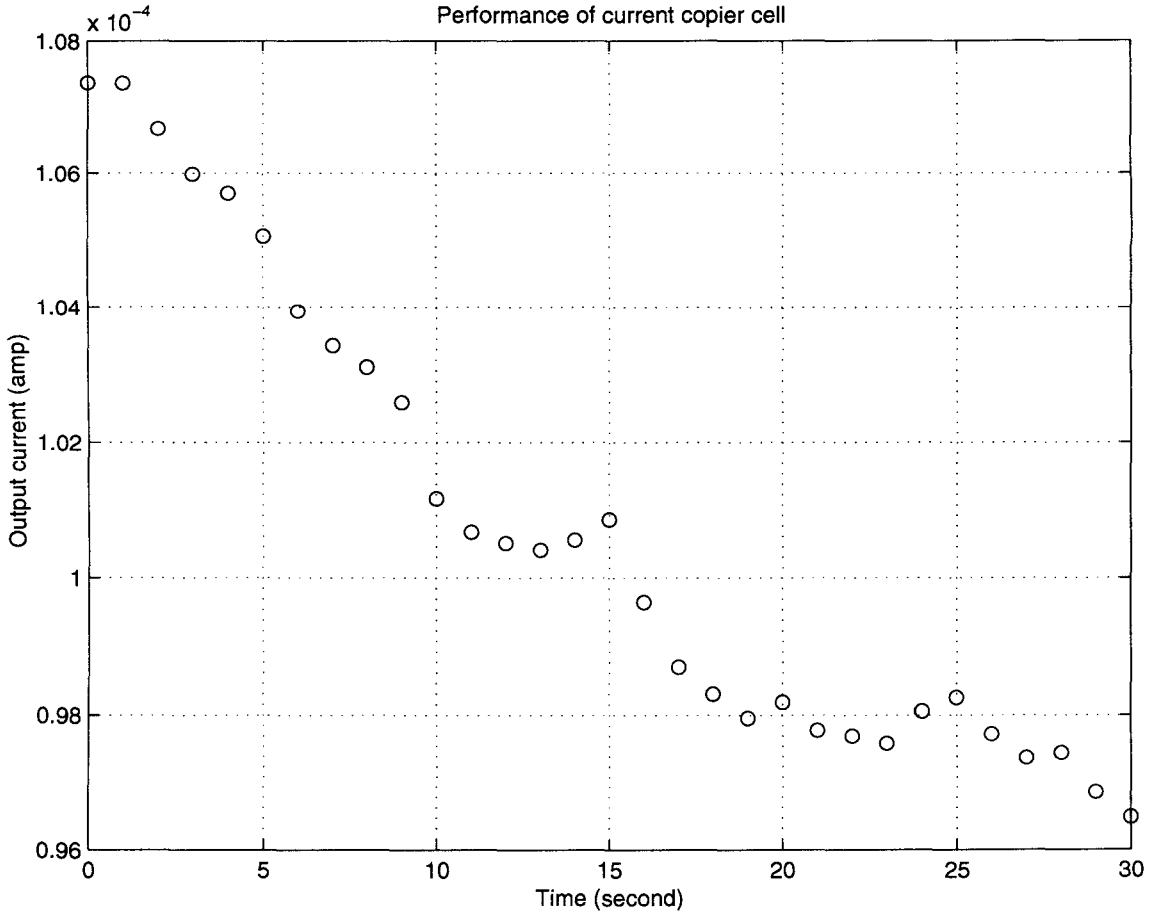


Figure 6.4: Performance of the current copier

equation 6.4, the deviated output current ΔI_{out} is squarely dependent on the leakage voltage ΔV . Also from equation 6.2, ΔV depends linearly on time T as long as the leakage current $I_{leakage}$ is a constant. Therefore, from equation 6.2 and 6.4 one might conclude that ΔI_{out} should have a square relationship with T , which is different from figure 6.4.

The reason is because figure 6.4 shows the first 30 seconds of the HOLD mode of the current copier. In this case ΔV is much smaller than the value of $2V - 2V_T$. Thus equation 6.4 can be approximated as

$$\Delta I_{out} = 2K(V - V_T)\Delta V \quad (6.5)$$

Therefore, the deviated output current ΔI_{out} has a linear dependence on the leakage voltage ΔV , i.e., ΔI_{out} is linearly dependent on T .

Dividing both ends of equation 6.5 by Δt , we can obtain

$$\frac{\Delta I_{out}}{\Delta t} = 2K(V - V_T) \frac{\Delta V}{\Delta t} \quad (6.6)$$

From equation 6.1 $\Delta V/\Delta t = I_{leakage}/C$. So equation 6.6 can be rewritten as

$$\frac{\Delta I_{out}}{\Delta t} = 2K(V - V_T) \frac{I_{leakage}}{C} \quad (6.7)$$

From figure 6.4, we can calculate the value of $\Delta I_{out}/\Delta t$ to be $0.36 \mu\text{A}/\text{second}$. Given the value of K, V, V_T , and C we can calculate the leakage current of the NMOS switch to be roughly 2.1pA .

Chapter 7 Classifier Stage

The final stage of the electronic nose chip is the classifier. The classifier stage receives the Euclidean distances calculated from the signal processing stage. These Euclidean distances represent the similarity between the input pattern and the stored odor patterns. As we have discussed, the shorter the Euclidean distance is, the more similar the input pattern and stored odor pattern is. So these Euclidean distances are compared and the odor corresponding to the shortest Euclidean distance is marked.

There are many ways to achieve the pattern recognition task. The classifier can be implemented to perform serial pattern recognition, but it also can be realized to classify the pattern in parallel. Moreover, correlation associative memory can also be used to provide another technique to pattern recognition. In this chapter these ideas will be discussed but only parallel classifier will be realized in VLSI implementation.

7.1 Serial pattern recognition

The idea of serial pattern recognition is to assign an initial answer to the classification problem, then verify if there is a better answer to the problem. A simple example can be used to illustrate the idea:

A teacher wants to find out who the tallest student is among n students in the classroom. First, he assigns a number to each student and assumes student number 1 is the tallest student in the class. Then, student number 2 is compared with student number 1 to see which one is taller. If student number 1 is taller, he is still assumed to be the tallest student in the class. But if student number 2 is taller, the answer to the question is modified. By repeating this comparison $n - 1$ times the teacher can obtain the final answer who the tallest student is.

The above example displays the fundamental idea of serial pattern recognition. The same idea can be applied to the odor recognition problem.

7.1.1 Description

The odor classification task is very similar to the example. First, the known odors are numbered as class number 1 to class number n for n different known odors. Then, the answer to the odor

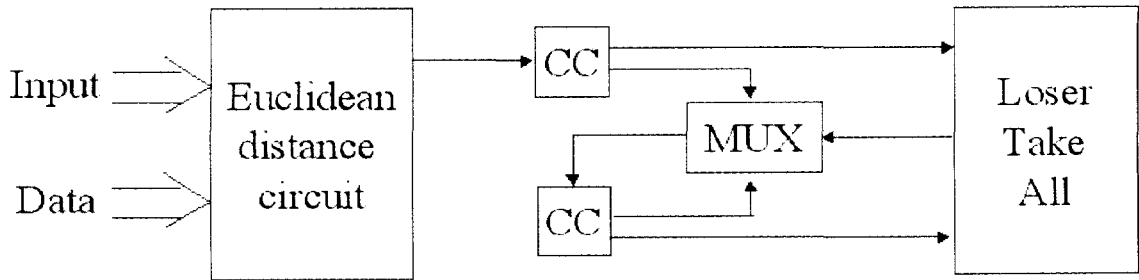


Figure 7.1: Serial pattern recognition

classification is set to be class 1. The Euclidean distance between the input signal vector and the data vectors are calculated for comparison. A simple code used for simulation is shown below:

```

Get  $Eu_1$ ;
Shortest =  $Eu_1$ ;
Answer = 1;
Counter = 1;
for Counter = 1 : n
    Get  $Eu_n$ ;
    If  $Eu_n < Shortest$ 
        Shortest =  $Eu_n$ ;
        Answer = Counter;
    else
        (Nothing changes)
  
```

Figure 7.1 is a simplified block diagram for the realization of serial pattern recognition used in the odor classification task. Input and data are sent to a Euclidean distance circuit. The Euclidean distance calculated is output to the top current copier. This current from the top current copier is compared to another current stored in the bottom current copier by a loser-take-all circuit. The smaller current is sent to the bottom current copier through a feedback loop. In other words, after every comparison, the bottom current copier is used to store the smaller Euclidean distance. This procedure is performed repeatedly until all the known odor patterns are compared and the final decision is made.

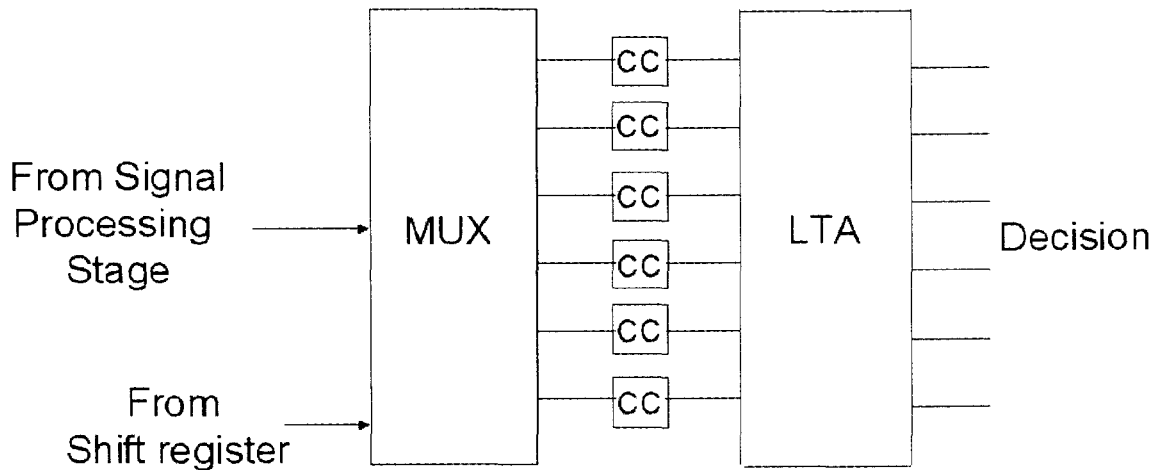


Figure 7.2: Parallel pattern recognition

7.1.2 Advantages and disadvantages

The serial pattern recognition technique has its advantages and disadvantages. As we discussed, to classify the patterns in serial, only two Euclidean distances are used for each comparison. So for a database containing n different odor patterns, $n - 1$ comparisons need to be made, i.e., the time to complete the odor classification task would be significantly longer than that of parallel classification.

On the other hand, since the serial pattern recognition only needs to perform comparison between two currents, the circuit area can be made much smaller than that of parallel pattern recognition.

7.2 Parallel pattern recognition

In contrast to serial pattern recognition, parallel pattern recognition performs the comparison in parallel instead of in serial. Taking our "Who is the tallest student in the class?" question for example, the teacher does not need to set an initial answer and compare the students one by one. Instead, the teacher just simply gathers the student in the schoolyard, makes them stand in a row, and picks up the tallest one. Comparing to serial pattern recognition, only one comparison needs to be done instead of $n - 1$ comparisons provided there are n students in the class.

This is made possible in hardware realization because of the loser-take-all (LTA) circuit. Different from the well-known winner-take-all circuit, LTA circuit raises the output associated with the lowest input while inhibiting all the other outputs.

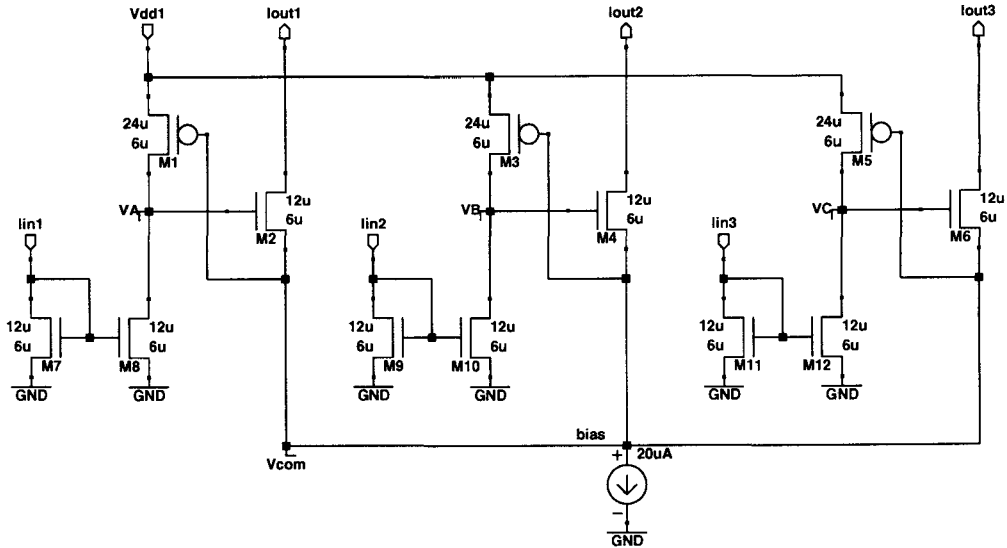


Figure 7.3: Schematic of the Loser-Take-All circuit

Figure 7.2 shows a block diagram for parallel pattern recognition. The Euclidean distances from signal processing stage are sent into different current copiers through the use of a multiplexor controlled by a shift register. All the outputs of current copiers are sent as the input of the LTA circuit. The outputs of the LTA circuit show the final decision for the classification.

7.2.1 Loser-Take-All circuit

Several different winner-take-all circuits[84, 85] and loser-take-all circuits[86] have been reported. Figure 7.3 is a schematic for our loser-take-all circuit. It is based on Patel's LTA circuit. As one can easily distinguish, the three-dimensional LTA circuit is composed of three cells, and each cell is constructed by four transistors. So the LTA circuit can be very easy to extend to multidimension by simply adding four transistors for one more dimension.

To analyze the circuit operation, first assume all the input currents $I_{in1}, I_{in2}, I_{in3}$ are the same for the LTA circuit. Also assume the transistors are perfectly matched. For this situation, V_A, V_B, V_C are equal and the bias current I_{bias} is distributed to the three outputs equally. So $I_{out1} = I_{out2} = I_{out3} = \frac{1}{3}I_{bias}$. Moreover, V_{com} is set accordingly to bias transistor M_1, M_3, M_5 to set the amount of input current.

Now if I_{in1} decreases slightly (assuming V_{com} does not change accordingly at this time, i.e., I_1 does not change), I_1 now is larger than I_{in1} , hence V_A increases to compensate the difference. Since V_{com} does not change, $V_A - V_{com}$ increases, and so does the output current I_{out1} . Since the summation of the output currents is equal to the bias current I_{bias} , the other two output currents decrease to the value $\frac{1}{2}(I_{bias} - I_{out1})$. Since the input currents I_{in2} and I_{in3} do not change, V_{com} is increased to compensate the decrease of the output current.

Moreover, since V_{com} is increased, I_3 and I_5 are decreased accordingly. Since I_{in2} and I_{in3} do not change, V_B and V_C are decreased to compensate the change. Remember V_{com} is increased, and V_B, V_C are decreased, $V_B - V_{com}$ and $V_C - V_{com}$ are decreased even more, so I_{out2} and I_{out3} are decreased even further, hence increases I_{out1} even more. This forms a feedback loop, and the analysis works iteratively until I_{out1} takes all the bias current I_{bias} while I_{out2}, I_{out3} are totally shut down.

As we just discussed, at the steady state, I_{out1} is equal to I_{bias} , while $I_{out2} = I_{out3} = 0$. Moreover, V_A is near the value V_{dd1} and V_B, V_C are close to GND. So adding amplifiers shown in Figure 7.4 after V_A, V_B, V_C ; binary signals can be obtained to indicate which cell the loser is. The losing cell outputs high while all the other cells output low.

7.2.2 Performance

Figure 7.5 displays the performance of a three-dimensional LTA circuit. The bias current is set to 100nA. The input current I_{in1} is set at $1\mu\text{A}$, and the other input current I_{in2} is set at $10\mu\text{A}$. Input current I_{in3} is swept from 10nA to 100uA. When I_{in3} is less than $1\mu\text{A}$, its output I_{out1} takes almost all the 100nA bias current, while shutting down the other two output currents. But at the point I_{in3} becomes larger than $1\mu\text{A}$, I_{out1} takes all the bias current and I_{out3} becomes extremely small. Since I_{in2} is never the lowest input of the circuit, its output is always near zero. The LTA circuit presents very good performance.

Setting V_{dd1} at 2V, the losing cell can be distinguished by reading V_A, V_B , and V_C through the use of amplifiers shown in figure 7.4. By setting V_t at 2.5V the performance is shown in figure 7.6.

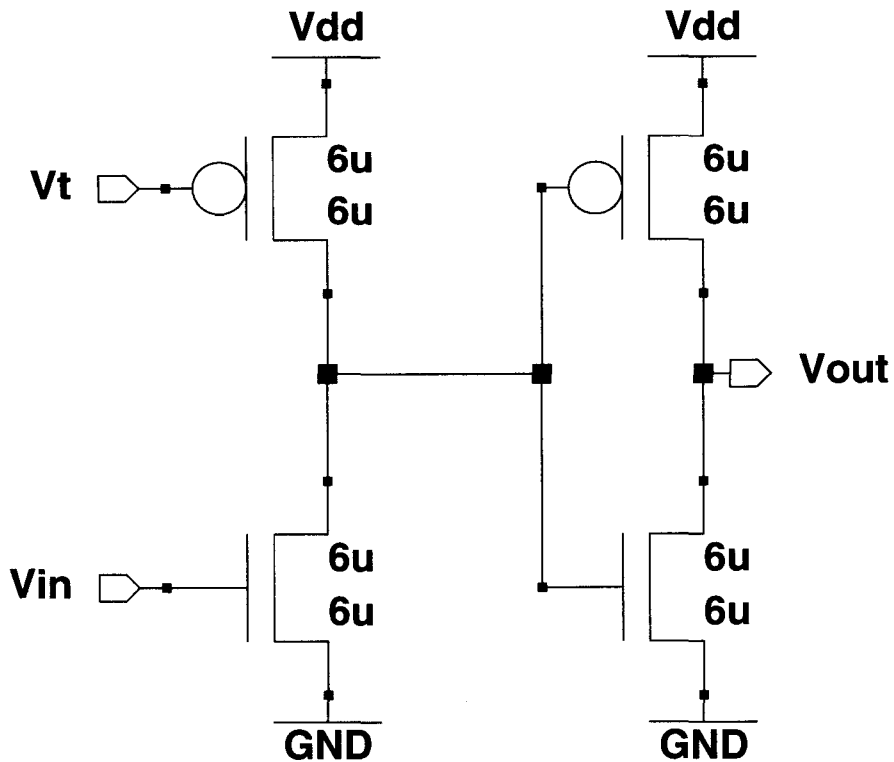


Figure 7.4: Schematic of the output amplifier

The loser-take-all circuit now outputs binary numbers denoting whether the cell is losing. The losing cell outputs 5V(1) while the other cells output 0V(0). This feature makes the outputs of the LTA circuit very easy to read.

7.2.3 Alteration of LTA circuit

An alternative way to build an LTA circuit can be described in two steps: first, a circuit to "invert" the input current is built, i.e., a circuit that outputs higher current if its input is lower. Secondly, an array of "inverse" output currents are sent to a winner-take-all (WTA) circuit. Combining this two circuits result in an LTA circuit as desired.

A divider can be used to invert the input current. For a standard four-transistor divider, the output current has the form

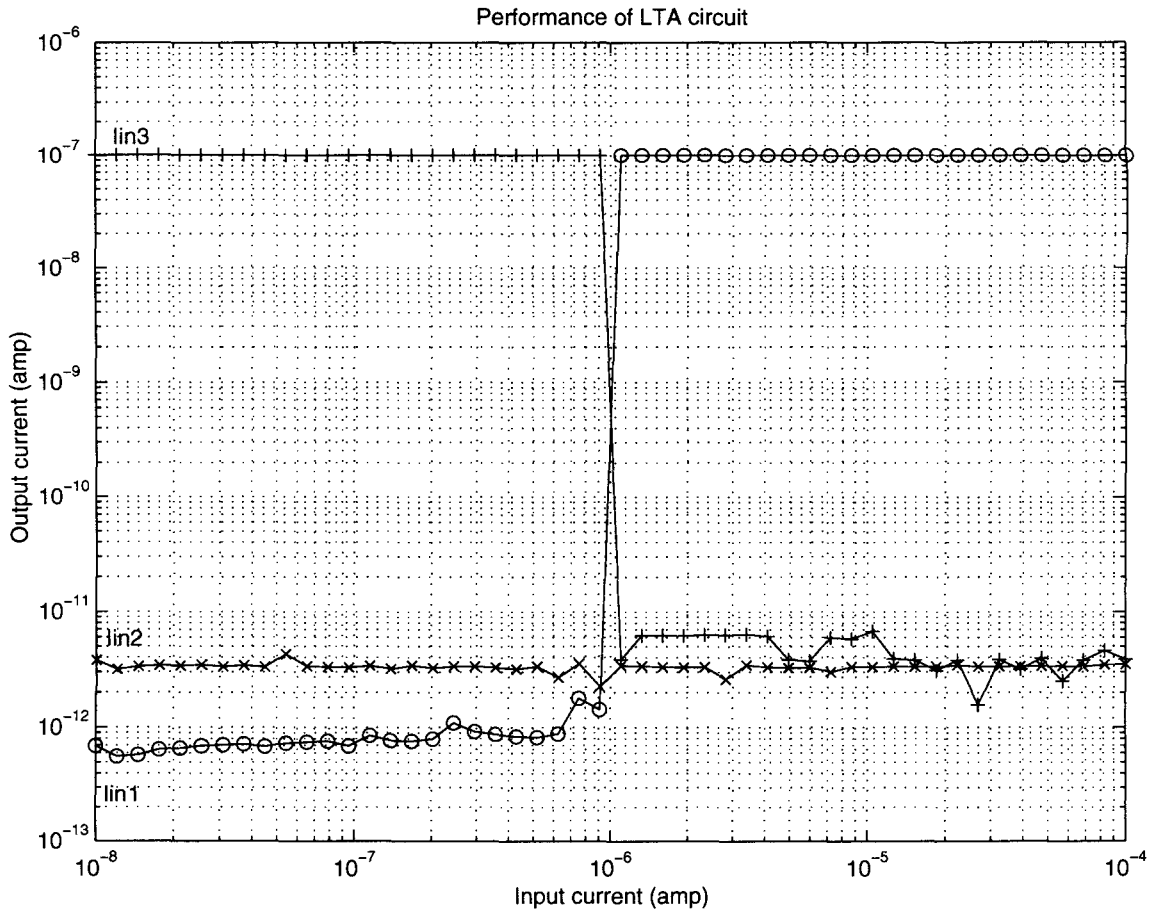


Figure 7.5: Performance of the LTA circuit (current output)

$$I_{out} = \frac{I_{ref1} I_{ref2}}{I_{in}}$$

Therefore, the higher the input current is, the lower the output current. By building n dividers for n Euclidean distance currents, the lowest Euclidean distance current will have the largest output. Performance of the divider is shown in figure 7.7.

A simple WTA circuit[84] is built and its performance is shown in figure 7.8. Contrary to the LTA circuit, the cell with the largest input takes all the bias current while inhibiting all the other cells. An overall performance of the combined circuit, i.e., the "alternative" LTA circuit, is shown in figure 7.9. It is two-dimensional, hence two dividers and a two-dimensional WTA circuit are used.

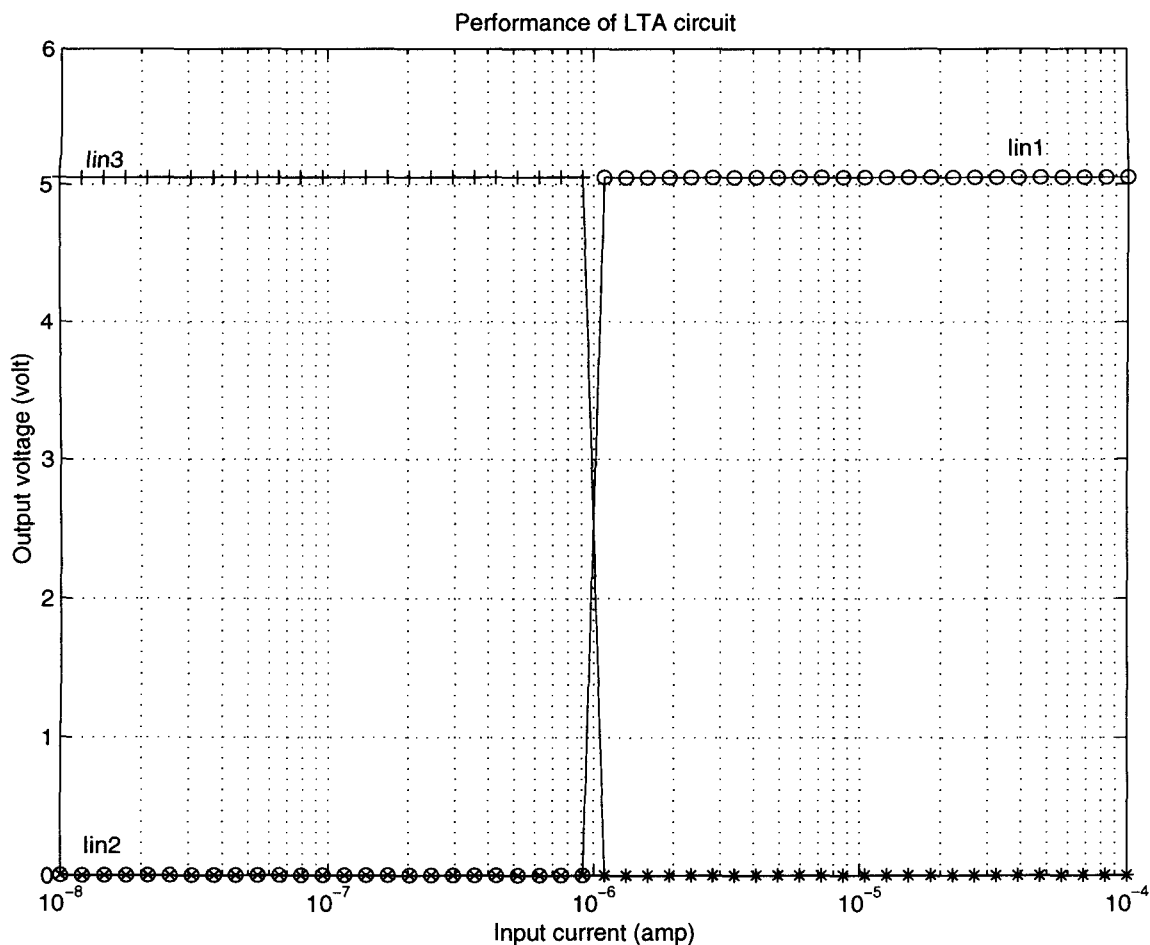


Figure 7.6: Performance of the LTA circuit (voltage output)

7.2.4 Drawback and improvement

The parallel pattern classifier is benefited by the power to process many inputs at the same time at the cost of chip area. The more dimensions the parallel pattern classifier has, the more chip area the circuit requires. It is just the opposite of a serial pattern classifier, which is small in chip area but needs much more time to process the data.

Another drawback of both serial and parallel pattern classifiers is their ambiguity when there are two or more very close inputs. Since the classifiers are based on comparators, so they cannot classify an input when it has almost the same Euclidean distances to two different classes. One way to improve the classifier is to enhance the ability so that it outputs the "probability" to a class instead of an "absolute" output decision. And if the probability to a class is higher than some percentage, the classifier just simply classifies the input to that class. Otherwise the classifier

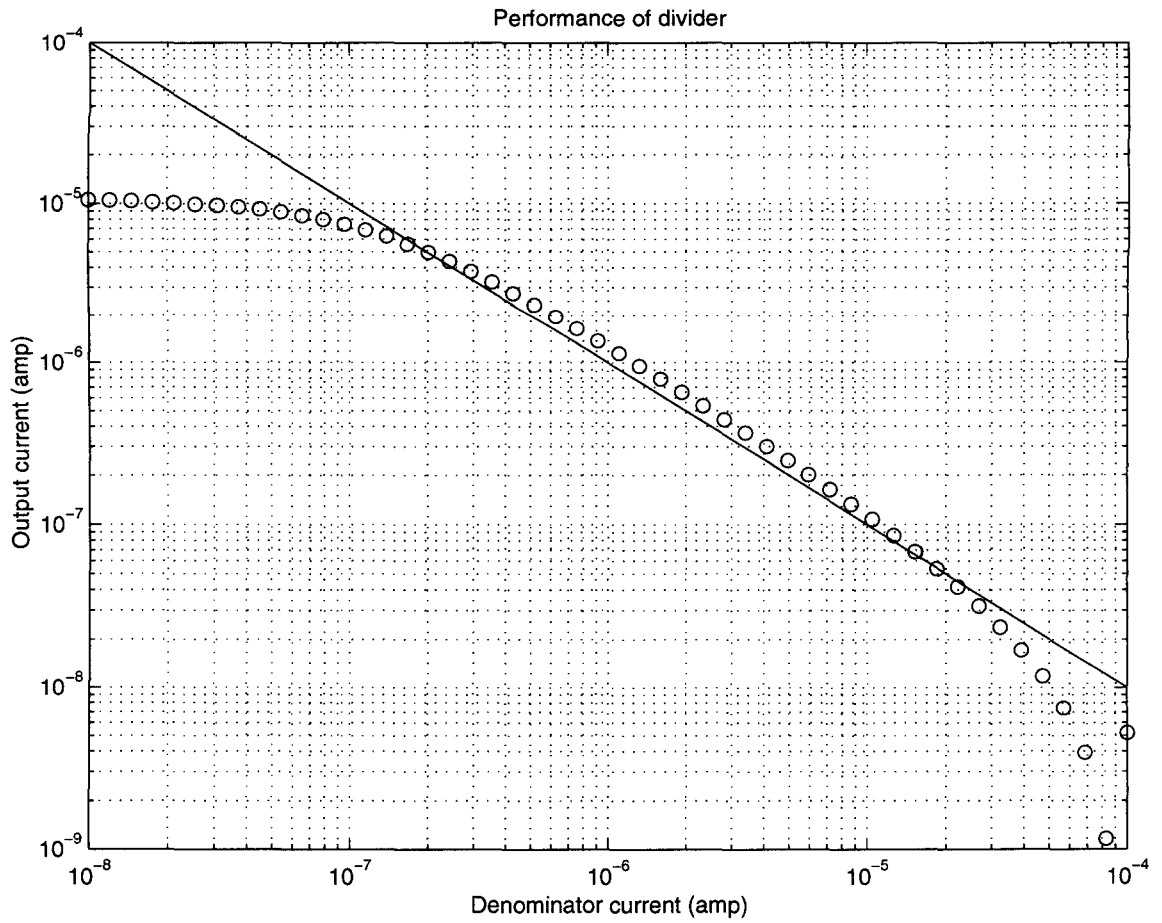


Figure 7.7: Performance of the divider circuit

outputs the probability of a class.

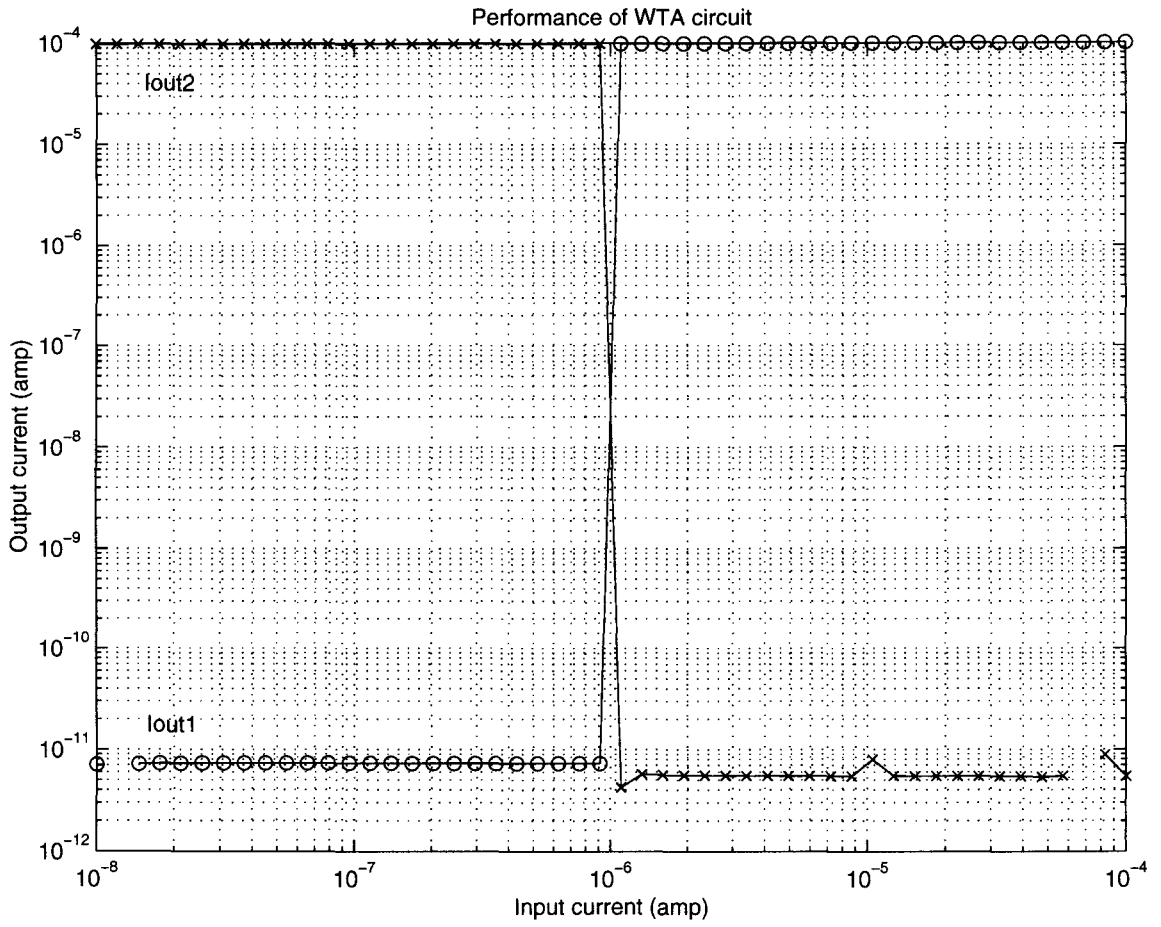


Figure 7.8: Performance of the WTA circuit

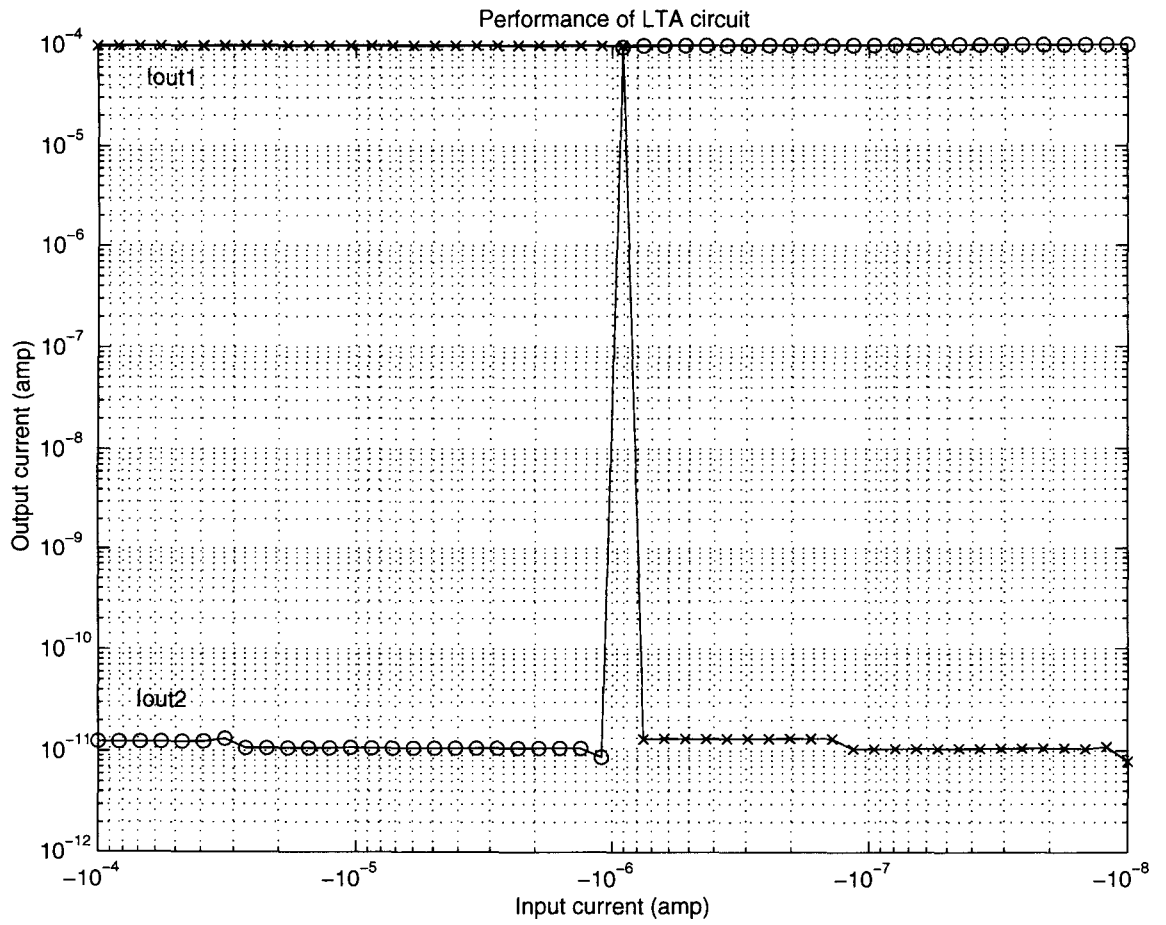


Figure 7.9: Performance of the alternative LTA circuit

Chapter 8 Conclusion

Four stages needed to build an electronic nose chip have been presented in the previous chapters. The sensor stage is constructed to adapt the carbon black-organic polymer sensor to a baseline value that is within suitable working range of the electronic nose chip. A current proportional to the odor concentration is output from the stage. Output currents from an array of sensor stages with different sensors compose a signal vector representing the input odor signature.

This signal vector is normalized using a city-blocks distance normalization circuit in the signal processing stage. During the learning state, this normalized signal vector is stored in a SRAM through the use of an A/D circuit in the database stage. In the sensing state, Euclidean distances between the normalized signal vector and data vectors generated from the database stage are calculated. The Euclidean distances serve as inputs of a loser-take-all circuit in the classifier stage. The shortest Euclidean distance raises the corresponding output and suppresses the others, and the raised output is the final answer to the odor classification task.

The whole electronic nose chip is controlled by a central control unit which generates all the control signals, decides the SRAM address to read/write, and arranges the time sequence of the signals. The control unit discussed in this dissertation is designed for two known patterns stored as three-dimensional vectors, but the final electronic nose chip is designed to store eight different odor patterns. The same principle can be used to extend the chip to more known odor patterns stored as higher-dimensional vectors.

The electronic nose chip is fabricated and its performance is tested. The power dissipation of the chip is measured and discussed. Longitudinal tests for the ability to learn and classify different odors is performed. The minimum detectable concentration of the chip is discussed. Chip response to two different analyte mixtures is measured and discussed. The effects of temperature is stated and discussed. The whole testing setup and the experimentation methodology is provided. At the end of the chapter, scalability to more channels is discussed, and possible future works of the electronic nose chip are introduced.

8.1 Chip performance

Performance of the electronic nose is tested. Power dissipation, longitudinal tests, minimum detectable level, temperature effects, and response to two analyte mixtures are discussed in the following sections.

8.1.1 Power dissipation

Power dissipation is a very important constraint when we want to make a wearable nose. Intuitively one does not want to have a wearable nose whose battery needs to be exchanged every single day. So the requirement of the power dissipation when designing our electronic nose chip is: the lower, the better.

In the real applications, the power dissipation of the electronic nose chip varies as the chip functions in different situations. For example, the power dissipated when the chip is really detecting some odor is different from the power dissipated when the chip is off-running. Moreover, since different odor concentration results in different sensor responses, the power dissipation varies as the odor concentration in our electronic nose chip. This mainly comes from the transconductance amplifier in the sensor stage. The higher concentration is, the higher output current from the transconductance amplifier.

To get a feeling, power dissipation at two different situations are measured. At the first situation, the chip is off-running, i.e. the chip does not detect anything. No odor is applied to the chip, and the power dissipation at this time is measured as 1.3 mW. The second situation is to set all the three sensors to have 100% resistance change. At this time the power dissipation is measured as 7.6 mW. Since our electronic nose chip is designed to detect signal within 100% resistance change as we have stated in section 4.2, the second situation is to measure the maximum power dissipation cost by the chip while the first situation is to measure the minimum.

The power dissipation of ADC0841 is measured as 15 mW and that of DAC0830 is 20 mW. So the electronic nose chip costs less energy than the A/D and D/A converters. We can conclude that most of the power dissipated from the circuits in this dissertation comes from these A/D and D/A converters. In fact, most of the power dissipated from the electronic nose chip itself is the central control unit, which contains mostly digital cells. To reduce the power dissipation to be even lower, on-chip analog memory cells should be implemented instead of SRAM. The instant advantage from doing that is to avoid the need to have A/D and D/A converters that cost most power. Moreover, if the memory cells are integrated on chip, chip interface we discussed in the dissertation can be

	D_x	D_y	D_z		D_{nx}	D_{ny}	D_{nz}
D_{11}	21.60	1.10	1.22	D_{n11}	9.572	0.502	0.558
D_{12}	32.92	1.53	1.71	D_{n12}	9.671	0.453	0.507
D_{13}	13.82	0.81	0.65	D_{n13}	9.563	0.586	0.474
D_{14}	22.51	1.41	1.41	D_{n14}	9.427	0.605	0.607
D_{15}	28.52	1.47	1.56	D_{n15}	9.596	0.503	0.535
D_{16}	17.21	1.07	1.05	D_{n16}	9.424	0.608	0.599
D_{17}	25.10	1.29	1.48	D_{n17}	9.551	0.503	0.578
D_{18}	16.25	0.85	0.95	D_{n18}	9.522	0.519	0.582
D_{19}	41.04	2.75	2.91	D_{n19}	9.375	0.621	0.657
D_{10}	36.72	1.87	2.07	D_{n10}	9.608	0.489	0.542

Table 8.1: Original and normalized data vectors from 10 times exposure to methanol

eliminated and the central control unit can be further reduced. An electronic nose chip with power dissipation in μW range is then expected.

8.1.2 Longitudinal tests

Longitudinal tests for the ability of the electronic nose chip to learn and classify different odors is tested. To test the chip, three different kinds of polymers, poly(N-vinylpyrrolidone), poly(styrene), and poly(ethylene-co-vinyl acetate), are chosen for the polymer sensors for the chip. The signals generated from these three sensors construct the three dimensions for the odor vector. The poly(N-vinylpyrrolidone) sensor denotes x-dimension, the poly(styrene) sensor denotes y-dimension, and the poly(ethylene-co-vinyl acetate) sensor denotes z-dimension. The data patterns from eight different chemicals: methanol(D_1), 2-propanol(D_2), hexane(D_3), ethyl acetate(D_4), acetone(D_5), toluene(D_6), ethanol(D_7), chloroform(D_8), are stored as data vectors in SRAM. Six chemicals: methanol(T_1), 2-propanol(T_2), hexane(T_3), ethyl acetate(T_4), acetone(T_5), benzene(T_6) are used to test the classifying ability of the electronic nose chip. Notice that $T_1 \dots T_5$ are known odor to the chip, while T_6 is a new odor. Therefore, $T_1 \dots T_5$ are used to test if the chip really "learns" the odor, and T_6 is used to test the ability of the chip to distinguish a new odor.

Ten exposures for each odor ($D_1 \dots D_8$) have been measured during a five-day span. Data patterns were taken twice a day, including one time in the morning and the other in the evening. So there are ten un-normalized data patterns for each odor after five days. All the data vectors were normalized in the signal processing stage of the chip. Table 8.1 is an example showing the ten original and normalized data vectors when the sensors were exposed to methanol.

Table 8.2 summarizes the eight data patterns stored in the chip. D_{nx} , D_{ny} , and D_{nz} are the three dimensions for the normalized data vectors ($D_{n1} \dots D_{n8}$) that are stored in SRAM. The magnitude of the stored data vector for each odor is the average over ten normalized data vectors for that

	D_{nx}	D_{ny}	D_{nz}
D_{n1}	9.5309 (0.0940)	0.5389 (0.0599)	0.5639 (0.0527)
D_{n2}	4.6385 (0.1546)	1.6277 (0.1075)	4.4509 (0.1072)
D_{n3}	0.1126 (0.0139)	0.8298 (0.1000)	9.6414 (0.1003)
D_{n4}	1.5783 (0.0724)	3.6545 (0.1120)	5.4855 (0.1401)
D_{n5}	2.3589 (0.0615)	4.7355 (0.1005)	3.6549 (0.0911)
D_{n6}	0.2919 (0.0217)	1.1569 (0.0434)	9.1708 (0.0617)
D_{n7}	7.8921 (0.1155)	1.1466 (0.0747)	1.6271 (0.1157)
D_{n8}	0.7387 (0.0409)	1.0327 (0.0441)	8.9175 (0.1233)

Table 8.2: Average of standard deviation of data vectors stored in the SRAM

specific odor. The standard deviation of the responses over ten trials is given in the parenthesis. The reference current for the normalization circuit is $10\mu\text{A}$. Eight different data vectors are shown in the table. The unit of the table is μA . Figure 8.1 shows the eight normalized data patterns with error bars. Although the values of the un-normalized data vary very much, all the patterns are normalized to range within $10\mu\text{A}$ for comparison.

The classifying ability of the electronic nose chip is tested by running six different chemicals through the chip separately. Six signal vectors ($T_1 \dots T_6$) are generated by the sensor stages, and six normalized signal vectors ($T_{n1} \dots T_{n6}$) are generated in the signal processing stage. The reference current of the normalization circuit is again $10\mu\text{A}$. The original and normalized signal vectors are summarized in table 8.3. The unit of the table is μA . Figure 8.2 shows the six un-normalized test patterns and Figure 8.3 shows six normalized test patterns.

The Euclidean distances between the normalized data vectors and normalized test vectors are calculated by the Euclidean distance circuit in the signal processing stage. The result are summarized in table 8.4. The unit of the table is μA .

The test chemicals $T_1 \dots T_5$, since they are already known odors for the electronic nose chip, can be easily classified into correct groups by the LTA circuit that raises the output cell with the shortest input Euclidean distance. But for benzene (T_6), because it is an unknown chemical to the chip, the chip would classify it to the class which is closest, toluene. One way to improve the chip could be

	T_x	T_y	T_z		T_{nx}	T_{ny}	T_{nz}
T_1	30	1.73	1.83	T_{n1}	9.466	0.552	0.587
T_2	4.4	1.4	4.2	T_{n2}	4.648	1.521	4.522
T_3	0.41	3.4	37.4	T_{n3}	0.107	0.854	9.632
T_4	1.8	4.2	6	T_{n4}	1.616	3.733	5.359
T_5	2.8	5.6	4.2	T_{n5}	2.383	4.741	3.603
T_6	1.6	4.8	33.6	T_{n6}	0.424	1.249	8.956

Table 8.3: Original and normalized test vectors

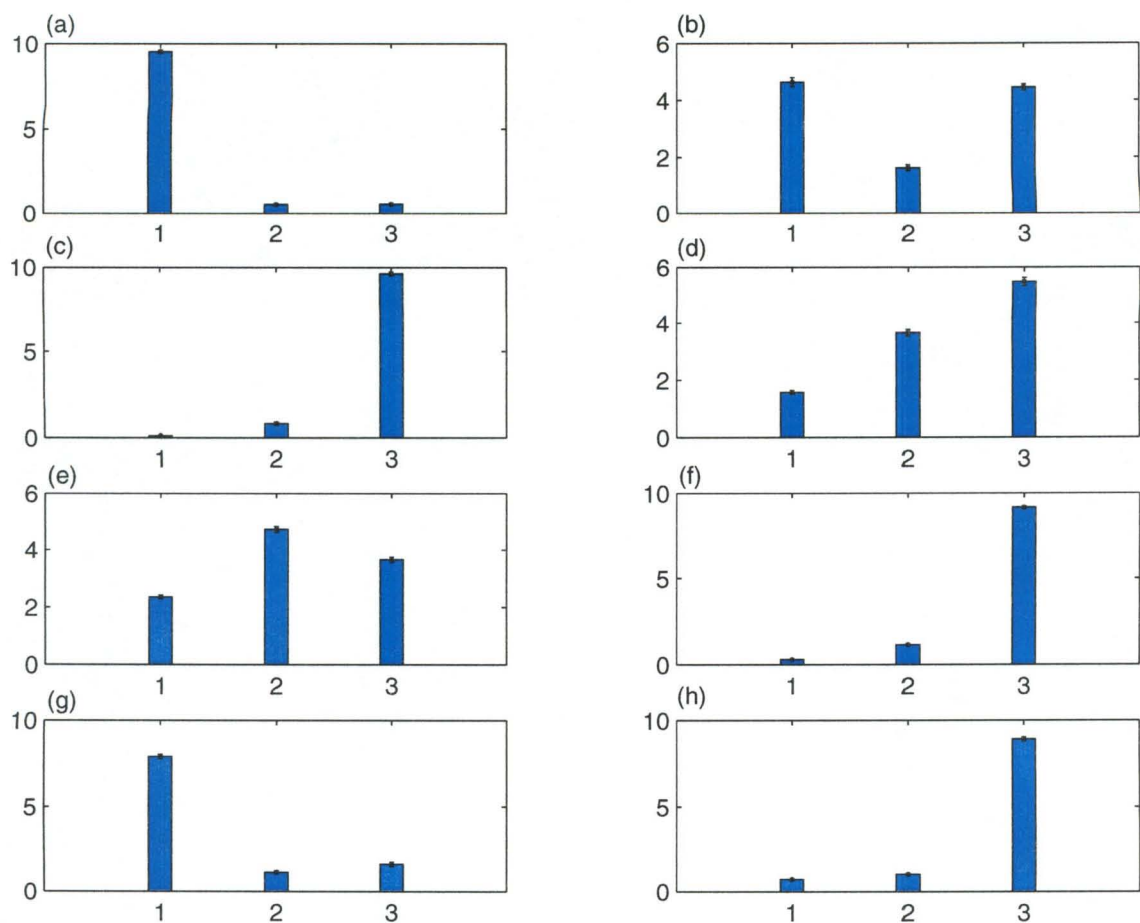


Figure 8.1: Normalized data patterns (a)methanol(D_1), (b)2-propanol(D_2), (c)hexane(D_3), (d)ethyl acetate(D_4), (e)acetone(D_5), (f)toluene(D_6), (g)ethanol(D_7), (h)chloroform(D_8)

to set up a threshold Euclidean distance D_t . If the shortest Euclidean distance is smaller than D_t , the test odor is classified to the class with the shortest distance. Otherwise, a new class is formed and the normalized test vector is stored as the data vector of the new class. In our experiment the threshold Euclidean distance current can be set at $0.25\mu A$.

Figure 8.4 is a three dimensional plot for the eight different normalized data vectors ($D_{n1} \dots D_{n8}$). The three different carbon black-organic polymer sensors form the three dimensions of the plot. From the figure we can see that the data patterns are very well separated. The six normalized test vectors ($T_{n1} \dots T_{n6}$) together with the normalized data vectors are shown in another three dimensional plot in figure 8.5. We can see from the figure that $T_{n1} \dots T_{n5}$ can be classified correctly to $D_{n1} \dots D_{n5}$. For test vector T_{n6} , although it is close to some data patterns (D_{n3}, D_{n6}, D_{n8}), the result is not as good as the other test odors.

	D_{n1}	D_{n2}	D_{n3}	D_{n4}	D_{n5}	D_{n6}	D_{n7}	D_{n8}
T_{n1}	0.127	7.369	15.118	11.418	10.285	14.615	4.884	14.026
T_{n2}	7.536	0.100	8.130	4.606	4.782	7.512	5.987	6.945
T_{n3}	15.247	8.211	0.017	6.234	8.825	0.822	13.551	1.293
T_{n4}	11.463	4.584	6.404	0.193	2.543	5.651	8.517	4.996
T_{n5}	10.374	4.770	8.893	2.796	0.083	8.149	6.846	7.837
T_{n6}	14.441	7.300	1.114	5.194	7.794	0.323	12.599	0.478

Table 8.4: Euclidean distances

8.1.3 Detection threshold

Two steps are taken to determine the detection threshold of the electronic nose chip. First, the minimum detectable signal for the electronics is determined. Then the detection limitation of the polymer sensor is found. By comparing these two limitations the detection threshold of the whole electronic nose chip can be determined.

To determine the minimum detectable signal for the electronics, first realize that the sensor stage outputs a current proportional to the signal interested. From what have been discussed in chapter 4, as long as there is a signal (differential input voltage to the transconductance amplifier), there will be a current output from the sensor stage. These output currents are sent into the city-blocks normalization circuit in the signal processing stage. Since there is a minimum current constraint for the normalization circuit, the minimum detectable signal is limited by the normalization circuit.

From the discussions in the previous chapters, we know that the output of the adaptive circuit is

$$V_p = V_{ref} \left(1 + \frac{dR}{R} \right) \quad (8.1)$$

Remember the inverting input voltage V_n of the transconductance amplifier is V_{ref} , the differential input voltage of the transconductance amplifier is

$$V_{diff} = V_p - V_n = V_{ref} \left(1 + \frac{dR}{R} \right) - V_{ref} = V_{ref} \frac{dR}{R}$$

The minimum input current of the normalization circuit is measured as 40nA. By measuring the relationship between the differential input voltage and output current of the transconductance amplifier, 40nA corresponds to 0.001V differential input voltage. By plugging in the number $V_{ref} = 2V$ the minimum detectable signal $(dR/R)_{min}$ can be determined as 0.05%.

Relationship between the odorant partial pressure and relative sensor resistance change dR/R has been studied by Severin in Nate Lewis' group[87, 88]. According to Severin's study, for a

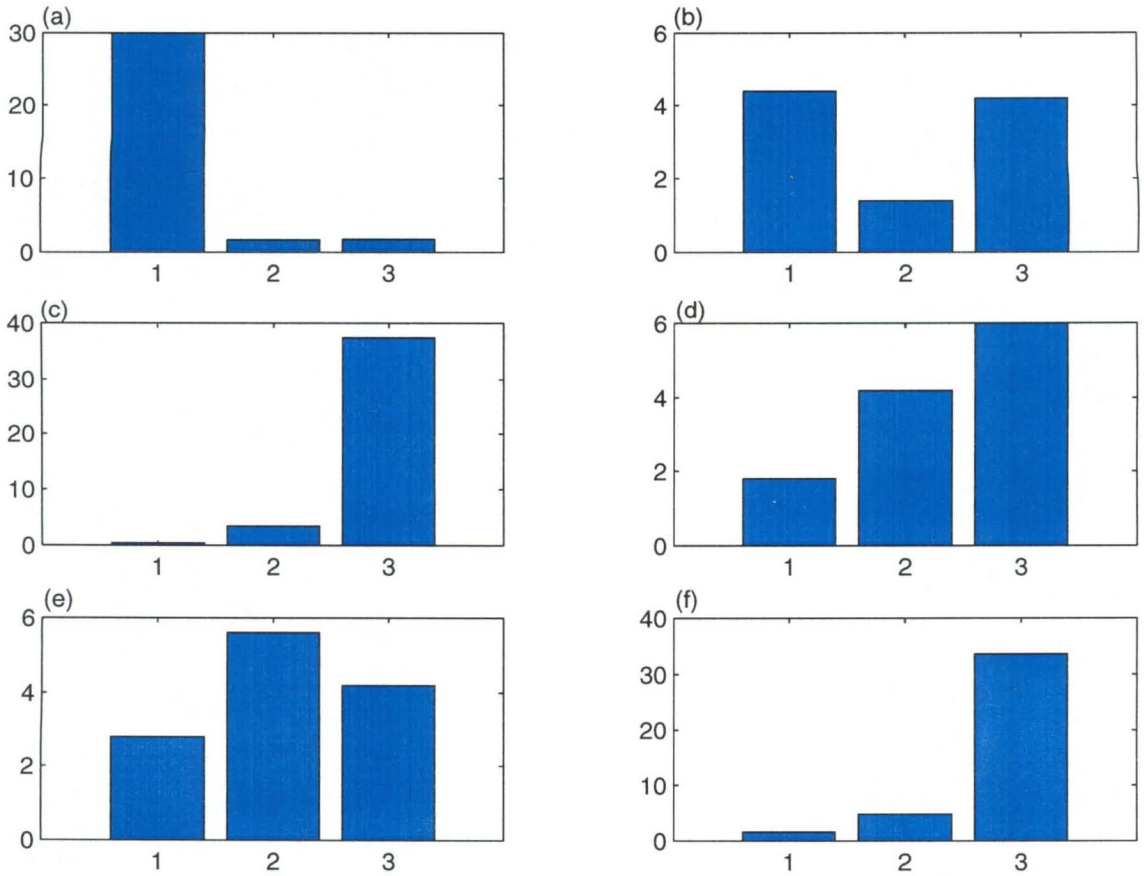


Figure 8.2: Un-normalized test patterns: (a)methanol(T_1), (b)2-propanol(T_2), (c)hexane(T_3), (d)ethyl acetate(T_4), (e)acetone(T_5), (f)benzene(T_6)

homologous series of alcohols ($n - C_nH_{2n+1}OH, 1 \leq n \leq 8$) and a homologous series of alkanes ($n - C_nH_{2n+2}, 5 \leq n \leq 10$ and $n = 12, 14$), 0.05% relative sensor resistance change is corresponding to odorant partial pressure ranging from 0.005 to 0.03.

The detection threshold of the polymer sensor has been investigated by Doleman in Nate Lewis' group at CalTech[89, 90]. The sensor can typically detect a minimum odorant partial pressure of approximately 4×10^{-5} of the odorant's vapor pressure. So the minimum detection level of the polymer sensor is much lower than that of the electronics. Thus we conclude that the detection threshold of the electronic nose chip is limited by the electronics at 0.05% relative differential sensor resistance change (0.005 to 0.03 odorant partial pressure for the odor studied).

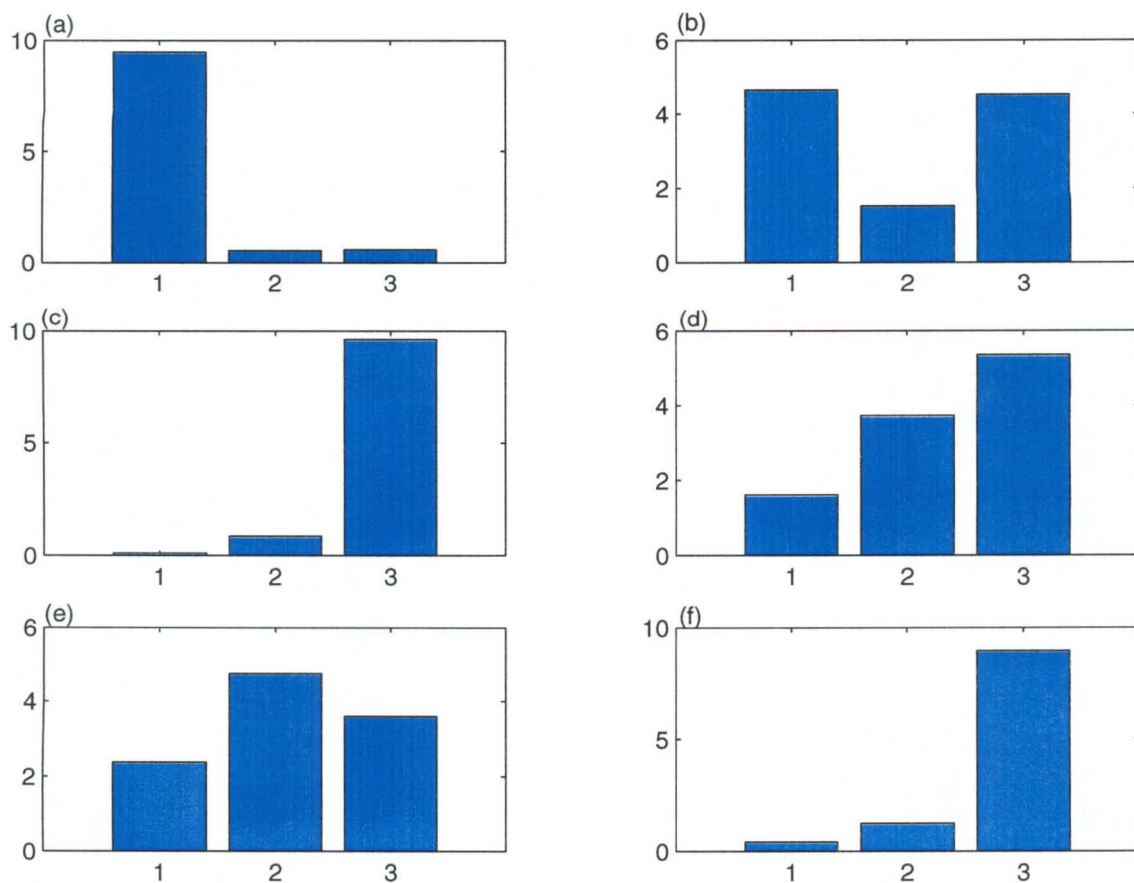


Figure 8.3: Normalized test patterns: (a)methanol(T_1), (b)2-propanol(T_2), (c)hexane(T_3), (d)ethyl acetate(T_4), (e)acetone(T_5), (f)benzene(T_6)

8.1.4 Response to analyte mixtures

Linearity in relative differential resistance versus odor concentration has been described in section 2.4. When a vapor is adsorbed into the polymer detector, the polymer swells and produces an increase in the electrical resistance. Although the absolute value of differential resistance of the sensor is sensitive to the fractional loading of the conductive filler in the insulating polymer of the conductive material, the relative swelling of the film remains constant as long as the filler material does not significantly affect the properties of the insulating portion of the composite. Therefore, for small fractional film swellings, the relative differential resistance dR/R is a linear function of the odor concentration. This is true when a single vapor is applied to the polymer film.

For analyte mixtures, as long as the concentration of analyte molecules is dilute in the polymer film, the relationship between swelling and odor concentration is expected to be linear. It is a

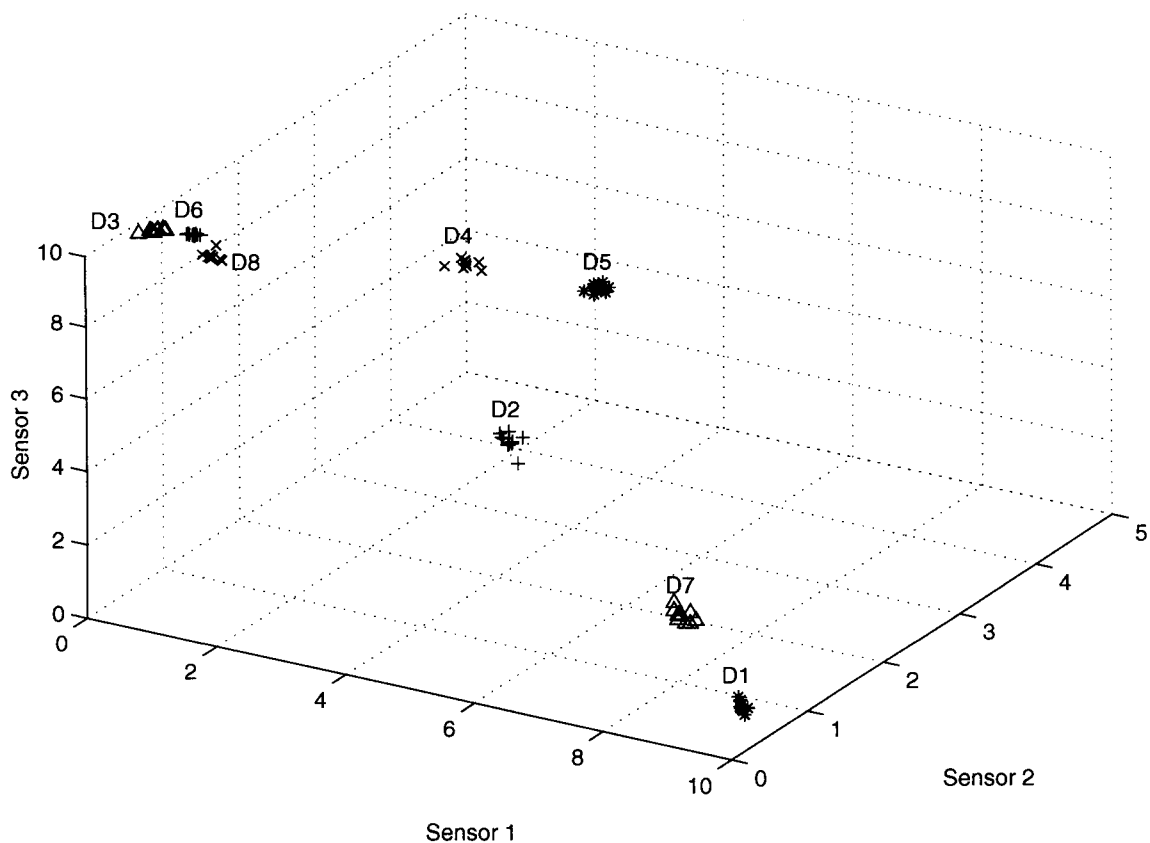


Figure 8.4: 3-D plot of the eight different normalized data patterns

good microscopic description of the signal transduction properties of the detectors when exposed to combinations of the analytes. Therefore, when two vapors in the air are simultaneously applied to the sensors, the relative differential resistance dR/R is the sum of the dR/R values obtained when each vapor is exposed separately to the sensors. Severin has investigated this issue thoroughly [87, 88] and kindly supported us the simulated input data to test the response of the electronic nose chip to analyte mixtures. In the experiment poly(ethylene-co-vinyl acetate), poly(ethylene oxide), and poly(styrene-co-butadiene) are used as sensors. Maximum relative differential resistance responses of the sensor array when exposed to simultaneous mixtures of benzene at $P/P^\circ=0.005, 0.01$, or 0.015 , and heptane at $P/P^\circ=0.005, 0.01$, or 0.015 . The result is shown in figure 8.6. Linearity in relative differential resistance versus odor concentration can be easily observed from the figure.

8.1.5 Temperature dependence

The signal transduction mechanism of the polymer sensor exploits the change in electrical properties of the detector materials caused by exposure to an analyte of interest. In order to affect the electrical

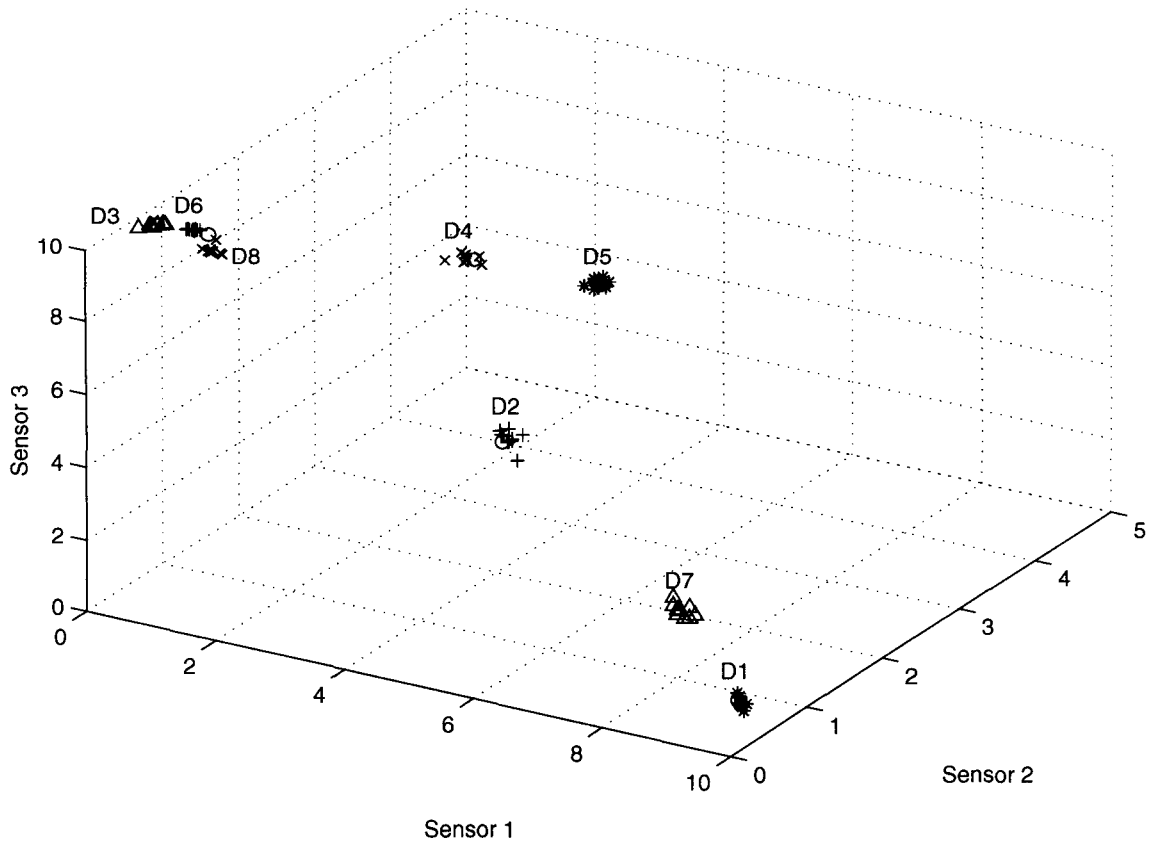


Figure 8.5: 3-D plot of the six normalized test patterns and the eight normalized data patterns. The test points are shown in circles 'o'. From the figure we can see the first five test odor can be classified easily to the correct class, while the 6th test odor still needs some further processing.

characteristics of the sensor, vapor must partition into the polymer film. The partitioning of the vapor into the polymer film has thermodynamic and kinetic components which are expected to be dependent on temperature. It has been observed that the amount of an analyte vapor sorbs into a polymer decreases exponentially with increasing temperature[91]. Therefore, decrease in the differential resistance response of the detectors is expected when increasing the temperature relative to the ambient temperature. This is consistent with the general strategy of lowering the temperature of the detectors relative to the temperature of the analyte vapor to achieve increased sensitivity. Temperature dependence of differential resistance responses exhibited by carbon black-polymer composite chemiresistors have been investigated in chapter 5 of Severin's thesis[88].

By the generosity of Severin to let me use his data as the input signals of my electronic nose chip, the temperature dependence of the nose chip can be examined. Three different polymers, poly(ethylene-co-vinyl acetate)(PEVA), poly(ethylene oxide)(PEO), and poly(4-vinyl phe-

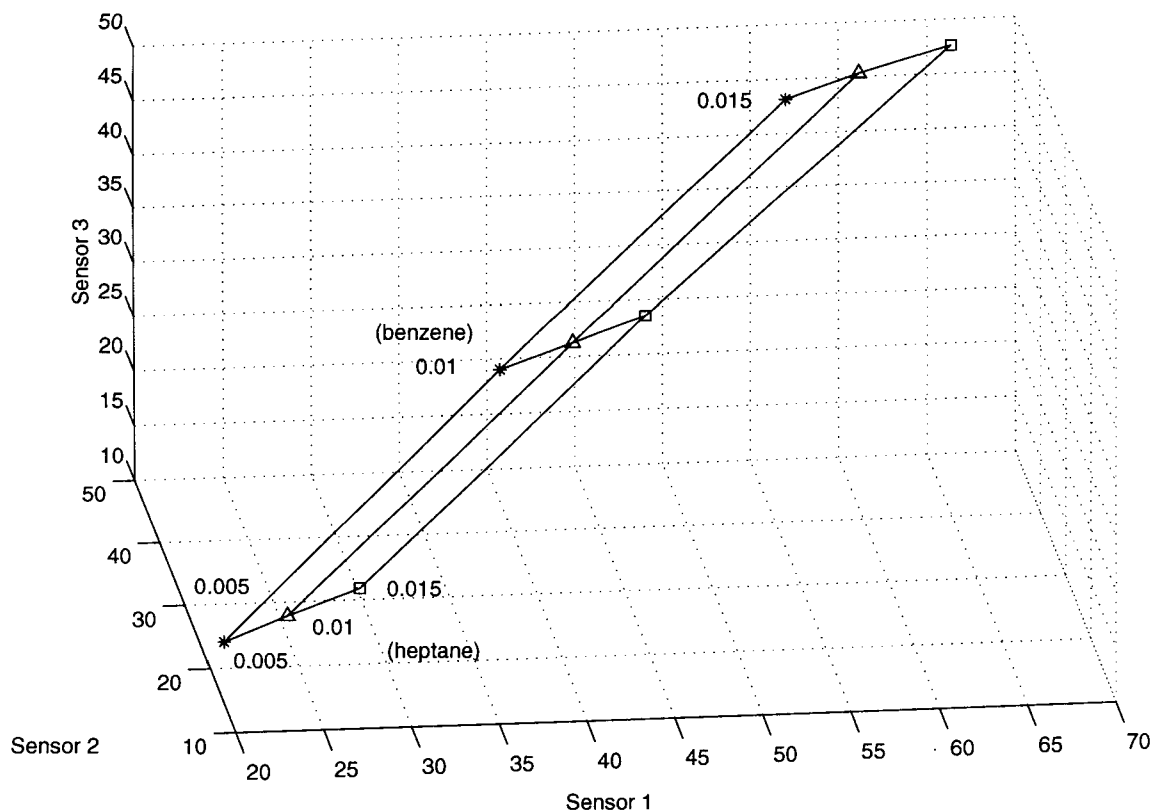


Figure 8.6: Maximum relative differential resistance responses of the sensor array when exposed to simultaneous mixtures of benzene at $P/P^\circ=0.005,0.01$, or 0.015 , and heptane at $P/P^\circ=0.005,0.01$, or 0.015 .

noI)(P4VP) were used as the sensors. Four different chemical vapors, 2-propanol, chloroform, ethanol, and methanol were applied to the polymer sensors at different temperatures. Differential relative resistance change dR/R of the sensors when exposed to different odors at different temperature were measured. In Severin's thesis PEVA was tested at 23° and 46° , PEO was tested at 22° and 47° , P4VP was tested at 23° and 43° . Assuming the temperature effect is not too severe in an one degree temperature change, the sensors can be seen to be tested at two different temperatures 23° and 45° . Therefore, the dR/R data can be applied as the inputs of the chip, and the output currents from the sensor stages are summarized in table 8.5.

Currents in table 8.5 serve as the input current of the normalization circuit, and the normalized currents are shown in figure 8.7. Although the variances of differential resistance response of different polymer sensors due to the change of temperature are not the same, normalized data shown in figure 8.7 still exhibits a good ability for the electronic nose chip to recognize the odor.

		PEVA(23°, 46°)	PEO(22°, 47°)	P4VP(23°, 43°)
2-propanol	23°	33.48	36.18	3.24
	45°	8.78	13.77	2.30
chloroform	23°	92.07	48.20	1.89
	45°	24.30	17.82	1.08
ethanol	23°	25.11	34.70	86.13
	45°	6.62	10.94	32.00
methanol	23°	4.19	18.09	133.92
	45°	7.70	5.81	54.54

Table 8.5: Output currents from 3 sensor stages when applying 8 different odors at different temperatures

8.2 Experimentation methodology

An automation system to measure the performance the circuits discussed in the dissertation have been constructed with three Keithley 236 instruments that can source current while measuring voltage or vice versa, one Keithley 6517 multimeter, and a PC. The Keithley instruments and PC are connected through IEEE-488. MATLAB code have been written to measure V-I or I-V characteristics. Codes have also been written to take the output signal by sweeping an input while maintaining the others. This automation system is used to test performance of the transconductance amplifier, normalization circuit, Euclidean distance circuit, absolute value circuit, and LTA circuit.

Tektronix TDS-420A Four Channel Digitizing Oscilloscope is used to test the performance of the peak detector. HP 8112A pulse generator is used to provide the pulse needed for the regenerative latch, and HP3325A function generator provides input signal for the peak detector to trace. The chip is enabled by HP 3610A DC Power Supply.

Figure 8.8 is the schematic for the electronic nose chip. Three different kinds of sensors are used, so three sensor stages are implemented. A three-dimensional normalizer and a three-dimensional Euclidean distance circuit are built in the signal processing stage. The central control unit introduced in chapter 6 is modified to store more data patterns for the database stage, then a eight-dimensional loser-take-all circuit serves as a nearest neighbor classifier. The three polymer sensors is placed at the terminals denoted *sensor*. *ref* is set at 2V by an off-chip voltage source. *sample* is controlled by a switch, whose value is GND for adaption and Vdd for sensing. *bias1* is set at 1.2V, *bias2* is set at 2V, and *bias* is set at 0.5V by three off-chip voltage sources. *pulse* is provided by a pulse generator with 10kHz frequency. *I_{ref}* is provided by a constant current sink. *C1* and *C2* are provided by a clock generator. *R* is controlled by a switch, whose value is Vdd to reset the electronic nose chip, and GND to enable the chip. *cap*, *c1*, *c2*, *c3*, *c4*, *c5* are external capacitors used to increase the time constants. *I_{out1}* and *I_{out2}* are outputs from LTA circuit.

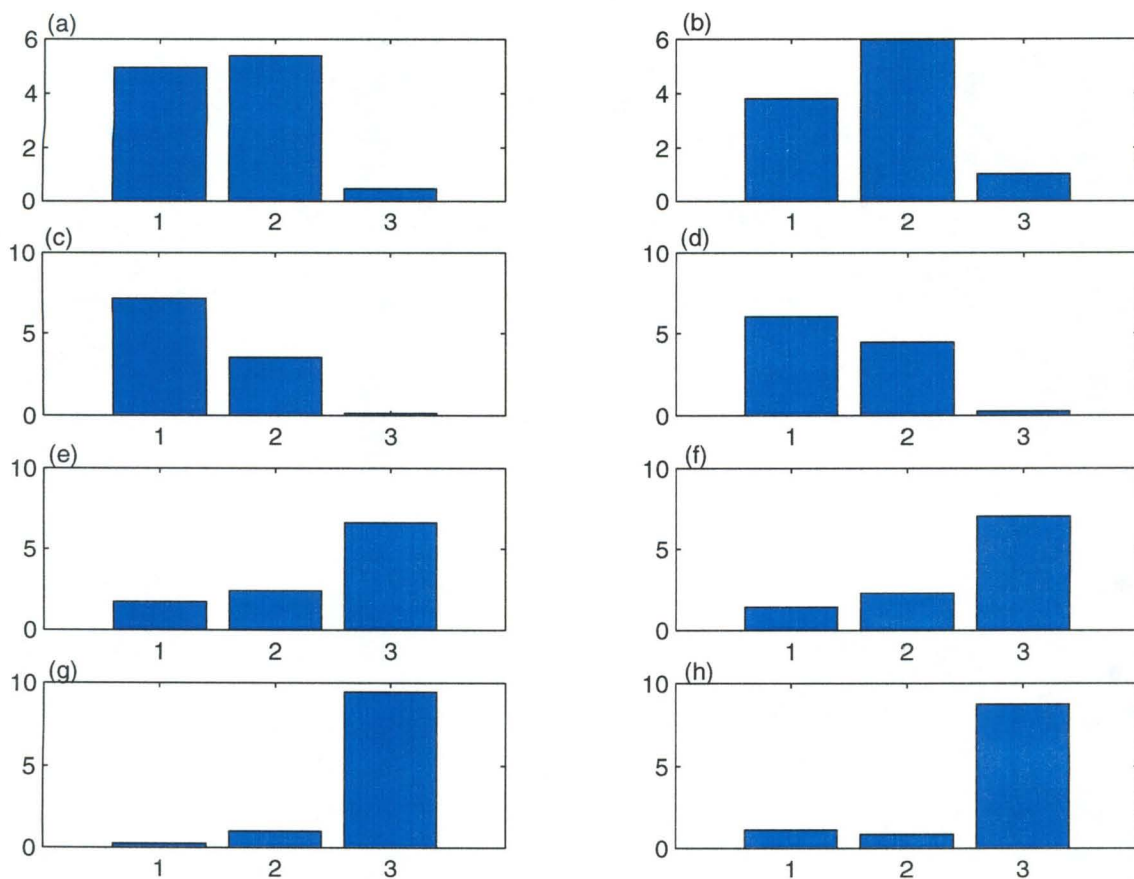


Figure 8.7: Temperature dependence to three polymer sensors (PEVA,PEO,PV4P). All the data are normalized using city-blocks distance normalization. (a)2-propanol, 23° (b)2-propanol, 45° (c)chloroform, 23° (d)chloroform, 45° (e)ethanol, 23° (f)ethanol, 45° (g)methanol, 23° (h)ethanol, 45°

Figure 8.9 shows the actual chip layout for the electronic nose chip. Four stages: sensor stage, signal processing stage, database stage, and classifier stage are labelled, as shown in the figure. The chip is fabricated by 1.2 μm 2-poly 2-metal process at MOSIS. The size of the chip is 2117 μm ×2117 μm .

8.3 Future works

8.3.1 Scalability

This dissertation shows the ability for the electronic nose chip to distinguish eight different odors by using three different carbon black-organic polymer sensors. We conclude that the processing ability of the chip to classify more odors can be enhanced by giving more sample odor patterns to learn and adding more different sensors. By processing more sample odors the database is increased and more

known odors are stored in the nose's memory. On the other hand, adding more different polymer sensors enables the nose chip to explore the odor space more thoroughly.

The chip in this dissertation is designed to process three channels of different polymer sensors. The size of the sensor stage in dimensionless units is 490λ by 940λ , one dimension of the signal processing stage is 220λ by 1230λ , and one dimension of the LTA circuit is 80λ by 100λ . In the $1.2\mu\text{m}$ process used to make the electronic nose chip, λ is equal to $0.6\mu\text{m}$. For one channel of polymer sensor, one sensor stage, one dimension of the signal processing stage, and one dimension of the LTA circuit is needed, i.e. $739200\lambda^2$ chip area is required for one polymer sensor. Therefore for a $1\text{cm} \times 1\text{cm}$ chip, circuits for 375 channels of polymer sensors can be implemented. If we take the chip area of wires and central control unit of the chip, we can confidently conclude that circuits for 300 channels of different polymer sensors can be implemented in a $1\text{cm} \times 1\text{cm}$ chip easily in terms of chip area consideration.

Scalability of the nose chip not only depends on chip area, but also on power dissipation. Remember 7.3mW is needed for a three polymer sensor chip. To implement a 300 polymer electronic nose, over 2W power dissipation is expected. This is undesired especially for our goal to build a wearable nose. Since it is relatively easy and cheap to have many polymers for the nose chip, the constraint of scalability of the electronic nose chip is on the power dissipation. Therefore, a 16 channel polymer sensor electronic nose chip is suitable for the goal towards a wearable nose and its power dissipation is expected to be within 25mW . Further reduction of power dissipation can be achieved by fully integration of the electronic nose chip.

8.3.2 Full integration

As we discussed in the subsection of power dissipation, to reduce the power cost by the electronic nose chip, one solution is to implement on-chip analog memory cells instead of digital memories. The first reason is because the analog memory costs much less power than its digital counterpart. In addition, by storing data in analog form the use of A/D and D/A converters, which cost most of the power, can be avoided. Finally, since the memory cell is on chip, chip interface can be highly eliminated, resulting in a much simpler central control unit, which is composed mostly of digital cells. Therefore, investigation of on-chip analog memory cells is one of the important future works of the 2nd generation electronic nose chip[76, 77, 78, 79].

To move toward a wearable electronic nose, in addition to on-chip analog memory cells, two elements need to be implemented on chip as well. The first thing is the polymer sensor. Discrete sensors have been used throughout this dissertation. So full integration of the electronic nose chip

would require the polymer sensors to be on chip with the electronics.

The other category that is not on chip in the first generation electronic nose chip is the reference voltages used in several different circuits. There have been a number of approaches that have been taken to realize voltage references in integrated circuits. One way to make a voltage reference is to use a zener diode that breaks down at a known voltage when reverse biased[92]. But it is not popular nowadays because the breakdown voltage of a zener diode is typically larger than the power supplies in modern circuits. The difference in the threshold voltage between an enhancement transistor and a depletion transistor has been used to build the voltage reference, too[93]. But it is not popular either because the actual value of the reference voltage is difficult to determine accurately because of the process sensitivity of the difference between the threshold voltage of an enhancement transistor and a depletion transistor. Another way is the bandgap voltage reference, which is the most popular for both bipolar and CMOS technologies today[94, 95, 96, 97]. All the reference voltage needed by the electronic nose chip can be implemented by building bandgap voltage references on chip.

Therefore, the 2nd generation electronic nose chip could be focused on building on-chip analog memory cells, integrated on-chip polymer sensors, and bandgap voltage references. To this point everything that is off-chip for the 1st generation electronic nose chip will be integrated on the same chip with less power dissipation, heading towards our goal to build up a wearable nose.

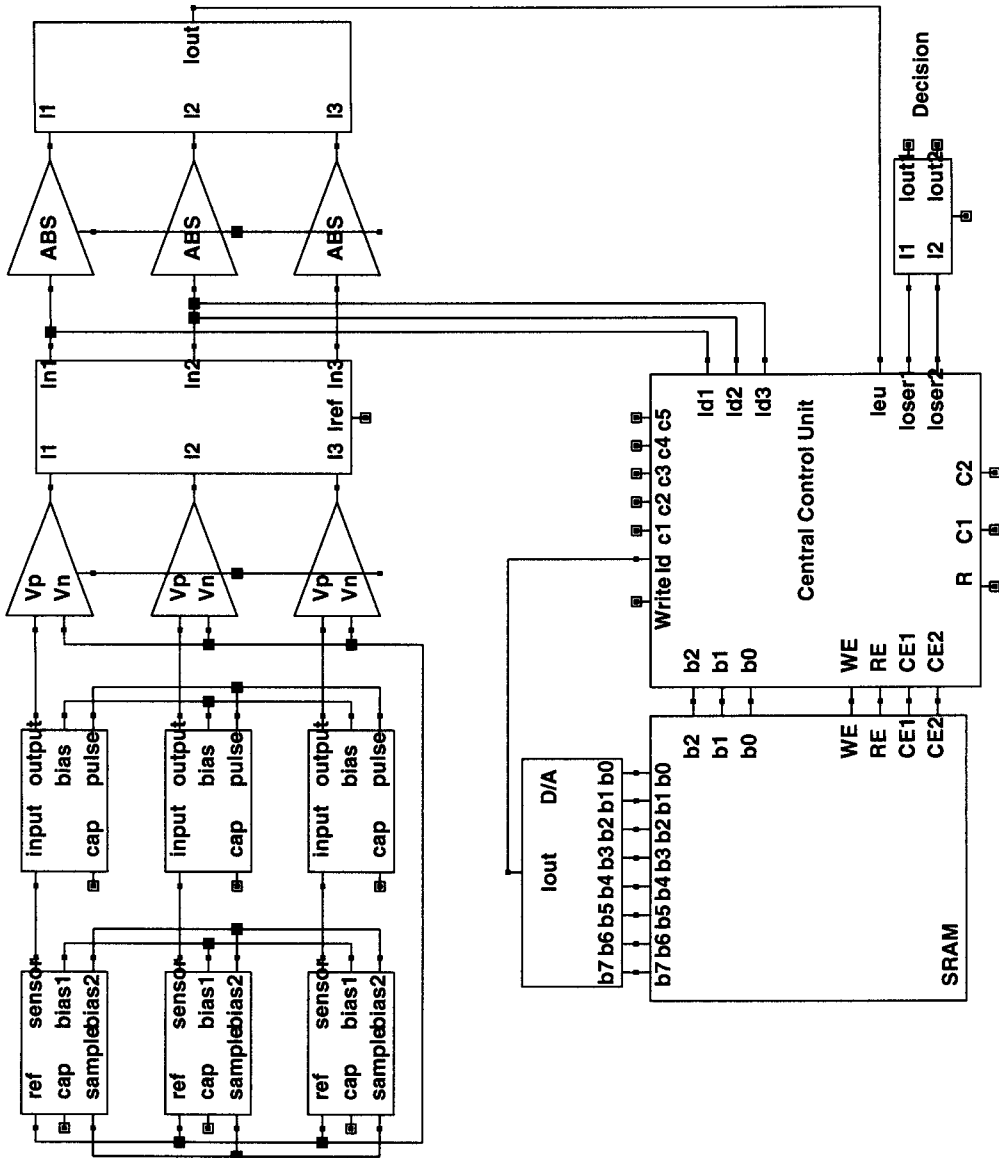


Figure 8.8: Circuit diagram for the electronic nose chip

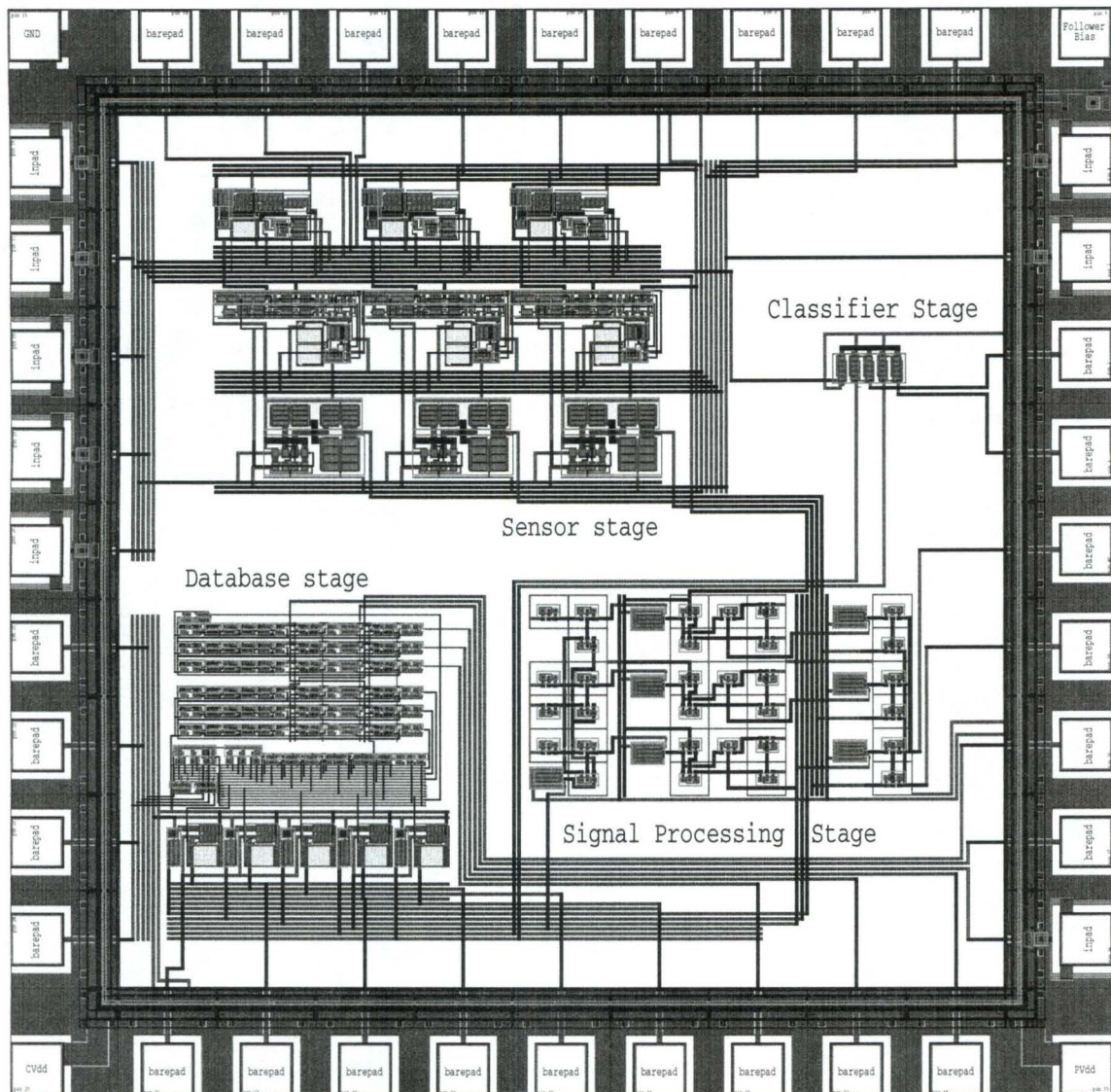


Figure 8.9: electronic nose chip Layout

Bibliography

- [1] Llobet, E.; Hines, E.L.; Gardner, J.W.; Franco, S. "Non-destructive banana ripeness determination using a neural network-based electronic nose" *Meas. Sci. Technol.* **1999**, 10, p.538.
- [2] Hines, E.L.; Llobet, E.; Gardner, J.W. "Neural network based electronic nose for apple ripeness determination" *Electronics Letters* **1999**, 35, p.821.
- [3] Gardner, J.W.; Shin, H.W.; Hines, E.L.; Dow, C.S. "An electronic nose system for monitoring the quality of potable water" *Sensors and Actuators* **2000**, B69, p.336.
- [4] Shin, H.W.; Llobet, E.; Gardner, J.W.; Hines, E.L.; Dow, C.S. "Classification of the strain and growth phase of cyanobacteria in potable water using an electronic nose system" *IEE Proceedings-Science Measurement and Technology* **2000**, 147(4), p.158.
- [5] Gardner J.W.; Craven, M.; Dow, C.; Hines, E.L. "The prediction of bacteria type and culture growth phase by an electronic nose with a multi-layer perceptron network" *Meas. Sci. Technol.* **1998**, 9, p.120.
- [6] Gardner, J.W.; Hines, E.L.; Molinier, F.; Bartlett, P.N.; Mottram, T.T. "Prediction of health of dairy cattle from breath samples using neural network with parametric model of dynamic response of array of semiconducting gas sensors" *IEE Proceedings-Science Measurement and Technology* **1999**, 146(2), p.102.
- [7] Gardner, J.W.; Shin, H.W.; Hines, E.L. "An electronic nose system to diagnose illness" *Sensors and Actuators* **2000**, B70, p.19.
- [8] Moncrieff, R.W. "An instrument for measuring and classifying odours" *J. Appl. Physiol.* **1961**, 16, p.742.
- [9] Wilkens, W.F.; Hatman, A.D. "An electronic analog for the olfactory processes" *Ann. NY Acad. Sci.* **1964**, 116, p.608.
- [10] Buck, T.M.; Allen, F.G.; Dalton, M. "Detection of chemical species by surface effects on metals and semiconductors" *Spartan Books Inc., USA* **1965**.
- [11] Dravnieks, A.; Trotter, P.J. "Polar vapour detection based on thermal modulation of contact potentials" *J. Sci. Instrum.* **1965**, 42, p.624.

- [12] Persaud, K.; Dodd, G. "Analysis of discrimination mechanisms of the mammalian olfactory system using a model nose" *Nature* **1982**, 299, p.352.
- [13] Ikegami, A.; Kaneyasu, M. "Olfactory detection using integrated sensors" *Proc. 3rd Int. Conf. Solid-State Sensors and Actuators (Transducers'85), Philadelphia, PA, USA, June 7-11 1985*, p.136.
- [14] Kaneyasu, M.; Ikegami, A.; Arima, H.; Iwanga, S. "smell identification using a thick-film hybrid gas sensor" *IEEE Trans. Components, Hybrids Manufact. Technol., CHMT-10* **1987**, p.267.
- [15] Gardner, J.W. "Pattern recognition in the Warwick Electronic Nose", *8th Int. Congress of European Chemoreception Research Organisation, University of Warwick, UK, July 1987*.
- [16] Gardner, J.W.; Bartlett, P.N.; Dodd, G.H.; Shurmer, H.V. "The design of an artificial olfactory system" *Chemosensory Information Processing, NATO ASI Series H: Cell Biology* **1990**, 39, p.131.
- [17] Gardner, J.W.; Bartlett, P.N. "Sensors and Sensory Systems for an Electronic Nose" *NATO ASO Series E: Applied Sciences* **1992**, 212.
- [18] Aishima, T. "Aroma discrimination by pattern recognition analysis of responses from semiconductor gas sensor arrays" *J. Agri. Food Chem.* **1991**, 39, p.752.
- [19] Hoffheins, B.S. "Using sensor arrays and pattern recognition to identify organic compounds" *MS Thesis, University of Tennessee, Knoxville, USA* **1989**
- [20] Abe, H.; Yoshimura, T.Y.; Kanaya, S.; Takahashi, Y.; Miyashita, Y.; Sasaki, S. "Automated odor-sensing system based on plural semiconductor gas sensors and computerised pattern recognition techniques" *Anal. Chim. Acta* **1987**, 194, p.1.
- [21] Shurmer, H.V.; Gardner, J.W. "Intelligent vapour discrimination using a composite 12-element sensor array" *Sensors and Actuators, B1* **1990**, p.256.
- [22] Pearce, T.C.; Gardner, J.W.; Friel, S.; Bartlett, P.N.; Blair, N. "Electronic nose for monitoring the flavour of beers" *Analyst* **1993**, 118, p.371.
- [23] Persaud, K.C. "Electronic gas and odour detectors that mimic chemoreception in animals" *Trends Anal. Chem.* **1992**, 11, p.61.
- [24] Slater, J.M.; Paynter, J.; Watt, E.J. "Multi-layer conducting polymer gas sensor arrays for olfactory sensing" *Analyst* **1993**, 118, p.379.
- [25] Freund, M.S.; Lewis, N.S. "A chemically diverse conducting polymer-based electronic nose" *Proc. Natl. Acad. Sci. USA* **1995**, 92, p.2652.

- [26] Slater, J.M.; Paynter, J. *Analyst* **1994**, 119, p.191.
- [27] Slater, J.M.; Watt, E.J. *Analyst* **1991**, 116, p.1125.
- [28] Ohnishi, M.; Ishibashi, T.; Kijima, Y.; Ishimoto, C.; Seto, J. "A molecular recognition system for odorants incorporating biomimetic gas-sensitive devices using Langmuir-Blodgett films" *Sensors Mater.* **1992**, 4(1), p.53.
- [29] Ballantine, D.S.; Rose, S.L.; Grate, J.W.; Wohltjen, H. "Correlation of surface acoustic wave device coating responses with solubility properties and chemical structure using pattern recognition" *Anal. Chem.* **1986**, 58, p.3058.
- [30] Baltes, H.; Lange, D.; Koll, A. "The electronic nose in Lilliput" *IEEE Spectrum* **1998**, september, p.35.
- [31] Dickinson, T.A.; White, J.; KaJ.S.; Walt, D.R. "A chemical-detecting system based on a cross-reactive optical sensor fiber" *Nature* **1996**, 382, p.697.
- [32] Dickinson, T.A.; Michael, K.L.; Kauer, J.S.; Walt, D.R. "Convergent, self-encoded bead sensor arrays in the design of an artificial nose" *Anal. Chem.* **1999**, 71, p.2192.
- [33] Nagle, H.T.; Schiffman, S.S.; Gutierrez-Osuna, R. "The how and why of electronic noses" *IEEE Spectrum* **1998**, september, p.22.
- [34] Hatfield, J.V.; Neaves, P.; Hicks, P.J.; Persaud, K.; Travers, P. "Towards an integrated electronic nose using conducting polymer sensors" *Sensors and Actuators* **1994**, B18-19, p.221.
- [35] Cole, M.; Gardner, J.W.; Lim, A.W.Y.; Scivier, P.K.; Brignell, J.E. "Polymeric resistive bridge gas sensor array driven by a standard cell CMOS current drive chip" *Sensors and Actuators* **1999**, B58, p.518.
- [36] Dickson, J.A.; Freund, M.S.; Lewis, N.S.; Goodman, R.M. "An integrated chemical sensor array using carbon black polymers and a standard CMOS process" *Technical Digest, Solid State Sensor and Actuator Workshop* **2000**, p.162.
- [37] Dickson, J.A.; Goodman, R.M. "Integrated chemical sensors based on carbon black and polymer films using a standard CMOS process and post-processing" *2000 IEEE International Symposium on Circuits and Systems*
- [38] Reed, R. R. *Neuron* **1992**, 8, 205.
- [39] Lancet, D.; Ben-Arie, N. *Curr. Biol.* **1993**, 3, 668.
- [40] Freund, M.S.; Lewis, N.S. *Proc. Natl. Acad. Sci. U.S.A.* **1995**, 92, 2652.

- [41] Shurmer, H. V.; Gardner, J. W. *Sens. Actuators B* **1992**, 8, 1.
- [42] Newman, A.R. *Anal. Chem.* **1991**, 63, A586.
- [43] Nakamoto, T.; Fukuda, A.; Moriizumi, T. *Sens. Actuators B* **1993**, 10, 85.
- [44] Ruschau, G.R.; Newnham, R.E.; Runt, J.; Smith, B.E. *Sens. Actuators* **1989**, 20, 269.
- [45] Talik, P.; Zabkowskawaclawek, M.; Waclawek, W. *J. Mater. Sci.* **1992**, 27, 6807. Lonergan, M.C.;
- [46] Doleman, B.J.; Sanner, R.D.; Severin, E.J.; Robert, H.G.; Lewis, N.S. *Anal. Chem.* **1998**, 70, 2560.
- [47] Severin, E.J.; Doleman, B.J.; Beaber, S.A.; Grubbs, R. H.; Lewis, N.S. *Chem. Mater.* **1996**, 8, 2298.
- [48] Doleman, B.J.; Lonergan, M.C.; Severin, E.J.; Vaid, T.P.; Lewis, N.S. *Anal. Chem.* **1998**, 70, 4177.
- [49] Severin, E.J.; Lewis, N.S. *Anal. Chem.* **2000**, 72, 2008.
- [50] Shurmer, H.V.; Corcoran, P.; James, M.K. *Sens. Actuators B* **1993**, 16, 256.
- [51] Doleman, B.J.; Severin, E.J.; Lewis, N.S. *Proc. Natl. Acad. Sci. USA* **1998**, 95, 5442.
- [52] Zaromb, S.; Stetter, J.R. *Sens. Actuators* **1984**, 6, 225.
- [53] Lundstrom, I; Erlandsson, R.; Frykman, U.; Hedborg, E.; Spetz, A.; Sundgren, H.; Welin, S.; Winqvist, F. *Nature* **1991**, 352, 47.
- [54] Norman, R.H. *Conductive Rubbers and Plastics* Elsevier: Amsterdam, 1970.
- [55] Medalia, A.I. *Rubber Chem. Technol.* **1986**, 59, 432.
- [56] Kirkpatrick, S. *Rev. Mod. Phys.* **1973**, 45, 574.
- [57] Lundberg, B.; Sundqvist, B. *J. Appl. Phys* **1986**, 60, 1074.
- [58] Jachym, B.J. *Carbon Black-Polymer Composites* Sichel, E. K., Ed.; Marcel Dekker, Inc.; New York, 1982; p 103.
- [59] Reboul, J. P. *Carbon Black-Polymer Composites* Sichel, E. K., Ed.; Marcel Dekker, Inc.; New York, 1982; p 79.
- [60] Surakamponorn, W.; Riewruja, V.; Kumwachara, K.; Surawatpunya, C.; Anuntahirunrat, K. "Temperature-Insensitive Voltage-to-Current Converter and Its Applications" *IEEE Transactions on instrumentation and measurement* **1999**, 48, pp.1270.

- [61] Szczepanski, S.; Wyszynski, A.; Schaumann, R. "Highly Linear Voltage-Controlled CMOS Transconductors" *IEEE Transactions on circuits and systems - I. Fundamental theory and applications* **1993**, 40, pp.258.
- [62] Opris, I.E.; Kovacs, G.T.A. "Large-signal subthreshold CMOS transconductance amplifier" *Electronics Letters* **1995**, 31, pp.718.
- [63] Wang, Z. "Novel linearisation technique for implementing large-signal MOS tunable transconductor" *Electronics Letters* **1990**, 26, pp.138.
- [64] Czarnul, Z.; Tsvividis, Y. "MOS tunable transconductor" *Electronics Letter* **1986**, 22, pp.721.
- [65] Tsvividis, Y.; Czarnul, Z.; Fang, S.C. "MOS transconductors and integrators with high linearity" *Electronics Letter* **1986**, 22, pp.245.
- [66] Sarpeshkar, R.; Lyon, R.F.; Mead, C. "A low-power wide-linear-range transconductance amplifier" *Analog Integrated Circuits and Signal Processing* **1997**, 13, pp.123.
- [67] Jeong, M.; Takagi, S.; Czarnul, Z.; Fujii, N. "Design of a novel linear 3-input CMOS OTA and its application to filter realization" *IEICE Trans. Fundamentals* **1997**, E80-A, pp.2548.
- [68] Wang, Z.; Guggenbuhl, W. "A voltage-controllable linear MOS transconductor using bias offset technique" *IEEE Journal of solid-state circuits* **1990**, 25, pp.315.
- [69] Gilbert, B. "Translinear circuits: a proposed classification." *Electronics Letters* 11(1), **1975**, pp.14-16.
- [70] Andreou, A.G.; Boahen, K.A. "Translinear Circuits in Subthreshold MOS" *Analog Integrated Circuits and Signal Processing* **1996**, 9, pp.141.
- [71] Minch, B.A.; Diorio, C.; Hasler, P.; Mead, C.A. "Translinear Circuits Using Subthreshold Floating-Gate MOS Transistors" *Analog Integrated Circuits and Signal Processing* **1996**, 9, pp.167.
- [72] Gilbert, B. "Translinear Circuits: An Historical Overview" *Analog Integrated Circuits and Signal Processing* **1996**, 9, 95-118.
- [73] Liu, S.I.; Chang, C.C. "A CMOS Square-Law Vector Summation Circuit" *IEEE Transaction on circuits and systems - II Analog and digital signal processing* **1996**, 43, pp.520.
- [74] Landolt, O.; Vittoz, E.; Heim, P. "CMOS Selfbiased Euclidean Distance Computing Circuit With High Dynamic Range" *Electronics Letters* **1992**, 28, pp.352.

- [75] Bult, K.; Wallinga, H. "A Class of Analog CMOS Circuits Based on the Square-Law Characteristics of an MOS Transistor in Saturation" *IEEE Journal of solid-circuits* **1987**, SC-22, pp.357.
- [76] Lachartre, D. "Switched-current low-power fast addressable analogue memory" *Electronics Letters* **1995**, 31, pp.1808.
- [77] Fujita, O.; Amemiya, Y. "A floating-gate analog memory device for neural networks." *IEEE Transactions on Electron Devices* **1993**, 40, p.2029.
- [78] Nakajima, K.; Sato, S.; Kitaura, T.; Murota, J.; Sawada, Y. *IEICE Trans. Electron.*, **1995**, E78-C, p.101.
- [79] Fujita, O.; Amemiya, Y.; Iwata, A. "Characteristics of floating gate device as analogue memory for neural networks", *Electronics Letters*, **1991**, 27, p.924.
- [80] Daubert, S.J.; Vallancourt, D.; Tsvividis, Y.P. "Current Copier Cells" *Electronics Letters* **1988**, 24, p.1560.
- [81] Gustat, H. "Small-Range Current Copier Cell" *Electronics Letters* **1991**, 27, p.1978.
- [82] Macq, D.; Jespers, P. "Charge Injection in Current Copier Cells" *Electronics Letters* **1993**, 29, p.780.
- [83] Daubert, S.J.; Vallancourt, D. "Operation and Analysis of Current Copier Circuits" *IEE Proceedings*, 137, p.109.
- [84] Lazzaro, J.P.; Ryckebusch, S.; Mahowald, M.A.; Mead, C.A. "Winner-Take-All Networks of O(N) Complexity" *Caltech Computer Science Department Technical Report* **1989**, Caltech-CS-TR-21-88.
- [85] Demosthenous, A.; Smedley, S.; Taylor, J. "A CMOS Analog Winner-Take-All Network for Large-Scale Applications" *IEEE Transactions on circuits and systems - I: Fundamental theory and applications* **1998**, 45, p.300.
- [86] Patel, G.N.; DeWeerth, S.P. "Compact Current-Mode Loser-Take-All Circuit" *Electronics Letters* **1995**, 31, p.2091.
- [87] Severin, E.J.; Doleman, B.J.; Lewis, N.S. "An investigation of the concentration dependence and response to analyte mixtures of carbon black/insulating organic polymer composite vapor detectors" *Anal. Chem.* **2000**, 72, p.658.
- [88] Severin, E.J. "Array-based vapor sensing using conductive carbon black-polymer composite thin film detectors" *PhD Thesis* **1999**

- [89] Doleman, B.J.; Lewis, N.S. "Comparison of odor detection thresholds and odor discriminabilities of a conducting polymer composite electronic nose versus mammalian olfaction" *Sensors and Actuators* **2001**, B72, p.41.
- [90] Doleman, B.J. "Study and development of an electronic nose and comparison with mammalian" *PhD Thesis* **1999**, p.130.
- [91] Zellers, E.T.; Han, M.W. *Analytical Chemistry* **1996**, 68, p.2409.
- [92] Mikolaj, V.; Belan, J.; Vojtechovsky, K. "Analysis of the voltage reference fluctuations of subsurface zener diodes" *Solid State Electronics* **1989**, 32, p.983.
- [93] Song, H.J.; Kim, C.K. "A temperature-stabilized SOI voltage reference based on threshold voltage difference between enhancement and depletion NMOSFETS" *IEEE J. Solid-State Circ.* **1993**, 28(6), p.671.
- [94] Reay, R.J.; Klaassen, E.H.; Kovacs, G. "A micromachined low-power temperature-regulated bandgap voltage reference" *IEEE J. Solid-State Circ.* **1995**, 30(12), p.1374.
- [95] Filanovsky, I.M.; Cai, S.S. "BiCMOS bandgap voltage reference with base current compensation" *INT J ELECTRON* **1996**, 81(5), p.565.
- [96] Nicollini, G.; Senderowicz, D. "A CMOS bandgap reference for differential signal-processing" *IEEE J. Solid-State Circ.* **1991**, 26(1), p.41.
- [97] Ferro, M.; Salerno, F.; Castello, R. "A floating CMOS bandgap voltage reference for differential applications" *IEEE J. Solid-State Circ.* **1989**, 24(3), p.690.